

MSN based biointerfaces to advance knowledge on ligand-stem cell interaction

Citation for published version (APA):

Zhang, X. (2024). *MSN based biointerfaces to advance knowledge on ligand-stem cell interaction*. [Doctoral Thesis, Maastricht University]. Maastricht University. <https://doi.org/10.26481/dis.20240228xz>

Document status and date:

Published: 01/01/2024

DOI:

[10.26481/dis.20240228xz](https://doi.org/10.26481/dis.20240228xz)

Document Version:

Publisher's PDF, also known as Version of record

Please check the document version of this publication:

- A submitted manuscript is the version of the article upon submission and before peer-review. There can be important differences between the submitted version and the official published version of record. People interested in the research are advised to contact the author for the final version of the publication, or visit the DOI to the publisher's website.
- The final author version and the galley proof are versions of the publication after peer review.
- The final published version features the final layout of the paper including the volume, issue and page numbers.

[Link to publication](#)

General rights

Copyright and moral rights for the publications made accessible in the public portal are retained by the authors and/or other copyright owners and it is a condition of accessing publications that users recognise and abide by the legal requirements associated with these rights.

- Users may download and print one copy of any publication from the public portal for the purpose of private study or research.
- You may not further distribute the material or use it for any profit-making activity or commercial gain
- You may freely distribute the URL identifying the publication in the public portal.

If the publication is distributed under the terms of Article 25fa of the Dutch Copyright Act, indicated by the "Taverne" license above, please follow below link for the End User Agreement:

www.umlib.nl/taverne-license

Take down policy

If you believe that this document breaches copyright please contact us at:

repository@maastrichtuniversity.nl

providing details and we will investigate your claim.

**MSN based biointerfaces to advance
knowledge on ligand-stem cell interaction**

Xingzhen Zhang

Copyright 2024© Xingzhen Zhang, Maastricht.
MSN based biointerfaces to advance knowledge on ligand-stem cell interaction
PhD Thesis, Maastricht University, Maastricht, the Netherlands.
ISBN: 978-94-6469-765-0
Cover Art: Jinmi Zou
Printed by ProefschriftMaken

All rights are reserved. For articles published, the copyright has been transferred to the respective publisher. No part of this thesis may be reproduced, distributed, or transmitted in any form or by any means without prior written permission from the author.

MSN based biointerfaces to advance knowledge on ligand-stem cell interaction

DISSERTATION

to obtain the degree of Doctor at Maastricht University,

on the authority of the Rector Magnificus,

Prof. dr. Pamela Habibović

In accordance with the decision of the Board of Deans,

to be defended in public

on Wednesday 28th February 2024, at 13:00 hours

by

Xingzhen Zhang

born on 7th August 1992 in Henan, China

Supervisor:

Prof. dr. Pamela Habibović

Co supervisor:

Dr. Sabine van Rijt

Assessment Committee:

Prof. dr. Roman Truckenmüller (Chair)

Dr. Matthew Baker

Prof. dr. Carmen Bartic, KU Leuven

Dr. Ingrid Dijkgraaf

Prof. dr. ir. Pascal Jonkheijm, University of Twente

Table of Contents

Chapter 1

General introduction	1
----------------------------	---

Chapter 2

2D biointerfaces to study stem cell-ligand interactions	9
---	---

Chapter 3

DNA modified MSN-films as versatile biointerfaces to study stem cell adhesion processes	59
---	----

Chapter 4

Development of mesoporous silica nanoparticle based films with tunable arginine-glycine-aspartate peptides global density and clustering levels to study stem cell adhesion and differentiation	99
---	----

Chapter 5

Effects of ligand-presenting dynamics on stem cell adhesion and migration ...	141
---	-----

Chapter 6

General discussion	173
--------------------------	-----

Chapter 7

Impact paragraph	189
------------------------	-----

Epilogue

Summary	195
Samenvatting	197
List of publications	199
Scientific communications	200
Acknowledgements	201
Curriculum Vitae	205

Chapter 1

General Introduction

Xingzhen Zhang and Sabine van Rijt

Department of Instructive Biomaterials Engineering, MERLN Institute for Technology-Inspired Regenerative Medicine, Maastricht University, Maastricht, the Netherlands.

General introduction

Regenerative medicine is an interdisciplinary field that aims to restore, replace, or regenerate damaged or diseased tissues and organs in the body [1]. Stem cells, characterized by their unique ability to self-renew and differentiate into specialized mature cells, are invaluable for regenerative medicine approaches [2]. Due to their versatile nature and regenerative capabilities, stem cells hold great therapeutic potential for the treatment of a wide range of diseases and injuries [3, 4]. The first use of stem cells in medicine can be traced back to the mid-20th century, when hematopoietic stem cell transplantation (HSCT) was performed to treat hematologic disorders, particularly leukemia [5, 6]. Since then, stem cell research and applications have significantly evolved, especially in the tissue engineering field, which aims to develop functional and native tissue-mimicking constructs, mostly using a combination of scaffolds, growth factors, and stem cells [7]. Although stem cells have great therapeutic potential, there have been few successful uses of stem cells in the clinic, even after several decades of research. There are still many challenges that need to be overcome to realize their clinical success, including how to elicit the desired stem cell behavior such as self-renewal and targeted lineage differentiation after implantation.

In the natural environment, the behavior, including regenerative capacity of stem cells is highly controlled by their extracellular matrix (ECM). The ECM is a complex and dynamic network comprising of multiple proteins and biomolecules, which provides structural support and biochemical cues to cells [8]. The ECM plays a crucial role in regulating stem cell fate, such as self-renewal and differentiation [9]. In particular, ECM proteins provide instructive biochemical cues through ligand interactions with integrin receptors expressed on stem cell membranes, known as integrin receptor-mediated stem cell adhesion. Integrins are transmembrane heterodimeric receptors consisting of α and β subunits [10]. The extracellular domain of integrins can recognize and bind to specific amino acid sequences present in ECM proteins, allowing cells to adhere to the ECM [11]. Intracellularly, integrins attach to the cell's cytoskeleton via a series of linker proteins. Integrin-mediated interaction not only provides stem cells anchoring points to the ECM but also transduces mechanochemical signals into cells, regulating diverse cellular functions including proliferation, migration, and differentiation [12].

Owing to such key functions in cell-ECM communication and in initiating cellular adhesions, integrins have been a common target in the biomaterials and tissue engineering fields [13]. Designing biomaterials capable of directing specific cellular behavior (e.g., adhesion, migration and differentiation) and promoting regenerative processes, has been a core challenge in the field of tissue engineering. A key starting point for designing interactive materials is to functionalize material surface with factors that promote cell adhesion. The capacity of a material to support cell adhesion is critical for stimulating proper tissue development at implant/tissue interfaces. Furthermore, cell attachment to a biomaterial scaffold is an important early step in the generation of *in vitro*-engineered tissue substitutes. In this regard, adhesive ligands such as Arg-Gly-Asp (RGD) peptides have been extensively used for material functionalization to enhance cell adhesion and tissue integration with the materials such as hydrogels and scaffolds [14, 15]. However, it has been demonstrated that the functionalization strategy, i.e., the way in which the adhesion ligand is incorporated into a material surface, has a significant impact on the ligand functionality and subsequent cell-material interactions. For example, previous studies have identified RGD density, spacing, and clustering as crucial ligand parameters in regulating integrin-mediated cell adhesion [16-18]. As such, there is a need to systematically understand how ligand parameters influence stem cell fate. Such knowledge will aid in the design and development of biomaterials by harnessing the potential of surface functionalization strategies for applications aimed at modulating cell function and tissue regeneration [19].

Synthetic 2D biointerfaces, which are 2D *in vitro* models that offer high control over surface properties, represent an interesting approach to study biological interactions at interfaces. Compared to complex 3D models, 2D biointerfaces are simplified systems with well-defined surface properties, allowing for better control and manipulation of experimental variables. It is important to note that while these 2D biointerfaces offer advantages in terms of controllable conditions, they represent a foundational step towards comprehending interactions within 3D environments. In addition, their surface properties are highly tunable and easy to modify, making them useful tools to study how specific ligand parameter regulates stem cell behavior. Moreover, by combining biointerfaces with nanotechnology, ligand-integrin interactions at subcellular and even nanoscale level can be studied.

The focus of the research described in this thesis is the use of a novel 2D biointerface based on nanoparticles to study ligand-integrin interactions in stem cells. First, **Chapter 2** provides an extensive literature review of recent developments in fabricating bioactive and cell-instructive 2D biointerfaces toward directing stem cell behavior, with a focus on stem cell adhesion. In this review, we first provided the reader with background information on stem cells, their natural environment, integrin-mediated cellular signaling and the importance of stem cell adhesion in dictating their behavior. Then we reviewed static biointerfaces with predefined biochemical signals and how such platforms were developed to study the effect of individual specific ligand parameters (ligand affinity, density, and patterning) on stem cell behavior. In the third section, we discussed strategies for the design of more complex dynamic platforms, which enable the display of biochemical cues with spatial or temporal control. Finally, we concluded with an outlook on current challenges and future designs of 2D biointerfaces.

One challenge in this field is designing biointerfaces that can be used to study multiple cue interactions simultaneously. Hence, in **Chapter 3**, we aimed to develop a flexible and versatile biointerface using mesoporous silica nanoparticles (MSN)-based films. MSN have promising characteristics to create 2D biointerfaces, which include high surface area, mesoporous structure and high control over their size and shape. Moreover, their surface can be easily functionalized with various chemical groups, which provides extensive possibilities for ligand modifications. Here, MSN were surface-functionalized with a PEG linker and single strand DNA (ssDNA) and spin-coated to create a film. The PEG linker was used as an antifouling linker to reduce unspecific ligand-surface interaction. DNA is a well-known versatile engineering tool, with the potential to incorporate multiple and diverse ligands into a single platform using a DNA hybridization strategy. As an example, we used Arg-Gly-Asp (RGD) ligand, which is a well-known peptide motif to interact with integrin receptors, and has been extensively exploited to understand and improve ligand-receptor interactions in many tissue-engineering applications [20]. In our design, a RGD ligand was coupled to a complementary DNA strand and attached to MSN based films via DNA hybridization. In this chapter, we first described the synthesis and characterization of PEG and DNA-modified MSN. The coating quality and surface structure of MSN films were characterized using different techniques including scanning electron microscope (SEM), water contact angle (WCA), and 3D laser scanning. DNA hybridization specificity and efficiency on the developed MSN films were also investigated.

Furthermore, using the developed films we also assessed the impact of immobilization PEG chain length on adhesion tripeptide RGD functionality and human mesenchymal stromal cells (hMSCs) adhesion. We demonstrated that an appropriate PEG chain length is required to achieve optimal RGD presentation and subsequent hMSC adhesion. Due to the high flexibility of our design, the platform developed here has wide applications for the study of ligand-stem cell interactions.

For example, in **Chapter 4**, we demonstrate the use of the developed MSN-based films to control ligand clustering at nanometer-scale. Previously it has been reported that ligand spatial distribution such as global density, micro patterns and spacing can significantly influence integrin-mediated adhesion processes [21]. Beyond that, the nanoscale pattern of these ligands on the surface is also critically important [22, 23]. For instance, ligand clustering at nanoscale has also been shown as an efficient approach to promote integrin clustering and the formation of focal adhesions [24]. However, how the ligand clustering levels at different global densities influence stem cell adhesion and subsequent differentiation is not known. Inspired by the nature of ECM, where ligands are clustered and organized at nanometer-scale to dictate cell behavior, we first developed MSN films with highly clustered ligands to probe the effect of RGD global density on stem cell adhesion. Importantly, we also investigated the impact of RGD nanoscale clustering level on stem cell adhesion and osteogenic differentiation by tuning the RGD functionalization ratio of silica nanoparticles. We demonstrated that both RGD global density and nanoscale clustering level play a role in stem cell adhesion. Higher RGD clustering levels led to increased formation of focal adhesions and expression of alkaline phosphatase in hMSCs. This chapter provides novel insight into the nanoscale ligand-stem cell interaction. Such information could be implemented into biomaterial design to achieve optimal performance of adhesive functional peptides.

In **Chapter 5**, we continued to explore the use of MSN-based films by establishing a dynamic platform and investigated the effect of ligand dynamics on stem cell behavior. In the body, the ECM remodels continuously, whereby biochemical cues change over time [25]. It is currently poorly understood how stem cells sense, adapt and behave in response to these changing signals. Therefore, a growing interest exists in the design of dynamic platforms to probe this dynamic ligand-stem cell interaction. Most of the studies as reviewed in **Chapter 2** used stimuli-responsive strategies to change ligand presentation in an “ON-OFF”

manner, which is limited to recapitulating the natural ECM kinetics due to the constant remodeling and turnover. To address this challenge, in **Chapter 5** we developed a novel dynamic biointerface based on the MSN-ssDNA films, similar to the one described in **Chapter 3**, to tune ligand kinetics by manipulating DNA hybridization dissociation rates. In this study, we employed several approaches such as Forster resonance energy transfer (FRET), surface plasmon resonance (SPR), and DNA points accumulation for imaging in nanoscale topography (DNA-PAINT), to study how different factors (DNA base pair length, hybridization buffer) influence the DNA hybridization processes. We found that different ligand kinetics provoked distinct cell morphology, adhesion and migration in hMSCs. Since the dynamic ligand-cell interaction is also involved in other diseases such as cancer, autoimmune disorders, and neurological conditions, the dynamic platform established here can also be used to advance our knowledge of various diseases, providing insights into the mechanisms underlying disease progression, identifying potential therapeutic targets, and facilitating the development of innovative treatment strategies.

In the discussion **Chapter 6**, we summarize the main findings obtained in **Chapter 3-5**, discussing their implications, and suggesting avenues for future research. Finally, we conclude the thesis with the impact paragraph **Chapter 7**, where we highlighted the scientific and social impact of our findings and potential future applications.

References

- [1] A.S. Mao, D.J. Mooney, Regenerative medicine: Current therapies and future directions, *Proc Natl Acad Sci U S A* 112(47) (2015) 14452-9.
- [2] R.A. Marklein, J.A. Burdick, Controlling stem cell fate with material design, *Adv Mater* 22(2) (2010) 175-89.
- [3] W. Zakrzewski, M. Dobrzyński, M. Szymonowicz, Z. Rybak, Stem cells: past, present, and future, *Stem Cell Res Ther* 10(1) (2019) 68.
- [4] R.S. Mahla, Stem Cells Applications in Regenerative Medicine and Disease Therapeutics, *Int J Cell Biol* 2016 (2016) 6940283.
- [5] A. Bazinet, G. Popradi, A general practitioner's guide to hematopoietic stem-cell transplantation, *Curr Oncol* 26(3) (2019) 187-191.
- [6] N. Granot, R. Storb, History of hematopoietic cell transplantation: challenges and progress, *Haematologica* 105(12) (2020) 2716-2729.
- [7] K. Dzobo, N.E. Thomford, D.A. Senthebane, H. Shipanga, A. Rowe, C. Dandara, M. Pillay, K. Motaung, Advances in Regenerative Medicine and Tissue Engineering: Innovation and Transformation of Medicine, *Stem Cells Int* 2018 (2018) 2495848.
- [8] K.H. Nakayama, L. Hou, N.F. Huang, Role of extracellular matrix signaling cues in modulating cell fate commitment for cardiovascular tissue engineering, *Adv Healthc Mater* 3(5) (2014) 628-41.
- [9] F. Gattazzo, A. Urciuolo, P. Bonaldo, Extracellular matrix: a dynamic microenvironment for stem cell niche, *Biochim Biophys Acta* 1840(8) (2014) 2506-19.
- [10] X. Zhang, S. van Rijt, 2D biointerfaces to study stem cell-ligand interactions, *Acta Biomater* 131 (2021) 80-96.
- [11] S. Chen, M. Lewallen, T. Xie, Adhesion in the stem cell niche: biological roles and regulation, *Development* 140(2) (2013) 255-65.
- [12] M.A. Schwartz, Integrins and extracellular matrix in mechanotransduction, *Cold Spring Harb Perspect Biol* 2(12) (2010) a005066.
- [13] X. Pang, X. He, Z. Qiu, H. Zhang, R. Xie, Z. Liu, Y. Gu, N. Zhao, Q. Xiang, Y. Cui, Targeting integrin pathways: mechanisms and advances in therapy, *Signal Transduction and Targeted Therapy* 8(1) (2023) 1.
- [14] O. Jeon, E. Alsberg, Photofunctionalization of alginate hydrogels to promote adhesion and proliferation of human mesenchymal stem cells, *Tissue Eng Part A* 19(11-12) (2013) 1424-32.
- [15] S.L. Bellis, Advantages of RGD peptides for directing cell association with biomaterials, *Biomaterials* 32(18) (2011) 4205-10.
- [16] J.A. Deeg, I. Louban, D. Aydin, C. Selhuber-Unkel, H. Kessler, J.P. Spatz, Impact of Local versus Global Ligand Density on Cellular Adhesion, *Nano Letters* 11(4) (2011) 1469-1476.

- [17] J.E. Frith, R.J. Mills, J.J. Cooper-White, Lateral spacing of adhesion peptides influences human mesenchymal stem cell behaviour, *J Cell Sci* 125(Pt 2) (2012) 317-27.
- [18] D.S.H. Wong, J.N. Li, X.H. Yan, B. Wang, R. Li, L. Zhang, L.M. Bian, Magnetically Tuning Tether Mobility of Integrin Ligand Regulates Adhesion, Spreading, and Differentiation of Stem Cells, *Nano Letters* 17(3) (2017) 1685-1695.
- [19] X. Zhan, Effect of matrix stiffness and adhesion ligand density on chondrogenic differentiation of mesenchymal stem cells, *J Biomed Mater Res A* 108(3) (2020) 675-683.
- [20] J.W. Lee, Y.J. Park, S.J. Lee, S.K. Lee, K.Y. Lee, The effect of spacer arm length of an adhesion ligand coupled to an alginate gel on the control of fibroblast phenotype, *Biomaterials* 31(21) (2010) 5545-51.
- [21] C. Selhuber-Unkel, T. Erdmann, M. Lopez-Garcia, H. Kessler, U.S. Schwarz, J.P. Spatz, Cell adhesion strength is controlled by intermolecular spacing of adhesion receptors, *Biophys J* 98(4) (2010) 543-51.
- [22] E.A. Cavalcanti-Adam, D. Aydin, V.C. Hirschfeld-Warneken, J.P. Spatz, Cell adhesion and response to synthetic nanopatterned environments by steering receptor clustering and spatial location, *Hfsp j* 2(5) (2008) 276-85.
- [23] Y. Kim, T.M. Koo, R. Thangam, M.S. Kim, W.Y. Jang, N. Kang, S. Min, S.Y. Kim, L. Yang, H. Hong, H.J. Jung, E.K. Koh, K.D. Patel, S. Lee, H.E. Fu, Y.S. Jeon, B.C. Park, S.Y. Kim, S. Park, J. Lee, L. Gu, D.H. Kim, T.H. Kim, K.B. Lee, W.K. Jeong, R. Paulmurugan, Y.K. Kim, H. Kang, Submolecular Ligand Size and Spacing for Cell Adhesion, *Adv Mater* 34(27) (2022) e2110340.
- [24] F. Karimi, A.J. O'Connor, G.G. Qiao, D.E. Heath, Integrin Clustering Matters: A Review of Biomaterials Functionalized with Multivalent Integrin-Binding Ligands to Improve Cell Adhesion, Migration, Differentiation, Angiogenesis, and Biomedical Device Integration, *Adv Healthc Mater* 7(12) (2018) e1701324.
- [25] W. Li, Z. Yan, J. Ren, X. Qu, Manipulating cell fate: dynamic control of cell behaviors on functional platforms, *Chem Soc Rev* 47(23) (2018) 8639-8684.

Chapter 2

2D biointerfaces to study stem cell-ligand interactions

Xingzhen Zhang and Sabine van Rijt

Department of Instructive Biomaterials Engineering, MERLN Institute for Technology Inspired Regenerative Medicine, Maastricht University, Maastricht, the Netherlands.

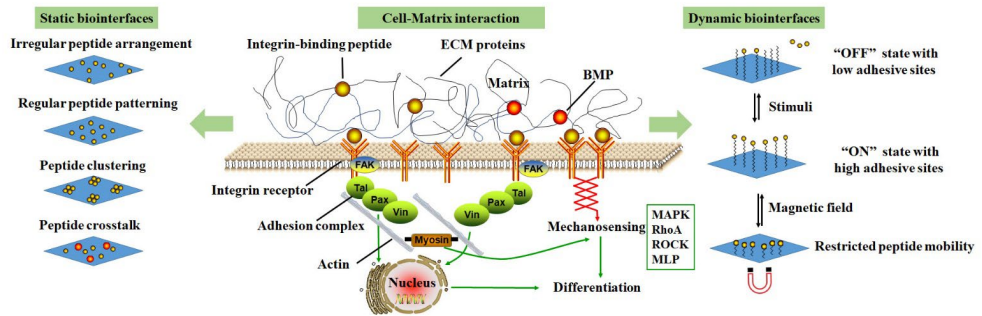
Abstract

Stem cells have great potential in the field of tissue engineering and regenerative medicine due to their inherent regenerative capabilities. However, an ongoing challenge within their clinical translation is to elicit or predict the desired stem cell behavior once transplanted. Stem cell behavior and function are regulated by their interaction with biophysical and biochemical signals present in their natural environment (i.e., stem cell niches). To increase our understanding about the interplay between stem cells and their resident microenvironments, biointerfaces have been developed as tools to study how these substrates can affect stem cell behaviors. This article aims to review recent developments on fabricating cell-instructive interfaces to control cell adhesion processes towards directing stem cell behavior. After an introduction on stem cells and their natural environment, static surfaces exhibiting predefined biochemical signals to probe the effect of chemical features on stem cell behaviors are discussed. In the third section, we discuss more complex dynamic platforms able to display biochemical cues with spatiotemporal control using on-off ligand display, reversible ligand display, and ligand mobility. In the last part of the review, we provide the reader with an outlook on future designs of biointerfaces.

Keywords

Stem cells; biointerfaces; dynamic biointerfaces; regenerative medicine; cell-material interaction

Graphical abstract



Stem cell adhesion to ECM components and ECM-inspired biointerfaces.

1. Introduction

Stem cells are unspecialized cells with an inherent ability to self-renew and with the potential to differentiate into specialized mature cells. As such, stem cells play an important role in tissue development, tissue homeostasis, and wound repair throughout life. For instance, in epithelial tissues, stem cells can compensate and replenish the cells that die from a wound or scratch to maintain tissue size and homeostasis [1]. Therefore, stem cells have attracted great attention in the field of regenerative medicine. In our bodies, stem cell interactions with the extracellular matrix (ECM) are crucial in directing stem cell behavior such as self-renewal, migration and differentiation [2]. This has resulted in a growing interest in the development of synthetic biomaterials that can mimic the natural ECM [3]. Especially in the field of regenerative medicine, biomaterials have been investigated as promising strategies to help regenerate or repair tissues and organs damaged by aging, cancer or other diseases, and as such, are regarded promising alternatives to mitigate the shortage of autografts and allografts [4-6]. The clinical success of biomaterials-based regenerative approaches is highly dependent on their ability to elicit cell behaviors that promote tissue healing. Specifically, biomaterials should provide structural and mechanical support and contain chemical and biological signals that can guide stem cell-mediated tissue regeneration processes [7]. Over the last decades, regenerative medicine has evolved from developing biocompatible but bioinert materials to materials that are biodegradable and bioactive (able to elicit a specific biological response) [8-11].

A popular strategy to create bioactive materials is by incorporating biochemical cues such as integrin-binding sequences to improve cell adhesion to the biomaterials. Accordingly, different adhesive peptides have been incorporated into various biomaterials, with tripeptide Arg-Gly-Asp (RGD) being the most popular one to enhance stem cell attachment and spreading [12-14]. RGD was initially recognized as the minimal integrin-binding domain of ECM protein fibronectin but is also present in several other ECM proteins including laminin and vitronectin [15]. Although RGD is very effective in promoting stem cell adhesion, it binds to many integrin receptors, therefore is not specific and does not recapitulate the composition diversity and structure complexity of natural ECM. Moreover, biochemical cue-mediated adhesion affects many downstream processes in stem cells that dictate their behavior. As such, it is very challenging to create a well-defined biomimetic microenvironment using only a single integrin-binding peptide

[16]. In addition, recent studies have shown the importance of ligand density, spacing, and clustering in mediating stem cell adhesion and promoting tissue-healing processes [17-19]. Therefore, there is a need for more systematic studies to improve our understanding on how individual external cues can affect stem cell behavior. Such information will improve the clinical translation of stem cell-based therapies by helping tissue engineers to rationally design improved bioactive biomaterials. In this context, synthetic 2D bioactive interfaces that offer high control over ligand presentation represent an interesting approach to study the impact of bioactive cues on stem cell behavior [20]. Specifically, 2D bioactive interfaces that can promote specific ligand binding with high control over their presentation, including their density, spacing, clustering and linkage strategies, are useful tools to improve our understanding on stem cell–ligand interactions in tissue regenerative processes.

In this review, we aim to provide an overview on recent developments on the fabrication of bioactive and cell-instructive 2D interfaces to study specific stem cell–ligand interactions. Studies using 3D systems such as hydrogels and scaffolds to research the effect of material properties and ligand chemistry on (stem) cell biology are outside the scope of this review and have been well-described elsewhere [21-24]. In this review, first, we will provide background information on stem cells and their interaction with the extracellular matrix (section 2). The next section (section 3) will focus on matrix biochemical features like ligand type, alignment, and density and their role in directing stem cell fate [25]. Specifically, we will focus on studies describing cell-instructive biointerfaces that can present cues in a static manner to decipher the role of ligand identity and density in directing stem cell adhesion, migration, or differentiation [26]. It should be noted that the matrix physical properties, such as surface topography, mechanical stiffness, and porosity, also play important roles in stem cell adhesion, migration, and differentiation capabilities [27-29]. These matrix properties and their effect on stem cells do not fit the scope of the current review, and are excellently reviewed elsewhere [29, 30]. In the next section (section 4), we review current chemical approaches for designing dynamic biosystems that are inherently dynamic or can recognize and respond to different external stimuli such as light, magnetism, sugar, and other biological factors to dynamically display biochemical cues [31-33]. Such dynamic biointerfaces can be used to increase our understanding on the importance of dynamic ligand presentation and their role in directing stem cell fate. We placed particular emphasis on dynamic ligand presentation and mobility using

stimuli-responsive materials. In the final section (section 5), we provide an outlook on future biointerface designs toward more biomimetic and diverse platforms.

2. Stem cells and their natural extracellular environment

2.1 Stem cells and stem cell niches

Generally, stem cells can be classified based on their potency (i.e., totipotent, pluripotent, or multipotent), which is their ability to differentiate in specialized cell types, or maturity (i.e., embryonic or adult) [34]. Cells of the pre-blastocyst (early embryo) are totipotent cells that can give rise to both extra-embryonic and embryonic tissues. Embryonic stem cells (ESCs) are originated from inner cell mass of a later-stage blastocyst cells [35, 36]. Although ESCs are pluripotent stem cells (PSCs) with limitless self-renewal and pluripotency, ethical problems arise by using embryos to isolate ESCs [37]. Induced pluripotent stem cells (iPSCs) are a group of ESCs-like cells with all of the hallmarks and potential of PSCs [38]. They are generated by epigenetically reprogramming somatic cells [39-41]. Easily accessible, iPSCs are characterized as having unlimited proliferation abilities and potential to differentiate into almost any adult cell type desired. Since the discovery in 2006 when Takahashi and Yamanaka used four transcriptional factors (Oct-4, Sox-2, Klf-4, and c-Myc) to reprogram adult cells into an embryonic state, iPSCs have become a promising cell resource used for treating human genetic disorders, modeling diseases, and screening drugs [42]. Despite their therapeutic promise, limitations and concerns with the clinical use of iPSC have arisen due to tumorigenicity and immunogenicity of these cells [43, 44].

Compared with PSCs, adult stem cells (ASCs), which are also known as somatic stem cells, show multipotency, giving rise to a more restricted range of differentiated specialized cells. Diverse ASCs reside in almost all human adult tissues throughout the human lifespan [45]; as such, they are easily harvested and do not have ethical concerns related to their use. ASCs can differentiate into various types of tissues lineages, offering an appealing cell source for clinical therapeutics. For example, mesenchymal stromal cells (MSCs) are highly researched ASCs that can differentiate into osteoblasts, chondrocytes, and adipocytes, and have anti-inflammatory and immune-modulatory properties. In addition, MSCs can be relatively easily obtained from the umbilical cord, bone marrow, and fat tissue by minimally invasive techniques and can be expanded for large-scale use [46]. Several studies have shown that MSCs functionality *in vivo* is not related to its multipotency [47] and so there is controversy over their

classification as stem cells [48]. Their main regenerative capabilities have been related to their ability to migrate to injured sites in response to environmental signals and release anti-inflammatory compounds to modulate the immune response and promote tissue regeneration [49]. As such, MSCs stimulate tissue-residing stem cells to regenerate new tissue and do not directly regenerate tissue themselves. Regardless of this controversy, MSCs are being investigated for various clinical applications including cardiac and orthopedic diseases (bone fracture, articular cartilage injury, osteoarthritis) [50-53].

Although ASCs have great therapeutic potential, there are still many challenges that need to be overcome to realize their clinical success. For example, we need to understand how we can elicit the desired stem cell behavior such as self-renewal, targeted lineage differentiation, and rapid proliferation once transplanted. In our bodies, ASCs reside in specialized microenvironments, referred to as stem cell niches. Each niche is tailored to meet the regenerative requirement for its respective tissue. In general, the stem cell niche is a complex assembly of multiple factors such as heterologous cellular components, various soluble factors secreted by cells, and structural extracellular matrix (ECM) proteins [54, 55]. Maintenance of stemness (the ability to preserve a stem cell's undifferentiated state) and differentiation into mature phenotypes are regulated by multifactorial cues collectively presented in their niches, which are called cell–niche interactions [56]. Many of the chemical cues from stem cell niches are provided by the ECM and are dynamic, changing in time and space. In addition, stem cells can also interact with supporting neighboring cells via secretion of soluble factors or direct cell contact, which are defined as cell–cell interactions. Although cell–cell interactions are important contributors to stem cell–niche interactions and reviewed in detail elsewhere [57, 58], we will focus in this review on the cues presented to stem cells solely by the ECM. In particular, we will focus on stem cell adhesion to the ECM, and its importance in dictating stem cell fate and ultimately regenerative processes.

2.2 Stem cell adhesion to ECM components

In the last two decades, the fundamental role of the ECM in regulating stem cell biology has gained increased attention [16, 59]. The ECM is an insoluble matrix, comprising multiple structural proteins, glycoproteins, and polysaccharides [60]. In addition, the ECM is a dynamic and complex microenvironment offering versatile cues to stem cells [61]. The native ECM structure has remodeling ability [62], which

plays a crucial role in regulating stem cell behavior, but the mechanisms of which are still poorly understood. Signal outputs from the ECM can be mainly categorized as biochemical cues such as biomolecule composition and protein assembly; biophysical cues such as matrix topography; and mechanical cues such as matrix stiffness [63]. Different chemical/physical parameters are presented to cells in a well organized way and integrate with stem cells to influence their diverse cellular functions, including adhesion, migration, and differentiation [64, 65]. In particular, ECM proteins provide instructive biochemical signals through ligand interactions with integrin receptors expressed on stem cell membranes, known as integrin receptor-mediated stem cell adhesion [66, 67]. Integrins are transmembrane heterodimeric receptors, consisting of α and β subunits. The integrin receptor family has 18 α - and 8 β -subunits, which interact noncovalently to form 24 distinct receptors [67]. Integrin receptors can consist of multiple combinations of α - and β -subunits and can recognize a variety of ECM proteins with different binding affinities. ECM proteins are recognized by, and interact with, integrin receptors via specific binding sequences including laminin-derived amino acid sequence RGD and Tyr-Lle-Gly-Ser-Arg (YIGSR), collagen I-derived sequence DGEA, and fibronectin-derived sequence PHSRN [68-70]. These sequences bind to distinct locations at the integrin receptors [71]. In addition, some amino acid sequences can bind to multiple integrin subtypes. For example, the RGD sequence is the most common recognition motif that binds to several different integrin dimers, i.e., $\alpha v\beta 1$, $\alpha v\beta 3$, $\alpha v\beta 5$, $\alpha v\beta 6$, $\alpha v\beta 8$, $\alpha 5\beta 1$, $\alpha 8\beta 1$, and $\alpha 11\beta 3$, and is found in multiple ECM proteins (fibronectins, vitronectin, collagen, tenascin, and laminin) [72]. The nature of the ECM proteins themselves is also important in determining the degree of stem cell adhesion and spreading, since different integrin receptors can be activated within stem cells [73]. Integrin-mediated interactions not only provide stem cells anchoring points to the ECM but are also an important factor in directing their fate. Generally, integrin activation is triggered by binding with ECM-derived ligands [67], and the activated integrin can further trigger binding events of multiple effector proteins, such as focal adhesion kinase (FAK), talin, paxillin, and vinculin. These effector proteins form adhesion complexes that transmit signaling from the ECM to other cytoplasmic proteins implicated in intracellular signaling pathways [74]. In addition, integrin-based adhesion complexes, which are tightly associated with the actin cytoskeleton, can activate intracellular mechanotransduction pathways, which involve phosphorylation of multiple signaling elements such as mitogen-associated protein kinase (MAPK), Rho kinase (RhoA), Rho-associated

protein kinase (ROCK) and myosin light chain (MLP) [29, 73]. Mechanotransduction regulates morphogenesis, migration and differentiation of stem cells by transmitting intrinsic mechanical force which is generated by actomyosin contractility and actin polymerization and extrinsic mechanical force which is externally applied via shear forces or tension from the ECM. The ECM sensing to the intrinsic mechanical force can further be transduced into biochemical signals and feed back to integrin-mediated adhesion [75].

The maturation of stem cell adhesion can be categorized into different stages, including nascent adhesion, focal adhesion, and fibrillary adhesion, that show variance in intracellular cytoskeletal organization, cell polarity, gene expression, and ultimately influence stem cell processes such as differentiation and migration. For example, cell migration is mediated by adhesion receptors and tightly regulated by adhesion processes. Effective migration requires constant formation of focal adhesions in the front direction of migration and detachment at the rear of cells [76]. Cell migration speed is dependent on cell adhesion strength mediated by integrin–ligand interactions, including ligand levels, integrin levels, and integrin–ligand binding affinities. An intermediate adhesion strength between the cells and the substrate may induce a highest migration speed [77]. In addition, cell adhesion has been reported to be crucial in determining MSC differentiation. Large adhesion, high cell spreading, and cytoskeletal tension could facilitate osteogenesis, whereas nonspreading and low intracellular tension facilitate adipogenesis [78, 79]. As such, stem cell adhesion represents an important process in controlling and predicting stem cell behavior. In the next two sections we will describe how 2D cell-instructive interfaces can be used to study important cell adhesion processes. In the next section static surfaces exhibiting predefined biochemical signals are discussed, while in the fourth section more complex dynamic platforms are described.

3. Static biointerfaces

Static interfaces with well-defined biochemical cues have been extensively developed as important tools to study the role of specific ligand parameters in stem cell adhesion and signal transduction [80]. The vast majority of published studies (89%) focus on incorporating the RGD sequence in the biomaterials and scaffolds to improve stem cell adhesion [81]. Although relevant, RGD is also highly unspecific. As such, the impact of the choice of ligand type as well as ligand density and distance on cell fate is currently understudied. In this section, we

describe how these static biointerfaces have been used as tools to study how ligand composition, affinity, density, and patterning can influence cellular biological processes, as summarized in Table 1. Such studies give us fundamental and progressive understanding on cell–interface interactions, which will help researchers in the field to improve their biomaterial designs.

Table 1 Elucidating stem cell–ligand interaction using static biointerfaces

Substrate	Ligand Properties	Cell type	Biological observations	Reference
Polystyrene	IKVAV ligand presentation	MC3T3	IKVAV containing multi-domain peptide significantly increased cell attachment, proliferation, osteo-differentiation and improved tissue integration <i>in vivo</i>	[82]
PS-PEO	Ligand type: RGD, RETTAWA, IKVAV and YIGSR	hBMSCs	hBMSCs cultured on these peptides displayed different morphologies and varying abilities to differentiate along osteogenic and adipogenic lineages	[83]
Gold	Ligand affinity to cyclic and linear RGD	MSCs	cycRGD peptide showed a higher affinity to integrin and promoted osteogenesis compared to linRGD	[84]
Glass	RGD and BMP-2 ligand interplay	hBMSCs	RGD and BMP-2 mimetic peptides acted synergistically to enhance hBMSCs osteogenesis	[85]
Self-assembled monolayers on gold	Ligand spacer to substrate	Swiss 3T3 fibroblasts	The PEG spacer to which the peptides were tethered influenced ligand-integrin interaction. Cell attachment decreased as PEG spacer length increased	[86]
Supported lipid bilayers	Ligand density	hMSC	Cell adhesion and osteogenic differentiation is positively correlated to ligand density	[87]
RGD-Cys-D1 nanopatterned PLLA	RGD local density	hMSCs	RGD nanopatterns with minimum interparticle distances below 70 nm resulted in larger cell condensates and enhanced chondrogenic differentiation	[88]
Protein-engineered fabrics	Ligand clustering	HUVEC	Ligand clustering enhanced integrin activation, focal adhesion and proliferation of cells	[89]
Fe nano-segments based barcoding	Nano-ligand frequency and sequence	hMSCs	Low nano-ligand frequency and terminally sequenced nano-ligands facilitated focal adhesion, mechanosensing and osteogenic differentiation of stem cells	[90]

3.1 Ligand type and affinity

Integrin activation and the strength of interaction greatly depend on the affinity and specificity between the particular integrin receptor and its ligand [91]. Therefore, different types of adhesive motifs can influence the lineage choice and functional pathways of stem cells by binding to distinct integrin receptors. To investigate this, Frith et al. proposed a controlled experimental approach to probe the effect of such specific integrin–ligand interactions on human bone marrow–derived mesenchymal stromal cells (hBMSCs) differentiation [83]. hBMSCs were chosen as a cell model as hBMSCs express a broad range of integrins in their undifferentiated state. A group of cell binding sequences RGD, RETTAWA, IKVAV and YIGSR were used to functionalize a nonfouling polystyrene-block-poly(ethylene oxide)-copolymer (PS-PEO) to fabricate a series of defined 2D substrates. RGD is known to bind to $\alpha v\beta 1$, $\alpha 8\beta 1$, $\alpha v\beta 1$, $\alpha v\beta 3$, $\alpha v\beta 5$, $\alpha 5\beta 1$, $\alpha 5\beta 6$, and $\alpha 11\beta 3$ integrins, while RRETAWA, IKVAV, and YIGSR can specifically recognize $\alpha 5\beta 1$, $\alpha 1$, and $\beta 1$ chain, respectively [69, 92-94]. Flow cytometry assays indicated hBMSCs expressed a broad range of integrin receptors and showed an increase in integrin $\alpha 5$ expression during osteogenesis and an increase in integrin $\alpha 6$ expression throughout adipogenesis. hBMSCs morphology, viability, and differentiation potential was affected by adhering to the different peptide motifs. Specifically, hBMSCs cultured on substrates presenting RGD peptides showed greatest spreading and a classic elongated morphology. In addition, presentation of RGD supported long-term viability of hBMSCs. The IKVAV peptide was observed to induce both osteo- and adipogenic differentiation. As such, this study shows that different bioactive motifs can activate specific integrin receptors which ultimately influence viability and lineage progression of hBMSCs. Along a similar line, the same authors compared the effect of RGD and IKVAV ligands on MSC adhesion [95]. Self-assembled adamantane-terminated polystyrene-b-poly(ethylene oxide) (PS-PEO-Ada) films were developed to which β -cyclodextrin (β -CD) modified peptide sequences (RGD and/or IKVAV) could be non-covalently conjugated. Adhesion studies demonstrated that MSC morphology was highly ligand dependent. Specifically, hMSCs on IKVAV conjugated substrates displayed rounded shapes, with significantly decreased cell spread area and poorly organized actin fibers that was predominantly localized to the cell periphery. Cells cultured on RGD conjugated substrates were well-spread and showed highly aligned stress fibers spanning the length of the cell.

Similarly, Mehta and co-workers reported that the osteogenic differentiation of MSCs encapsulated within collagen I-derived DGEA ligand-modified substrates was enhanced when compared with that functionalized with RGD [96]. Specifically, the osteocalcin expression and mineral deposition of MSCs cultured in DGEA peptide-containing gels were 50% and 1-fold higher compared to RGD modified surface. From these studies, it is clear that MSCs adhesion through specific integrin receptors plays an important role in MSC differentiation processes. Furthermore, these studies also showed that various types of short peptide sequences can be used to allow different levels of integrin specificity, which could not be achieved with whole ECM proteins.

Apart from specificity of different integrin–ligand pairing, other reports have demonstrated that the conformation of the peptide can also modulate integrin affinity, influencing the cytoskeleton of the cell and ultimately directing differentiation pathways of MSCs. In one study, cyclic peptide RGDfC (cycRGD) or linear peptide GRGDSC (linRGD) was immobilized on gold substrates [84]. MSCs cultured on monolayers presenting a high-affinity cycRGD peptide promoted osteogenesis, giving greater tension in the cytoskeleton, while cells on monolayers presenting the lower-affinity, linRGD peptide displayed a high expression of myogenic markers. Overall, the utilization of specificity and affinity between integrin receptors and correlated ECM bioactive motifs to control stem cell fate and to elicit desired cell differentiation has significant implications for designing tissue engineering therapies.

3.2 Multiple ligand interplay

Stem cell differentiation is closely regulated by the native ECM, which contains a mixture of soluble and immobilized proteins with distinct functions. While RGD has been used as a “default” integrin-binding site for biomaterial functionalization, its functionality is affected by its contextual sequence presentation within fibronectin. Previous studies demonstrated that the co-presentation of RGD and its synergy sequence PHSRN significantly affected the spreading and proliferation of MSCs [97, 98]. As such, the importance of crosstalk and interplay between different ligands in regulating stem cell behavior has been highlighted [85]. To study the importance of ligand crosstalk, recent studies have focused on developing biointerfaces functionalized with two ligands. For example, incorporating a combination of RGD and osteogenic bone morphogenic protein (BMP)-2 mimetic peptide to study their synergistic effect on the differentiation of hBMSCs has

recently been investigated [99]. The BMP-2 peptide is known to induce hBMSCs osteoblast differentiation, and also weakly supports cell adhesion [100, 101]. Functionalized surfaces were prepared by grafting glass surfaces with RGD and BMP-2 peptides, alone and in combination. hBMSCs cultured on RGD surfaces mainly preserved their stemness, while hBMSCs cultured on BMP-2 surface showed targeted osteogenic commitment. More importantly, the osteogenic commitment of hBMSCs was accelerated on RGD and BMP2 bifunctionalized surfaces as compared to BMP-2-only surfaces. Thus, the osteoinductive effect of BMP-2 peptide was enhanced in the presence of adhesive RGD peptides, suggesting that integrin signaling played a role in the activation of BMP-2 receptors. These findings not only provided important information on signaling pathways that govern the transition of stem cells from their stemness state towards the osteoblastic lineage, but also contributed to the development of custom-designed *in vitro* cell culture biointerfaces.

In a similar work, recombinant human BMP-6 and its co-presentation with integrin ligands cyclic-RGD were nanopatterned on gold-coated glass substrates via a protein-repellent PEG linker [102]. BMP-6, a member of the transforming growth factor (TGF)- β superfamily, plays an important role in osteoblast differentiation through downstream smad signaling pathways [103]. Both RGD and BMP-6 ligands were covalently immobilized on the surface to prevent internalization, allowing sustained interaction with the cells. The results in this study suggested that co-presentation of BMP-6 and RGD to mouse myoblast C2C12 cell cultures promoted focal cell adhesion and enhanced cellular Smad phosphorylation levels, indicating enhanced BMP mediated osteoblast signaling. In addition, BMP-6 added to culture media with the presence of RGD ligands were less effective in inducing Smad complex activation compared to BMP-6 immobilized on the surfaces. These results indicated that co-presentation of BMP-6 and RGD ligands can enhance cell adhesion and BMP-mediated signaling activity.

Recently, Gentile et al. developed a platform using a multilayered electrospun membrane based on PLGA and nanohydroxyapatite (nHA), which could incorporate three types of fragments into the different nanolayers [104]. The peptides were KRSR, which is known to enhance cell adhesion and proliferation; NSPVNSKIPKACCVPTLSAly, which is derived from BMP-2 and has shown potential to guide MSC differentiation into osteoblasts; and FHRRIKA, which is known to promote mineralization. Using this system, it was demonstrated that the

addition of peptides resulted in the significant increase in the expression levels of osteogenic markers including alkaline phosphatase (ALP), osteopontin, and osteocalcin. Furthermore, the functionalized membrane promoted bone tissue regeneration 4 weeks after implantation in a rat calvarial defect model. This approach shows that incorporating multiple bioactive ligands into biomaterial constructs have high potential to improve tissue regeneration processes.

3.3 Ligand spacer

In addition to ligand specificity and affinity, the length of the spacer between adhesion ligands and substrates also plays a vital role in directing stem cell response. One common strategy to improve the bioactivity of biomaterials is to couple adhesive moieties to the material surface through a nonfouling linker such as polyethylene glycol (PEG). The ultimate efficacy of bioactive ligands used for surface functionalization is likely to be affected by the length of the spacer. In order to evaluate the effect of spacer length of immobilized RGD peptides on the control of attachment and spreading of Swiss 3T3 fibroblasts, self-assembled RGD monolayers were developed as model substrates by the Mrksich group [86]. RGD was immobilized on gold surfaces via PEG linkers, where the distance separating the glycol groups and the peptide ligand could be controlled by using oligo (ethylene glycol) groups with either tri-, tetra-, penta-, or hexa (ethyleneglycol) units. As the length of the oligo(ethylene glycol) groups increased, cell adhesion and spreading decreased. The strength of the cell–substrate interaction also decreased on monolayers with longer glycol groups. Interestingly, cell attachment and spreading on monolayers presenting longer glycol oligomers was RGD density-dependent, while cell attachment and spreading on monolayers presenting short glycol oligomers did not change with RGD density. The differences in cell attachment to substrates presenting different oligo(ethylene glycol) groups was attributed to a change in binding affinity between the peptide and integrin receptor, indicating that spacer length is a considerable parameter for the design of bioactive materials.

In another study, Lee et al. investigated how RGD attached to different spacer arm lengths influenced fibroblast phenotype [105]. The authors found that alginate gels functionalized with RGD peptides containing varying spacer arm lengths strongly affected the adhesion and proliferation of fibroblasts when the total concentration of the peptides was kept constant. An increase in spacer arm length contributed to enhanced cell spreading and proliferation in both 2D and 3D

culturing systems. It was hypothesized that as the spacer arm length diminished the steric hindrance of conjugated ligands, enhancing the accessibility to the RGD peptides. They found that a spacer ranging from four to twelve glycine units were required for RGD peptides to properly bind to the cellular integrin receptor and allow effective adhesion of fibroblasts when cultured in 2D systems. In a follow-up study, Lee and colleagues further studied the effect of spacer arm length on stem cell differentiation using mouse-derived bone marrow stromal cells (D1 stem cells) [106]. Osteogenic and adipogenic differentiation of these stem cells was promoted when the spacer arm length of RGD peptide increased. Thus, the spacer length of RGD—and perhaps other cell adhesion ligands—can play an important role in regulating proliferation and differentiation of stem cells.

In another recent work by Chen et al., the impact of PEG antifouling layer length on stem cell adhesion using various types of cell adhesion peptides was studied [107]. Cell-specific adhesive peptides (KRSR, YIGSR, VAPG) were tethered onto a layer of PEG at variable chain lengths including short (tetraethylene glycol, OEG4), medium (octaethylene glycol, OEG8), and long (polyethylene glycol, PEG2K, Mn = 2000 Da). PEG spacers of medium length had a substantial effect on the performance of functional peptides by affecting both peptide antifouling properties and surface density. The OEG8 ligand was shown to be the optimal length to provide antifouling properties and low non-specific cell adhesion to the attached surfaces. KRSR, YIGSR, and VAPG attached to OEG8 could promote selective cell adhesion. In contrast, PEG linkers with either a short spacer (OEG4) or a long spacer (PEG2K) led to unspecific cell adhesion or low cell adhesion, respectively. In addition, a dual-ligand (RGD and BMP2 peptide mimetic)-modified surface using OEG8 as antifouling linker demonstrated controlled hMSCs differentiation towards the osteoblast phenotype by providing both efficient antifouling and enough peptide density of RGD and BMP2 on the surface to allow adhesion and differentiation. This study provides general guidelines on selecting optimal PEG linker lengths to ensure proper function of adhesion peptides when creating 2D biointerfaces.

In conclusion, PEG has been extensively used as nonfouling spacers for surface engineering. The spacer arm length of adhesion ligands can influence the performance of functional peptides, therefore regulating stem cell–interface interactions. The knowledge obtained from these platforms is useful to determine

the correct spacer length when incorporating adhesive ligands in biomaterials and scaffolds.

3.4 Ligand density

Stem cell adhesion to the ECM is mediated by the recognition and molecular interaction between adhesion ligands and transmembrane integrin proteins. Integrin-mediated adhesion is a prelude after which many cellular signaling cascades follow and has significant implications in long-term cell behavior [108, 109]. Ligand density and spacing are critical parameters in regulating stem cell behavior since proper spatial arrangement of ligands is required for integrin clustering and activation [110]. Variations in ligand density and arrangement can drive changes in cellular force tension, cytoskeletal organization and signal transduction, which altogether modulate cellular adhesion and differentiation [111-113]. In order to investigate how biomaterial parameters like ligand density and ligand spacing regulate stem cell biological responses, various bioactive interfaces have been explored on which the ligands can be displayed stochastically at various densities or uniformly arranged at different lateral spacing [114] (Fig. 1A). One strategy to control ligand density is the use of self-assembled monolayers (SAM) of alkanethiolates on gold surfaces. By modulating the ratio of ligand-alkanethiol conjugates, a surface with different average ligand densities could be formed [84]. In work performed by Jonkheijm's group, a recombinant knottin protein containing RGD sequences and multivalent tryptophan was designed for cell adhesion studies [115]. This knottin was tethered on cucurbit[8] (CB[8])-methylviologen (MV²⁺)-modified gold surfaces through supramolecular chemistry. CB[8] is a macrocyclic host molecule that can bind two aromatic guest molecules simultaneously, and has been extensively explored for dynamic cell adhesive surfaces where guest binding can be controlled by external conditions [33]. The surface coverage of the knottins could be controlled by valency and concentration. A series of knottin variants was created by varying the number of tryptophan moieties, which act as an anchorage motif and can form heteroternary complexes with CB[8]- MV²⁺ (Fig. 1B). Surface plasmon resonance spectroscopy was used to study the interaction between knottins and the CB[8] and MV²⁺ surface. A higher valency of tryptophan residues on knottin resulted in an increased affinity for assembly and an enhanced coverage of knottin on the surface, which eventually contributed to elongated cell spreading and pronounced focal adhesion. This study preliminarily illustrated that the RGD ligand density has an effect on cell adhesion. In addition, CB[8]-mediated assembly

of multivalent knottins displaying RGD ligands is a promising strategy for biomaterials with tunable interactions with cells.

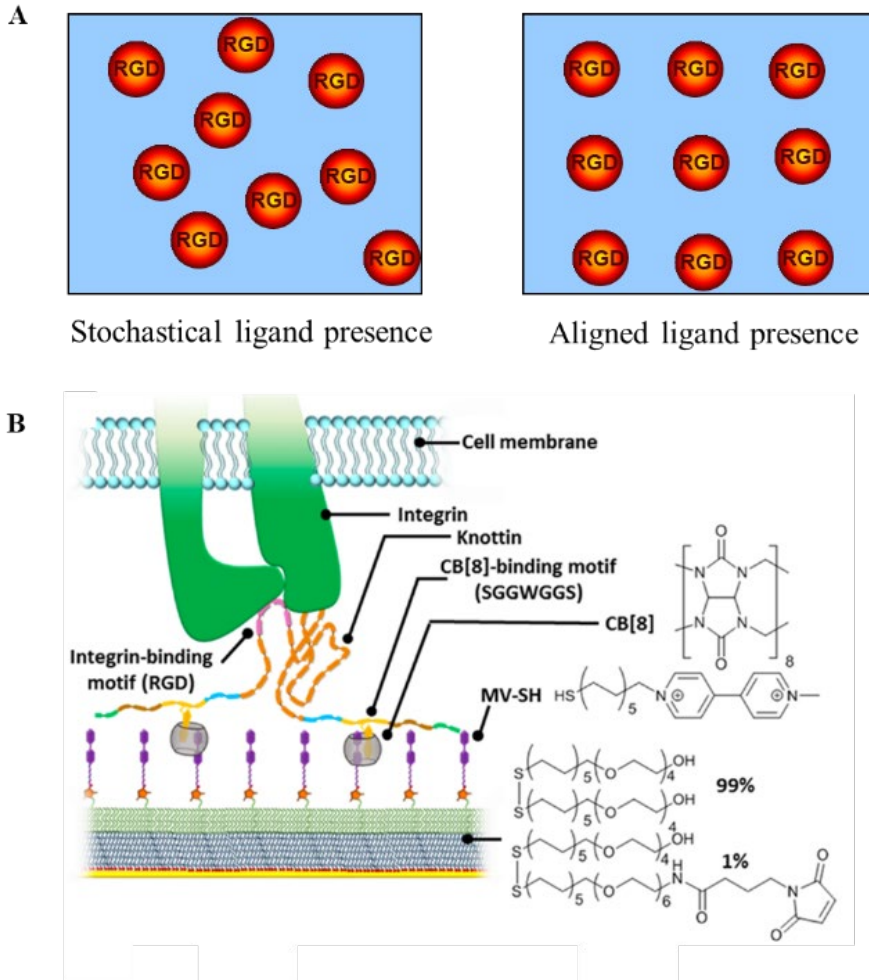


Figure 1. (A) Cartoon representation of stochastic ligand presence versus aligned ligand presence. (B) Schematic representation of the integrin-binding knottin constructs noncovalently bound to cucurbit[8]-methylviologen (MV²⁺)-modified gold surfaces through the formation of two ternary complexes. Reprinted with permission from ref. 115.

Biological interfaces based on supported lipid bilayers (SLB) have also been used as model systems to study how ligand density and lateral movement of anchored ligands over a 2D surface affect cell adhesion. SLBs are cell membrane-mimetic supramolecular architectures, consisting of lipids [116]. SLBs have been widely employed as biological interfaces due to their easily tunable properties such as biospecificity, mobility, and ligand density. For example, by adjusting the molar concentration of functional lipids to which the ligands are tethered, the density of predesigned ligand molecules can be easily controlled. In addition, compared to substrates where peptides are covalently conjugated to self-assembled monolayers of alkylthiolates or block copolymers on gold, substrates based on SLBs could integrate responsive and mobile ligands into the system due to inherent dynamics of noncovalent bonds [33, 117, 118]. Furthermore, the mobility of ligands on SLBs could be tuned by adjusting the alkyl chain composition of base lipids, which determines the phase behavior of SLBs. For example, SLBs consisting of lipids with 1,2-dioleoyl-sn-glycero-3-phosphocholine (DOPC) present mobile ligands while SLBs consisting of lipids 1,2-dipalmitoyl-snglycero-3-phosphocholine (DPPC) present immobile ligands at physiologically compatible temperatures. In one report, SLB-based systems were employed to investigate the role of ligand density and mobility on hMSC fate decision [87]. To modulate the lateral mobility of ligands immobilized on a surface, SLBs were created consisting of either DOPC lipids to allow the presentation of mobile ligands or DPPC lipids to allow presentation of immobile ligands on the surface. DOPC conjugated with biotin (DOPE) were used to link RGD on surface. RGD peptide density over the surface could be tuned by adding different amounts of DOPE (ranging from 0.01 mol% to 1.0 mol%) to DOPC. Cell density increased with increasing RGD functionalization degree due to the creation of a higher number of adhesive sites. Enhanced osteogenic differentiation capacity of hMSCs was observed when cultured on 1 mol% biotin DOPE-conjugated SLBs compared to 0.01 mol% biotin DOPE-conjugated SLBs, suggesting a positive role of ligand clustering in dictating hMSC lineages. In addition to osteogenic differentiation, the RGD surface density can be tailored at the nanoscale to steer hMSCs into chondrogenic commitment by regulating cell adhesion. The process of MSCs toward chondrogenic differentiation requires cellular aggregation (condensation) that is mediated by cell-cell adhesion communication, which involves multiple signaling molecules such as N-cadherin and gap-junction proteins [119]. It has been reported that both functional group

composition as well as RGD nanopatterns can be used to steer MSCs towards chondral regeneration [120].

In another study, RGD-dendrimer-based nanopatterns on poly(lactic acid) (PLLA) were developed by immersing PLLA substrates in aqueous solutions of an RGD-tailored dendrimer (RGD-Cys-D1) [88]. RGD surface density was tuned by using a range of dendrimer concentrations (4×10^{-9} – 10^{-2} (% w/w)). It was shown that a dendrimer concentration of 2.5×10^{-8} (% w/w) led to nanopatterns in which 90% of the surface contained a minimum interparticle distance of 70 nm (d_{mixn}), a threshold value needed to promote effective cell adhesion. In addition, cell condensation, an important process required for chondrogenic differentiation, was evaluated for hMSCs cultured on different RGD-Cys-D1 nanopatterned surfaces. It was shown that intermediate adhesiveness of cells to substrates with dendrimer concentrations of 2.5×10^{-8} (% w/w) resulted in larger cell condensation and enhanced chondrogenic differentiation. In a follow-up study, the authors further analyzed and compared the chondrogenic differentiation potential of human BM-MSCs derived from osteoarthritis (OA) or healthy (H) donors on RGD-Cys-D1 PLLA nanopatterned substrates, using a three-dimensional (3D) pellet culture system as reference model [121]. It was shown that RGD-Cys-D1 PLLA nanopatterned substrates could enhance the adhesion and formation of pre-chondrogenic condensates from OA- and H-derived BM-MSCs compared to the 3D cell pellet culture reference model. Moreover, MSC-derived from OA exhibited bigger aggregate areas, more compact aggregates, and higher expression of chondrogenic makers (tenascin, sex determining region Y-box9 and collagens type II) compared to H-derived MSCs when cultured on the RGD-dendrimer-PLLA nanopatterned substrates. This study suggests that 2D biointerfaces are also useful tools for use as disease models.

Advances in surface engineering and surface fabrication techniques also enabled the development of platforms with patterned and ordered ligand distribution. These platforms have been used to study how ligand lateral spacing at micrometer or even nanometer length scales influence cellular behavior [111, 122]. For example, self-assembled maleimide-functionalized polystyrene-block poly(ethylene oxide) copolymers (PS-PEO-Ma) have been employed to nanopattern cysteine–GRGDS peptides at different lateral spacing ranging from 34 to 62 nm. hMSCs cultured on PS-PEO-Ma surfaces presenting smaller lateral nanospacing of RGD peptides (34 nm and 44 nm) showed larger cell areas, well

defined stress fibers, and more mature adhesions, whereas hMSCs cultured on surfaces with a larger spacing (62 nm) of RGD peptides exhibited smaller cell areas, normal fibroblastic morphology, disorganized actin cytoskeleton, and more nascent adhesions. Furthermore, significant osteogenic differentiation of hMSCs was only observed on 34 nm-spaced RGD substrate. Conversely, upregulation of the adipogenic markers in hMSCs was confirmed on 62 nm-spaced RGD surfaces after 7 days of incubation. These findings suggested that the lateral spacing of RGD peptides can alter the cells' ability to spread, form mature adhesion, and differentiate into specific lineages [123]. In a follow-up study, the authors further investigated the underlying molecular mechanisms defining the impacts of ligand lateral spacing on stem cell adhesion and differentiation. A panel of real-time localization and activity biosensors for focal adhesion (FA) proteins and mechanotransduction signaling pathway modulators (Rho GTPases) was applied to monitor hMSC temporal response. hMSC cultured on 32 nm-nanospaced RGD surfaces recruited more activated focal adhesion kinase (FAK) and steroid receptor coactivator (Src) proteins, showed more myosin IIA co-localized within actin and FAK, and consequently formed stable and increased FAs compared to hMSCs cultured on the larger, 64 nm-spaced RGD surfaces. Additionally, hMSCs on the 32 nm-spaced substrates exhibited larger and mature vinculin-positive complexes, and higher tension force per FA compared to cells on the 62 nm-spaced substrates. In addition, upregulation of active Rac1, enhanced RhoA activity, greater YAP/TAZ activation, and increased RUNX2 activity in hMSCs on smaller RGD nanospacing was responsible for hMSCs' commitment toward an osteogenic fate. To conclude, this study validated a profound relevance between ligand lateral spacing and initiating hMSC cellular mechanotransduction via differential coupling of FAK/Src/Rac1/myosin IIA/YAP/TAZ signaling pathways [124].

To study the effect of clustered ligand distributions on integrin activation, a series of elastin-like engineered protein fabrics with precisely controlled global and local ligand densities have been developed [89]. It was demonstrated that ligand clustering could enhance integrin activation, cell focal adhesion and proliferation. However, this ligand clustering-enhanced integrin activation required a global ligand density near the ligand's effective dissociation constant ($K_{D,eff}$) of $12,000 \pm 1,000$ RGD μm^{-2} . In another approach, a barcoding system was developed to investigate how ligand frequency and sequence within the barcode influences stem cell adhesion and differentiation [90]. Tunable nanoscale and spatial RGD presentation of barcoding substrates was achieved by tuning the electrodeposition

conditions, while nanoscale intra-barcode (local) ligand density and macroscale (total) ligand density on surface was constant in all groups (Fig. 2A). Low ligand frequency using the same sequences and terminally sequenced ligands at the identical frequency facilitated focal adhesion and spreading of hMSCs, showing significantly higher attached cell number, spread area, and vinculin expression both *in vitro* and *in vivo* (Fig. 2B). Moreover, FA-assisted mechanotransduction and osteogenic differentiation of hMSCs by stimulating nuclear translocation of RUNX2 and YAP mechanotransducer, and ALP expression was observed. As such, this study demonstrated that ligand sequences and frequency within nanostructures are critical parameters in *in vitro* and *in vivo* regulation of diverse cell functions, which sheds novel insights into designing biomaterials with heterogeneous nano-ligand sequences to control stem cell behaviors.

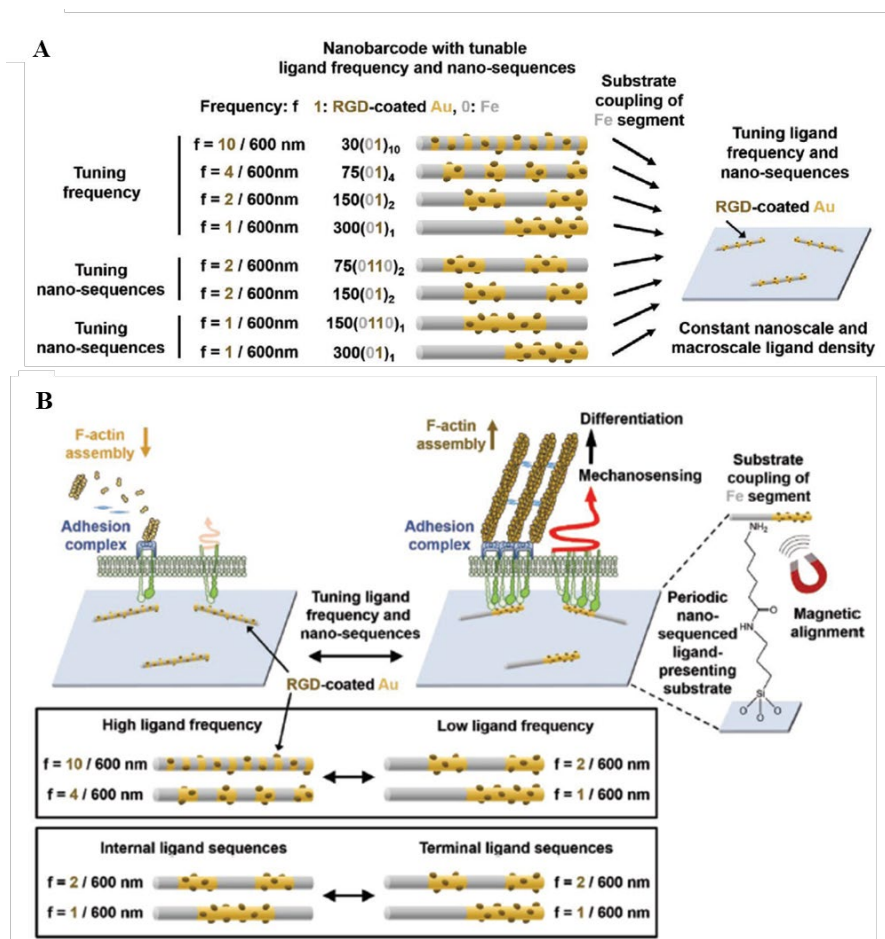


Figure 2. (A) Schematic representation of a heterogeneous barcoding system including RGD-bearing Au and RGD-free Fe nano-segments to independently present tunable frequency and sequences of RGD in nano-segments. (B) Low-frequency and terminally sequenced nano-ligands facilitating focal adhesion and mechanosensing, thus mediating differentiation of stem cells. Reprinted with permission from ref. 90.

4. Dynamic biointerfaces

The in the previous section discussed static biointerfaces have provided the field with important information on the role of key interfacial parameters in regulating stem cell behaviors. However, in the body the ECM remodels continuously, where biochemical cues change in space and time. It is currently poorly understood how stem cells sense, adapt and behave, including adhesion and migration, in response to these changing signals. Therefore, more recently, dynamic biointerfaces have been developed to study the dynamic interaction between stem cells and biological signals presented in extracellular environments. Dynamic biointerfaces, a new concept within the field of synthetic ECM-mimicking 2D interfaces, are defined by highly tunable surface properties capable of controllable and modular biochemical cue presentation [125]. Diverse stimuli-responsive materials that can respond to physiochemical stimuli (e.g., light, chemicals, magnetism, electric field) together with various chemical strategies (e.g., supramolecular chemistry, host-guest chemistry) have been investigated to create well controlled and dynamic biointerfaces. These dynamic systems enable on-off presentation of ligands, reversible control over single ligand display, or even dynamic manipulation of ligand mobility over time, to study dynamic ligand presentation on stem cell behavior, as summarized in Table 2. In this section, different ways to create dynamic synthetic biointerfaces and their biological effect on stem cells are discussed.

Table 2 Elucidating stem cell–ligand interaction using dynamic biointerfaces

Ligand properties	Stimuli	Materials	Application	Ref.
On-off ligand presentation	Elastase	Fmoc blocking PEG-RGD via dialanine linker	“ON” state promoted adhesion and high integrin $\beta 5$ co-localization of hMSC	[126]
	Light	DMNPB-caged RGD	Four-fold higher adherent cell densities were observed on “ON” state	[127]
	Electric potential	Viologen, CB[8] and tripeptide ternary complex on gold	After cell adhesion, electrochemical reduction lead to the release of the peptide and detachment of cells	[128]
Reversible ligand presentation	Sugar	(DOPA)4-S5-GRGDS binding with PBA	Dynamic ligand presentation enabled dynamic modulation of hBMSCs adhesion	[129]
	Magnetic force	MNP-(AuNP-RGD)	Reversible nanoscale ligand oscillations regulated adhesion and differentiation of hMSCs both <i>in vitro</i> and <i>in vivo</i>	[130]
	Light	β -CD/Azo-E7	The release of Azo-E7 peptides weakened adhesion and mobility of BMSCs	[131]
	Electric potential	RGD/Sulfonate/Au	Switchable surfaces dynamically modulated stem cell adhesion, morphology and differentiation, with a higher RGD accessibility leading to osteogenesis	[132]
	Magnetic force	PEG-MNP@SiO ₂ -RGD	Low RGD mobility promoted adhesion, spreading, osteogenic differentiation of hMSCs	[133]
Ligand mobility	Magnetic force	PEG-SPION@SiO ₂ -RGD	Nanoscale motion of RGD influenced the adhesion and differentiation of hMSCs both <i>in vitro</i> and <i>in vivo</i>	[134]

4.1 On-off presentation of ligands

One approach to develop dynamic biointerfaces is to regulate single ligand presentation by functionalizing the surface with stimuli-responsive linkers to which the adhesive ligands are tethered. These stimuli-responsive platforms can switch either from “ON” to “OFF”, or from “OFF” to “ON” upon triggering by various stimuli such as light, electrical potential, enzymes, or other molecules [135-138]. This ON-OFF switching can change adhesive ligands accessibility for stem cell binding, thereby enabling temporal control over stem cell adhesion. Most examples make

use of photo-cleavable or enzyme-cleavable linkers to create ON-OFF systems. For example, Roberts et al. fabricated an elastase-cleavable platform to investigate the mechanisms of hMSC growth and differentiation as a function of dynamic integrin binding [126]. The platform was created by immobilizing RGD on glass, followed by coupling with an elastase-sensitive dialanine (AA) linker and fluorenylmethoxycarbonyl (Fmoc) (Fig. 3A). In this set-up, Fmoc worked as a blocking group, sterically preventing cells from interacting with the RGD ligands, represented as the “OFF” state with low adhesive sites. Upon elastase pretreatment, cleavage of the AA linker resulted in the removal of the Fmoc blocking group, hence exposing RGD to the cells, representing the “ON” state, resulting in high hMSC adhesion. hMSCs cultured on the RGD surfaces (“ON” state) exhibited supermature adhesions (SMAdhs) with a high co-localized expression of integrin $\beta 5$ (vitronectin receptor) and BMP-2 receptor. In contrast, hMSCs that were exposed to the “OFF” state showed poor adhesion, which was found to be mediated predominantly by the integrin $\beta 1$ receptor (fibronectin receptor), and no significant BMP receptor co-localization could be observed. Integrin $\beta 5$ has been identified previously as being important in MSC osteogenic commitment [139]. In addition, the adhesion changes could further influence stem cell phenotype and long-term growth. MSC growth markers STRO-1 and activated leukocyte cell adhesion molecule (ALCAM) as well as the osteoblast markers osteopontin (OPN) and osteocalcin (OCN) were checked at 21 days in culture. MSCs on RGD surfaces and the enzyme-cleaved surface showed high expression levels of OPN and OCN, and low levels of STRO-1 and ALCAM. These data suggest that there is a delicate adhesion/tension balance controlling hMSC growth and lineage commitment.

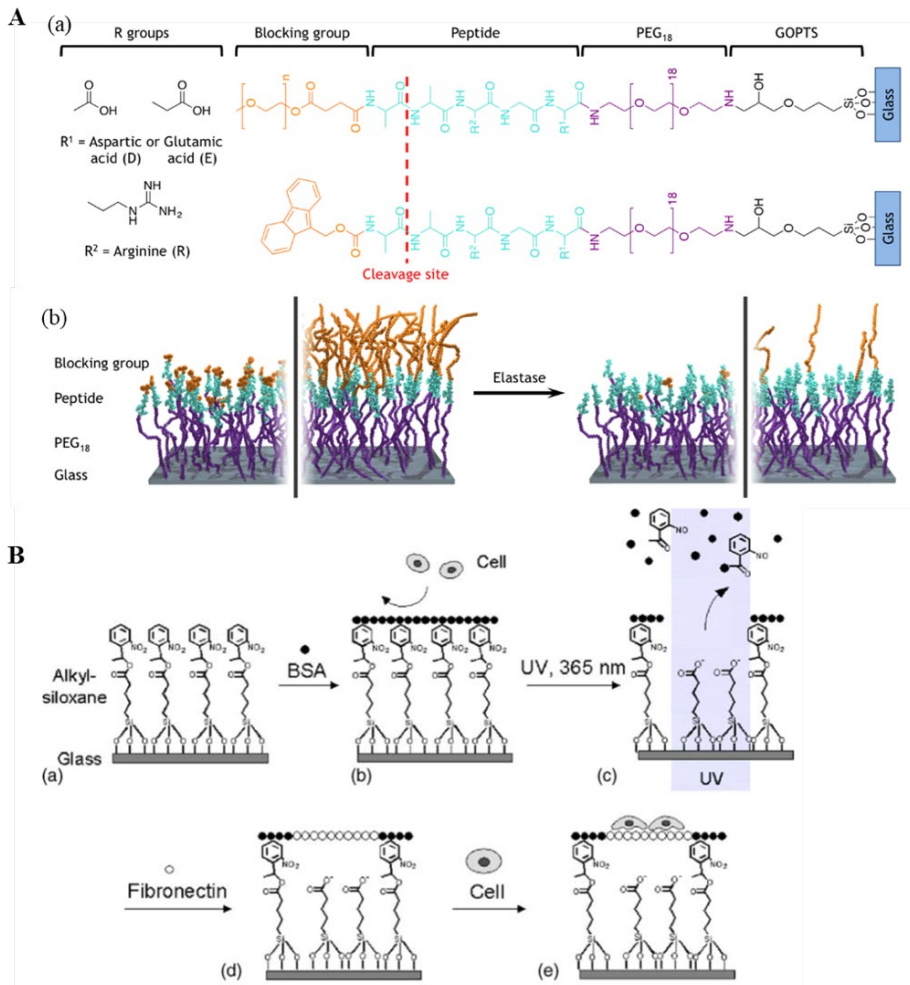


Figure 3. (A) Enzyme-cleavable dynamic surface for MSC growth. (a) Chemical structure of the Fmoc- and PEG-blocked RGD surfaces illustrating the elastase cleavage site. (b) Cartoon illustration of uncleaved “OFF” substrate and enzymatically activated “ON” substrate. Reprinted with permission from ref. 126. (B) The photoactivated substrates used to regulate cell adhesion. (a) Glass modification with a photocleavable 2-nitrobenzyl group. (b) BSA adsorption to substrate to prevent unspecific cell adhesion. (c) UV light illumination at 365 nm used to release the 2-nitrobenzyl group, leading to desorption of BSA from the surface. (d) and (e) Addition of fibronectin used to promote specific cell adhesion. Reprinted with permission from ref. 144.

Similar to the above described enzyme-cleavable system, utility of light-triggered activation of adhesive peptides is another strategy that has been investigated to create “ON-OFF” biointerfaces. Using light as a stimuli has many advantages such as low invasiveness and possibilities for spatiotemporal control. Furthermore, light has a broad wavelength spectrum, ranging from the UV-visible region (200–800 nm) to the near-infrared region (800–2500 nm), making light-responsive systems flexible in their use. However, only light at higher wavelengths (far red to infrared region) can penetrate tissue, making its *in vivo* use more limited [140-142]. There are very few studies focusing on the impact of dynamic ligand presentation in an *in vivo* environment. To this end, Lee and co-workers proposed a platform that enabled temporal control over bioligand presentation using external light triggers to dynamically modulate cell adhesion both *in vitro* and *in vivo* [127]. In their platform, cell-adhesive RGD peptides were modified with a 3-(4,5-dimethoxy-2-nitrophenyl)-2-butyl ester (DMNPB) caging group on its integrin-receptor-binding site. This caging group functionalized as a photolabile group, which could be removed from the surface when exposed to light with a specific wavelength ($\lambda \sim 350\text{--}365$ nm), thus resulting in the presentation of the active bioligand RGD. The non-UV light-exposed caged RGD surface supported very low numbers of adherent NIH3T3 fibroblasts. In contrast, four-fold higher adherent cell densities were observed on the UV-activated surface. High RGD uncaging efficiency by UV light was also confirmed in an *in vivo* study using caged fluorescein as an analog. Following subcutaneous implantation in mice and transdermal UV light exposure, high numbers of cells adhered uniformly to the biomaterial’s surface. Spatial RGD presentation and cell patterning using transdermal illumination could also be achieved. Such transdermal time-regulated presentation of bioligands can be harnessed to direct tissue reparative responses associated with implanted biomaterials.

The aforementioned enzyme-cleavable and photocleavable strategies are generally used for bulk monolayer modulation of ligands, but cannot be used to manipulate ligands at (sub)cellular levels. Dynamic control over cell adhesion at the (sub)cellular level has been achieved by using light and electrochemically responsive systems [143]. In one such example, a photocleavable biointerface was developed to regulate (single) stem cell adhesion [144]. Photocleavable 2-nitrobenzyl groups were assembled over glass via an alkylsiloxane linker, followed by bovine serum albumin (BSA) absorption on the surface to prevent cell adhesion (Fig. 3B). UV illumination could trigger a photocleavage reaction of nitrobenzyl

group, leading to a targeted release of BSA from the surface. After that, adhesive protein fibronectin was added to promote selective cell adhesion to UV exposed spots. By controlling the sizes of the illuminated regions, cell-adhesive spots could be limited to smaller than single cells. Moreover, a photomask was used to create activated cell-adhesive patches in arbitrary designs for cell patterning. The subcellular-sized adhesive patch not only regulated cell adhesion, but also induced cell migration and proliferation.

Alternatively, electrochemically responsive systems provide another effective approach to control single cell adhesion by applying voltage to individually addressable electrodes [143]. Jonkheijm's group recently reported the utilization of electroactive supramolecular biointerfaces to regulate cell adhesion at the single cell level. Electrochemically controlled release of cells was achieved by using a redox-active supramolecular ternary complex consisting of electroactive viologen (organic compounds with the formula $(C_5H_4NR)^{2n+}$) and a tripeptide as guest molecules and host molecule CB[8] [128]. In this study, gold surfaces were functionalized with viologen, which can bind to the CB[8] host molecule to form a ternary complex with a second guest, the RGDS-modified WGG tripeptide. Self-assembly of the RGD-conjugated ternary complexes yielded an adhesive surface for cell attachment by integrin–RGD-mediated interaction. Cells could efficiently attach to and spread on surfaces with the ternary RGD complex. An electrical potential was employed to trigger the dissociation of the RGD ternary complex, thus removing over 90% of cells from the surface and the remaining cells displaying a round morphology. When the strategy was applied to electrode arrays, the developed supramolecular strategy was confirmed to be applicable to trigger cell adhesive response at a single cell level. This supramolecular approach enabled controlled adhesion and release, and provides the possibility to study details of biological processes at the (sub)cellular level.

The above examples of dynamic biointerfaces can be used to temporally control cell adhesion down to single cells, and represents an important tool to understand how ECM remodeling affects (stem) cell adhesion processes.

4.2 Reversible ligand presentation

Although platforms based on on-off ligand presentation are an efficient strategy to study stem cell adhesion processes, their regulation process is irreversible and does not allow repeatable cycles. Reversible ligand presentation on interfaces, therefore, would more closely mimic the native ECM, where ligand presentation is

dynamic and reversible. For instance, tissue repair involves a continual and circular conversion between cell attachment and detachment at the wound site, which is guided by reversible ECM ligand presentation [145]. Recently, sophisticated biointerfaces that enable reversible display of adhesive ligands, and subsequently switchable modulation of cell behaviors, have been researched using catechol-boronate covalent chemistry, host-guest chemistry, magnetic force, light-responsive and potential-responsive materials [125]. For example, a sugar-responsive biointerface based on catechol-boronate interactions was proposed to dynamically manipulate stem cell adhesion behavior [146]. In this study, mussel-inspired peptides ((DOPA)₄-S₅-GRGDS) composed of catechol-containing sequence (DOPA), a spacer and a cell-binding sequence (GRGDS) were designed (Fig. 4A). DOPA can reversibly bind with phenylboronic acid (PBA) polymer-grafted substrates through the dynamic formation of catechol/PBA ester. The bare PBA polymer-based substrate showed excellent cell-repellent properties as a result of the high hydrophilicity of the polymer brushes. The introduction of (DOPA)₄-S₅-GRGDS significantly improved hBMSCs adhesion to the surface, mediated by RGD–integrin interactions. Introduction of a sugar (e.g., glucose or fructose) could induce the release of surface-bound peptides via competitive molecular exchange of the catechol group with PBA, thus triggering the detachment of hBMSCs. Interestingly, the detached cells could readhere by refreshing the (DOPA)₄-S₅-GRGDS peptide-containing medium. Considering that the platform uses a sugar-sensitive stimulus and that the peptide design is flexible, this platform can be used to study the effect of dynamic presentation of various types of ligands under physiological conditions.

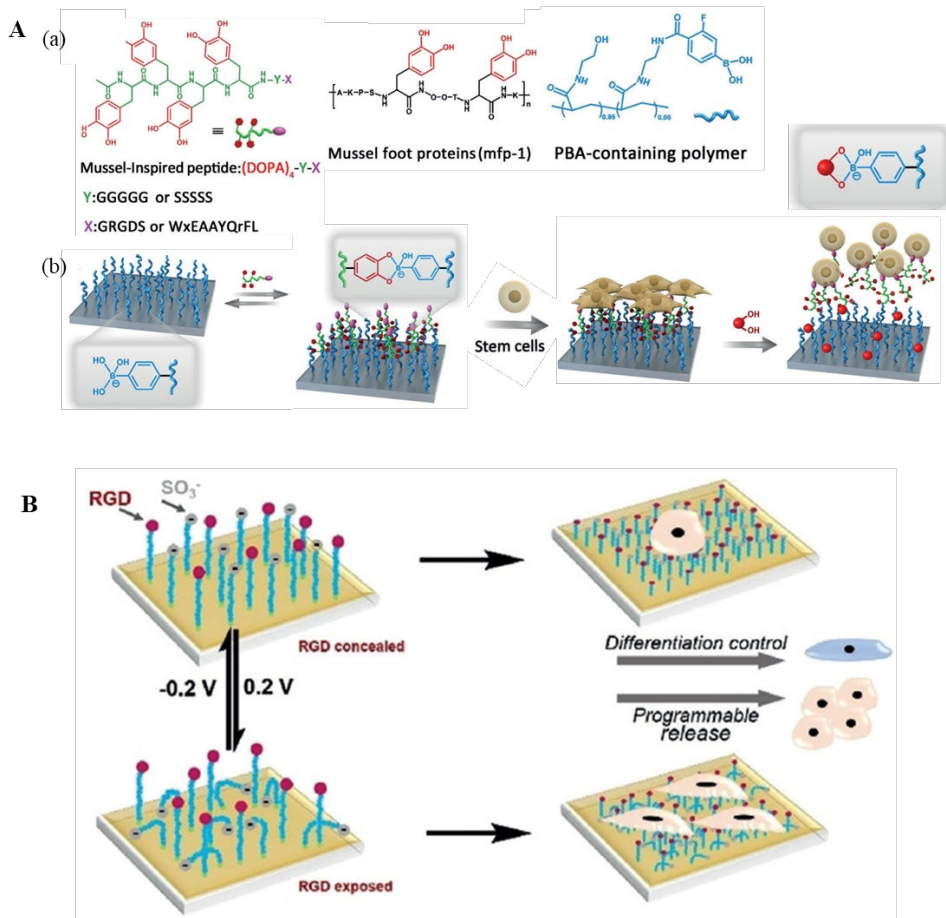


Figure 4. (A) Sugar-responsive dynamic biointerface. (a) The chemical structure of mussel-inspired peptides with catechol groups and bioactive motifs, the natural mussel foot proteins, and the PBA-containing polymers. Reprinted with permission from ref. 146. (b) Schematic representation showing how the sugar-responsive dynamic biointerface can be used to modulate stem cell adhesion behavior. (B) Schematic illustration of the reversible electrochemical surface for the dynamic manipulation of cell behavior. Reprinted with permission from ref. 132.

Magnetic force is another stimulus that has been used to create reversible dynamic interfaces. Magnetic fields have the ability for high tissue penetration without exerting cytotoxicity even in high-intensity applications [147]. As such, magnetic fields can act as an appealing stimuli to allow remote control over ligand

display in *in vivo* applications [148]. So far, several novel magnetically responsive platforms based on nanostructures (e.g. nanoswitches, nanocoils and nanoligands) have been designed to remotely and reversibly control stem cell adhesion and differentiation *in vitro* and *in vivo*. For example, Bian's group developed a magnetic nanoswitch platform to reversibly control RGD presentation [130]. To this end, magnetic nanoparticles (MNP) were coupled to underlying RGD-modified gold nanoparticle (AuNP) via a long flexible linker, to form MNP-(AuNP-RGD) heterodimers on a substrate. The MNP acted as nanocage, which could be magnetically manipulated to reversibly uncage and cage RGD. hMSC cellular adhesion and differentiation as a function of reversible RGD presentation using the magnetic nanoswitch was investigated. After 12 h, hMSCs cultured on magnetically switched "ON" substrates promoted cellular adhesion, enhanced spread area, and increased vinculin expression compared to hMSCs cultured on magnetically switched "OFF" substrates. In addition, magnetic switching from "OFF" to "ON" at 12 h induced stem cell focal adhesion and spreading after 24 h. The reversible magnetic nanoswitch not only regulated cell adhesion, but also influenced stem cell differentiation over a longer culture period, where continuously switching "ON-OFF" drove hMSCs towards osteogenic differentiation. Furthermore, when subcutaneously implanted in nude mice, the heterodimer-grafted substrate was able to regulate cell adhesion *in vivo*, when magnetic switching to the "ON" state significantly promoted the formation of focal adhesions and subsequent stem cell spreading, which was not observed in the "OFF" state. In parallel, Kang's group developed a cell-adhesive RGD ligand-presenting magnetic nanocoil which allowed cyclic and nanoscale stretching ("ON") and shrinking ("OFF") of ligands using magnetic fields to regulate stem cell adhesion [149]. Specifically, helical shaped CoFe nanocoils were functionalized with PEGylated RGD peptides and chemically coupled to aminated material surfaces. Application of a magnetic field to the resulting surfaces containing RGD ligand-bearing nanocoils, could tune ligand nanospacing of the nanocoils without modulating the ligand-presenting surface area per nanocoil, resulting in constant macroscale ligand density during switching between ON and OFF states. The magnetic switching "ON" significantly promoted focal adhesion and integrin $\beta 1$ expression compared to magnetic switching "OFF", suggesting that nanospaced RGD declustering (nanostretching) can activate cell adhesion. In addition, magnetic switching from "OFF-ON-OFF" and "ON-OFF-ON" could initiate intracellular mechanotransduction and osteogenic differentiation in hMSCs in a reversible manner, by stimulating higher nuclear translocation of YAP

mechano-transducers and facilitating expression of RUNX2/ALP (early markers) and osteocalcin (late marker) of hMSCs. Furthermore, this system could also be used to study the mechanosensing-mediated differentiation of stem cells *in vivo*. Following from this work, the same group reported a magnetically responsive biointerface that enabled control over both spatial (macroscale) and temporal RGD presentation [150]. Negatively charged and mobile magnetic nanoligands, containing a superparamagnetic core and PEG-RGD shell, were electrostatically coupled to a positively charged substrate. The macroscale density and nanoscale movement of nanoligands could be tuned by magnetic attraction and facilitated cell adhesion and mechanosensing-mediated differentiation of hMSCs. Furthermore, remote and effective manipulation of hMSCs adhesion via control of nanoligand movement was also demonstrated *in vivo*. These magnetically responsive systems indicate that reversible RGD “ON-OFF” via magnetic force offers an effective approach to regulate and elucidate dynamic cell-ligand interaction both *in vitro* and *in vivo*, which can benefit ultimate clinical utility of dynamic biointerfaces.

Photoswitchable molecules such as azobenzene, stilbenes, and spiropyran also have been researched for the design of reversible functional platforms [151-153]. Photoswitchable molecules are chromophores that are capable of isomerizing by illumination at a specific wavelength between two (or more) species [154]. Previously, a photoisomerizable, azobenzene-based, supramolecular host-guest chemistry has been used to reversibly display adhesive moieties [131]. Specifically, azobenzene can bind with supramolecular hosts such as cucurbit[8]urils and cyclodextrins to form a supramolecular complex. UV irradiation (at 365 nm) can cause photoisomerization of azobenzene, resulting in a conformation change that triggers dissociation of the complex. This process is reversible by using visible light. In this study, dual-responsive surfaces based on β -cyclodextrin (CD)/azobenzene interaction were constructed to regulate the migration of BMSCs by dynamic display of peptides. Azobenzene-grafted MSC-affinitive E7 peptides (Azo-E7) were bound to a β -cyclodextran (β -CD)-modified, antifouling brush polymer-based substrate. Addition of competing guest molecules amantadine hydrochloride (Ama) and/or UV irradiation triggered the release Azo-E7 peptides from the CD surface to different extents, thus weakening cell adhesion. The migration rate of BMSCs exposed to the CD/E7 surface was three times faster than that on the glass control slide. However, subsequent Ama (20 μ mol/L) and UV-irradiation treatment of the CD/E7 surface caused a reduction of BMSC migration rate. This work provides an attractive approach to control stem cell mobility.

In addition to photoresponsive platforms, electrochemically responsive platforms based on a potential-induced conformational transitions of molecules have also been used to manipulate reversible cell adhesion. For example, an approach for electrochemically controlled release of cells based on ferrocene (Fc)/CD and an aptamer-modified, dual-functionalized graphene substrate has been reported [31]. Fc-aptamer AS1411 conjugate bound to the CD-modified graphene surface through Fc/CD host–guest chemistry. Cells attached to this surface through the presence of aptamer AS1411, which has shown high binding affinity to cells. Oxidation of ferrocenyl moieties decreased the binding affinity of Fc to CD, which triggers the release of AS1411, and subsequently the release of cells from the substrates. Regenerated and multi-cycle cell catch-and-release on graphene substrate was realized by reversible manipulation of Fc/CD host–guest interaction. In another example of electrochemically responsive platforms, a mixture of RGD-modified 11-mercaptopundecanoic acid (MUA) and negatively charged, sulfonate moieties–modified MUA was used to modify a gold surface to form an electrode-patterned, self-assembled monolayer (SAM) [132]. When applying a negative voltage, the negatively charged sulfonate moieties were repelled from the gold electrode surface, which concealed RGD. Once a positive potential was applied, the functionalized SAM went through a conformational change, switching the surface from concealing RGD (an adhesion-resistant state) to exposing RGD, thus offering an adhesion-promoting state (Fig. 4B). As a result, this surface allowed for the controlled adhesion and release of stem cells. Higher RGD accessibility under a positive voltage promoted stem cells to adhere and lead to osteogenesis, whereas lower RGD accessibility under a negative voltage caused programmable cell release and adipogenesis.

In summary, dynamic biointerfaces presenting reversible ligand presentation enable dynamic modulation of cell adhesion by applying targeted stimuli. In addition, reversible stem cell adhesion influenced stem cell morphology, which ultimately can guide stem cell differentiation. As such, these systems are important tools to understand the importance of reversible dynamic ligand presentation in guiding stem cell processes.

4.3 Ligand mobility

Another way to create dynamic biointerfaces is by looking at ligand mobility, which refers to a ligand's movement relative to a surface, similar to the bilateral movement of ligands and receptors on cellular membranes. Thus far, various

strategies have been explored to dynamically tune ligand mobility to investigate its effect on stem cell behavior, especially in relation to cell migration and adhesion dynamics. For instance, Sheetz's group reported the use of SLB to tune RGD lateral mobility [155]. It was observed that mobile RGD surfaces resulted in clathrin-mediated endocytosis of integrin- β 3 clusters and adhesion turnover, showing co-localization of adaptor protein Dab2 and activated integrin- β 3 clusters in HeLa cells. These results indicated the critical role of ligand mobility in regulating cell migration and adhesion dynamics. However, this work was done in an immortalized cancer cell line, and very little is currently known about the role of ligand mobility in regulating stem cell behavior.

In work done by Wong et al., dynamic control over RGD tether mobility could be achieved using a magnetic force and its effect on hMSCs was studied. To achieve this, a monolayer of RGD-grafted MNPs were attached to a glass substrate via flexible PEG linkers, which gave the RGD a high degree of mobility. PEG-RGD mobility could be significantly restricted by applying a downward magnetic attraction to the MNPs (Fig. 5). It was reported that the RGD ligand mobility had a vital role in regulating adhesion and cellular mechanosensing of hMSCs: those cultured on substrates exposed to a magnetic field that restricted RGD tether mobility showed improved adhesion, subsequent spreading, and osteogenic differentiation at a later stage, compared to hMSCs cultured on substrates with high RGD tether mobility [133]. This was attributed to restricted RGD tether mobility facilitating cellular traction force development and mechanical feedback, thereby contributing to a faster and enhanced activation of downstream mechanotransduction signaling involving the Yes-associated protein (YAP) transcriptional regulator. This novel magnetic responsive-based approach is an excellent tool enabling remote and noncontact modulation over ligand mobility.

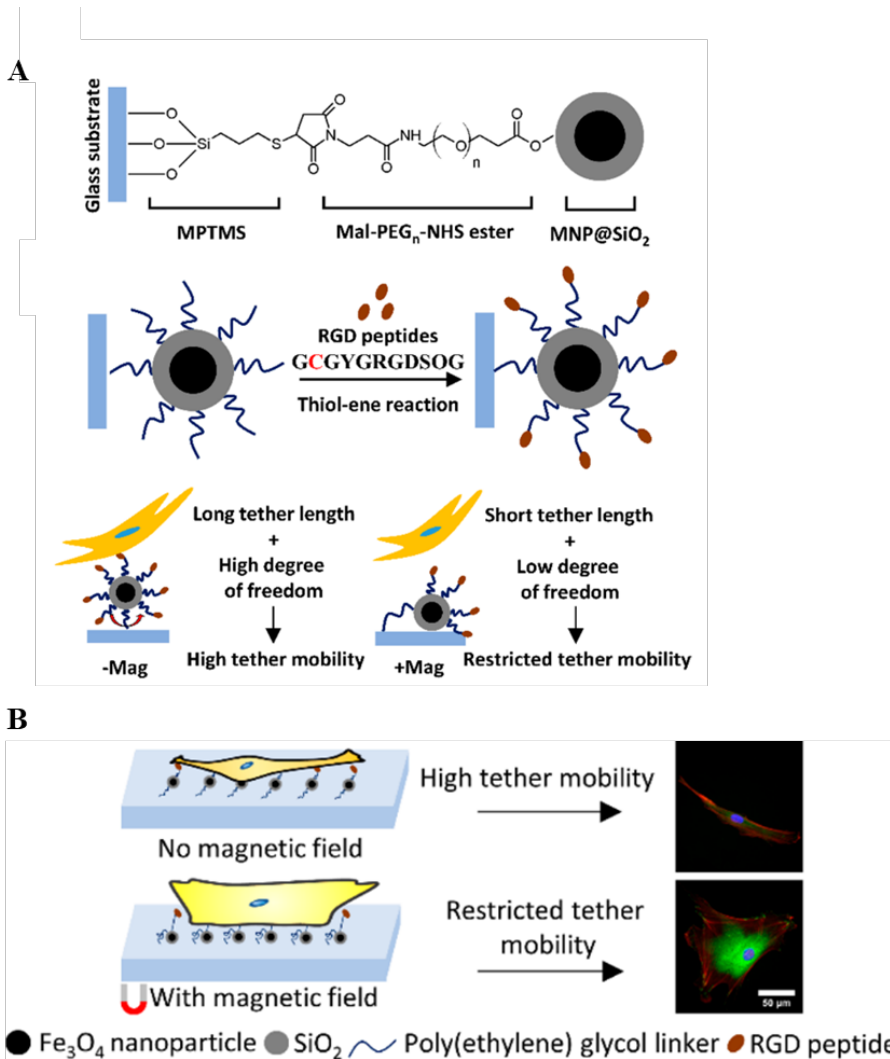


Figure 5. (A) Schematic showing a monolayer of RGD-bearing MNP substrate attached to a glass surface using a PEG linker (top panel), grafting of RGD peptides onto MNPs via thiol-ene reaction (middle panel), and the proposed tunable integrin ligand tether mobility for cell studies (bottom panel). (B) Schematic showing the effect of dynamic ligand mobility on cell morphology. Reprinted with permission from ref. 133.

In a similar study reported by the same research group, a dynamic biointerface that permits ligand mobility regulation of adhesive ligand presentation using oscillating

magnetic fields was developed [134]. Specifically, RGD peptide–modified superparamagnetic iron oxide nanoparticles (SPION) were anchored to a glass substrate via a long flexible PEG linker (Mn = 5000 Da), which allowed controllable motion of the RGD ligand. The temporal regulation of multimodal RGD ligand motion at the nanoscale could be achieved by applying magnetic field with different oscillation frequency. “Slow” ligand motion speeds under a low magnetic oscillation frequency (0.1 Hz) significantly promoted integrin binding with RGD, hMSC adhesion and osteogenic differentiation, whereas “fast” ligand oscillation under a high magnetic oscillation frequency (2 Hz) inhibited integrin ligation and cellular adhesion. Interestingly, temporal switching of the ligand oscillation between “slow” and “fast” enabled reversible modulation of cell adhesion and spreading. This study presented an appealing approach to mimic dynamic integrin–ligand binding by tuning nanoscale ligand motion.

Taken together, these approaches to tune ligand mobility and subsequent integrin-ligand binding demonstrate a critical role in dynamic ligand presentation to steer adhesion and differentiation of stem cells.

5. Outlook and Conclusions

The development of instructive synthetic biointerfaces has helped researchers working in the field of biomedical sciences and regenerative medicine understand the importance of ligand density, mobility, and dynamicity in determining (stem) cell behavior. In particular in the field of regenerative medicine, knowledge on how stem cells respond to specific cues could help researchers rationally design bioactive materials. We reviewed biointerfaces presenting ligands in a highly defined and static manner and how such platforms are useful tools to study how individual interfacial properties (ligand affinity, density, and patterning) modulate stem cell behaviors, and aid our fundamental understanding about cell–material interactions. However, one limitation of static biointerfaces is the lack of dynamicity. The highly dynamic nature of the native extracellular environment plays an important role in the maintenance and regeneration of tissues. As such, there has been a growing interest in the design of smart biointerfaces with dynamic complexity. With progressive advances in chemistry, materials synthesis and modifications, biointerfaces with the ability to manipulate dynamically ligand presentation, including on-off and reversible features, have been prepared. These platforms have shown dynamic ligand presentation and ligand mobility have a crucial role in controlling stem cell adhesion and directing stem cell differentiation

and migration, findings that are undoubtedly of great importance for various biomedical applications.

Despite these tremendous advancements in the development of biointerfaces, especially considering that this is still a young field of research, various challenges need to be addressed to create ever more complex ECM-biomimicking interfaces. For one, more complex biological characterizations need to be performed in order to understand how dynamic adhesion processes influence other cell behaviors such as stem cell differentiation; currently, most studies have been limited to investigating cell adhesion processes only. In addition, other stem cell types should be included in these studies, as most studies have been limited to hBMSCs. Also other ligands that promote cell adhesion, their functionality, bioactivity, and specificity should be explored. Most dynamic systems use RGD, which has many advantages such as commercially available at low costs, low immunogenicity, easy synthesis and modification. However, RGD binds to a wide range of integrin species [156], making it nonspecific. This makes RGD less interesting for tissue engineering approaches where specific interactions are needed. Several studies have already shown that more specific integrin binding ligands influence lineage progression of hBMSCs [83]. Moreover, RGD also shows inferior integrin-binding affinity compared to native ECM proteins in complex *in vivo* environments, making the translation to clinical applications difficult [68].

Another challenge to consider is designing biointerfaces that can mimic the multi-responsive and stimuli-adaptive nature of the native ECM [157]. In several static platform the importance of ligand crosstalk was already demonstrated [99]. Current dynamic biointerfaces are limited in their capacity to present multiple ligands reversibly or respond to multiple stimuli in one system. Also the timescales need to be considered for future studies; most of the developed dynamic biointerfaces can effectively change surface adhesiveness on demand by changing the amount of RGD adhesive sites that are available to the cells, but another way to control the surface adhesiveness can be achieved by regulating temporal kinetics of RGD presentation over the surface. Such platforms give information on stem cell adhesion kinetics at biologically relevant timescales. Finally, future work could also look into translation of these 2D systems to 3D dynamic environments, which could endow these biomaterials with properties closer to a natural ECM. Interestingly, the recognition of the importance of ECM dynamicity for regenerative approaches has resulted in an extremely rapid interest in the field of dynamic

hydrogels, while incorporating dynamic control over ligand presentation in 3D are not so widely implemented [158-160]. Creation of 3D model systems to study cell–interface interactions could also speed up the translation from lab research to clinical applications.

Some of the properties that have been investigated in the static interfaces would also be interesting to investigate using dynamic systems such as the role of dynamic ligand spacing on stem cells' function. One study investigating the role of reversible integrin clustering on cell behavior showed the effect of integrin receptor clustering on filopodia protrusion development of cells. In this study, a multivalent DNA “nano-spring” was used to construct a structure-stretchable nanomachine to reversibly control integrin clustering by regulating dynamic spacing arrangement of bioligands [161].

To conclude, this review discussed recent developments in the development of cell-instructive biointerfaces to study stem cell processes and stem cell–ligand interactions. These studies have highlighted the importance of ligand type, density, spacing, crosstalk and dynamicity. These findings can be used to improve the design criteria of tissue engineering constructs to improve material-cell interactions, and promote specific stem cell behavior. Better designed materials will undoubtedly lead to better tissue repair outcomes. Although many challenges still exist in this field, we strongly believe that with sustained efforts and cooperation from chemists, biologists, and materials scientists, more complex platforms with highly programmable and controllable properties will be developed that can be used to obtain important knowledge on biochemical cue presentation and stem cell regenerative processes.

Conflicts of interest

There are no conflicts to declare.

Acknowledgments

The authors acknowledge China Scholarship Council (grant number 201806220082) for financial support.

References

- [1] C. Blanpain, E. Fuchs, Stem cell plasticity. Plasticity of epithelial stem cells in tissue regeneration, *Science* 344(6189) (2014) 1242281.
- [2] M. Ahmed, C. Ffrench-Constant, Extracellular Matrix Regulation of Stem Cell Behavior, *Curr Stem Cell Rep* 2(3) (2016) 197-206.
- [3] D. Jhala, R. Vasita, A Review on Extracellular Matrix Mimicking Strategies for an Artificial Stem Cell Niche, *Polym. Rev.* 55(4) (2015) 561-595.
- [4] Y. Zhang, D. Wu, X. Zhao, M. Pakvasa, A.B. Tucker, H. Luo, K.H. Qin, D.A. Hu, E.J. Wang, A.J. Li, M. Zhang, Y. Mao, M. Sabharwal, F. He, C. Niu, H. Wang, L. Huang, D. Shi, Q. Liu, N. Ni, K. Fu, C. Chen, W. Wagstaff, R.R. Reid, A. Athviraham, S. Ho, M.J. Lee, K. Hynes, J. Strelzow, T.C. He, M. El Dafrawy, Stem Cell-Friendly Scaffold Biomaterials: Applications for Bone Tissue Engineering and Regenerative Medicine, *Front Bioeng Biotechnol* 8 (2020) 598607.
- [5] R. Sinha, M. Cámara-Torres, P. Scopece, E. Verga Falzacappa, A. Patelli, L. Moroni, C. Mota, A hybrid additive manufacturing platform to create bulk and surface composition gradients on scaffolds for tissue regeneration, *Nature Communications* 12(1) (2021) 500.
- [6] S. Camarero-Espinosa, C. Tomasina, A. Calore, L. Moroni, Additive manufactured, highly resilient, elastic, and biodegradable poly(ester)urethane scaffolds with chondroinductive properties for cartilage tissue engineering, *Materials Today Bio* 6 (2020) 100051.
- [7] M. Navarro, A. Michiardi, O. Castaño, J.A. Planell, Biomaterials in orthopaedics, *Journal of the Royal Society, Interface* 5(27) (2008) 1137-58.
- [8] C.L. Salgado, B.I.B. Teixeira, F.J.M. Monteiro, Biomimetic Composite Scaffold With Phosphoserine Signaling for Bone Tissue Engineering Application, *Front. Bioeng. Biotechnol.* 7 (2019) 16.
- [9] B. Derkus, B.O. Okesola, D.W. Barrett, M. D'Este, T.T. Chowdhury, D. Eglin, A. Mata, Multicomponent hydrogels for the formation of vascularized bone-like constructs in vitro, *Acta Biomaterialia* 109 (2020) 82-94.
- [10] G.S. Hussey, J.L. Dziki, S.F. Badylak, Extracellular matrix-based materials for regenerative medicine, *Nature Reviews Materials* 3(7) (2018) 159-173.
- [11] Y.H. Tsou, J. Khoneisser, P.C. Huang, X. Xu, Hydrogel as a bioactive material to regulate stem cell fate, *Bioact Mater* 1(1) (2016) 39-55.
- [12] T. Führmann, R.Y. Tam, B. Ballarin, B. Coles, I. Elliott Donaghue, D. van der Kooy, A. Nagy, C.H. Tator, C.M. Morshead, M.S. Shoichet, Injectable hydrogel promotes early survival of induced pluripotent stem cell-derived oligodendrocytes and attenuates longterm teratoma formation in a spinal cord injury model, *Biomaterials* 83 (2016) 23-36.

- [13] E. Mauri, A. Sacchetti, N. Vicario, L. Peruzzotti-Jametti, F. Rossi, S. Pluchino, Evaluation of RGD functionalization in hybrid hydrogels as 3D neural stem cell culture systems, *Biomater Sci* 6(3) (2018) 501-510.
- [14] L.B. Gallagher, E.B. Dolan, J. O'Sullivan, R. Levey, B.L. Cavanagh, L. Kovarova, M. Pravda, V. Velebny, T. Farrell, F.J. O'Brien, G.P. Duffy, Pre-culture of mesenchymal stem cells within RGD-modified hyaluronic acid hydrogel improves their resilience to ischaemic conditions, *Acta Biomater* 107 (2020) 78-90.
- [15] M.D. Pierschbacher, E. Ruoslahti, Cell attachment activity of fibronectin can be duplicated by small synthetic fragments of the molecule, *Nature* 309(5963) (1984) 30-33.
- [16] F. Gattazzo, A. Urciuolo, P. Bonaldo, Extracellular matrix: a dynamic microenvironment for stem cell niche, *Biochim Biophys Acta* 1840(8) (2014) 2506-19.
- [17] G. Maheshwari, G. Brown, D.A. Lauffenburger, A. Wells, L.G. Griffith, Cell adhesion and motility depend on nanoscale RGD clustering, *Journal of Cell Science* 113(10) (2000) 1677.
- [18] J. Li, Y. Chen, N. Kawazoe, G. Chen, Ligand density-dependent influence of arginine-glycine-aspartate functionalized gold nanoparticles on osteogenic and adipogenic differentiation of mesenchymal stem cells, *Nano Research* 11(3) (2018) 1247-1261.
- [19] F. Karimi, A.J. O'Connor, G.G. Qiao, D.E. Heath, Integrin Clustering Matters: A Review of Biomaterials Functionalized with Multivalent Integrin-Binding Ligands to Improve Cell Adhesion, Migration, Differentiation, Angiogenesis, and Biomedical Device Integration, *Adv Healthc Mater* 7(12) (2018) e1701324.
- [20] K.M. Ferlin, M.E. Prendergast, M.L. Miller, B.N. Nguyen, D.S. Kaplan, J.P. Fisher, Development of a dynamic stem cell culture platform for mesenchymal stem cell adhesion and evaluation, *Mol Pharm* 11(7) (2014) 2172-81.
- [21] C.M. Madl, B.L. LeSavage, R.E. Dewi, K.J. Lampe, S.C. Heilshorn, Matrix Remodeling Enhances the Differentiation Capacity of Neural Progenitor Cells in 3D Hydrogels, *Advanced Science* 6(4) (2019) 1801716.
- [22] M.J. Kratochvil, A.J. Seymour, T.L. Li, S.P. Pasca, C.J. Kuo, S.C. Heilshorn, Engineered materials for organoid systems, *Nat Rev Mater* 4(9) (2019) 606-622.
- [23] M.G. Haugh, T.J. Vaughan, C.M. Madl, R.M. Raftery, L.M. McNamara, F.J. O'Brien, S.C. Heilshorn, Investigating the interplay between substrate stiffness and ligand chemistry in directing mesenchymal stem cell differentiation within 3D macro-porous substrates, *Biomaterials* 171 (2018) 23-33.
- [24] M.G. Haugh, S.C. Heilshorn, Integrating Concepts of Material Mechanics, Ligand Chemistry, Dimensionality and Degradation to Control Differentiation of Mesenchymal Stem Cells, *Curr Opin Solid State Mater Sci* 20(4) (2016) 171-179.

- [25] N.J. Walters, E. Gentleman, Evolving insights in cell-matrix interactions: elucidating how non-soluble properties of the extracellular niche direct stem cell fate, *Acta Biomater* 11 (2015) 3-16.
- [26] P. Bugga, M. Mrksich, Dynamic Substrates for Cell Biology, *Curr Opin Colloid Interface Sci* 38 (2018) 80-87.
- [27] G. Abagnale, M. Steger, V.H. Nguyen, N. Hersch, A. Sechi, S. Joussem, B. Denecke, R. Merkel, B. Hoffmann, A. Dreser, U. Schnakenberg, A. Gillner, W. Wagner, Surface topography enhances differentiation of mesenchymal stem cells towards osteogenic and adipogenic lineages, *Biomaterials* 61 (2015) 316-326.
- [28] G. Abagnale, A. Sechi, M. Steger, Q. Zhou, C.-C. Kuo, G. Aydin, C. Schalla, G. Müller-Newen, M. Zenke, I.G. Costa, P. van Rijn, A. Gillner, W. Wagner, Surface Topography Guides Morphology and Spatial Patterning of Induced Pluripotent Stem Cell Colonies, *Stem Cell Reports* 9(2) (2017) 654-666.
- [29] K.H. Vining, D.J. Mooney, Mechanical forces direct stem cell behaviour in development and regeneration, *Nat Rev Mol Cell Biol* 18(12) (2017) 728-742.
- [30] F. Xing, L. Li, C. Zhou, C. Long, L. Wu, H. Lei, Q. Kong, Y. Fan, Z. Xiang, X. Zhang, Regulation and Directing Stem Cell Fate by Tissue Engineering Functional Microenvironments: Scaffold Physical and Chemical Cues, *Stem Cells Int* 2019 (2019) 2180925.
- [31] L. Feng, W. Li, J. Ren, X. Qu, Electrochemically and DNA-triggered cell release from ferrocene/beta-cyclodextrin and aptamer modified dual-functionalized graphene substrate, *Nano Research* 8(3) (2015) 887-899.
- [32] T. Heydari, M. Heidari, O. Mashinchian, M. Wojcik, K. Xu, M.J. Dalby, M. Mahmoudi, M.R. Ejtehadi, Development of a Virtual Cell Model to Predict Cell Response to Substrate Topography, *Acs Nano* 11(9) (2017) 9084-9092.
- [33] J. Brinkmann, E. Cavatorta, S. Sankaran, B. Schmidt, J. van Weerd, P. Jonkheijm, About supramolecular systems for dynamically probing cells, *Chem Soc Rev* 43(13) (2014) 4449-69.
- [34] V.K. Singh, A. Saini, M. Kalsan, N. Kumar, R. Chandra, Describing the Stem Cell Potency: The Various Methods of Functional Assessment and In silico Diagnostics, *Front Cell Dev Biol* 4 (2016) 134.
- [35] C.M. Madl, S.C. Heilshorn, Engineering Hydrogel Microenvironments to Recapitulate the Stem Cell Niche, *Annu Rev Biomed Eng* 20 (2018) 21-47.
- [36] J.A. Thomson, J. Itskovitz-Eldor, S.S. Shapiro, M.A. Waknitz, J.J. Swiergiel, V.S. Marshall, J.M. Jones, Embryonic stem cell lines derived from human blastocysts, *Science* 282(5391) (1998) 1145-7.
- [37] K. Koga, B. Wang, S. Kaneko, Current status and future perspectives of HLA-edited induced pluripotent stem cells, *Inflamm Regen* 40 (2020) 23.
- [38] M. Wei, S. Li, W. Le, Nanomaterials modulate stem cell differentiation: biological interaction and underlying mechanisms, *J Nanobiotechnology* 15(1) (2017) 75.

- [39] G. Liu, B.T. David, M. Trawczynski, R.G. Fessler, Advances in Pluripotent Stem Cells: History, Mechanisms, Technologies, and Applications, *Stem Cell Rev Rep* 16(1) (2020) 3-32.
- [40] Z.P. Zhang, J.T. Zhang, S.C. Huang, X.Y. He, L.X. Deng, Double sperm cloning (DSC) is a promising strategy in mammalian genetic engineering and stem cell research, *Stem Cell Res Ther* 11(1) (2020) 388.
- [41] R. Zahumenska, V. Nosal, M. Smolar, T. Okajcekova, H. Skovierova, J. Strnadel, E. Halasova, Induced Pluripotency: A Powerful Tool for In Vitro Modeling, *Int J Mol Sci* 21(23) (2020).
- [42] Y. Qiao, O.S. Agboola, X. Hu, Y. Wu, L. Lei, Tumorigenic and Immunogenic Properties of Induced Pluripotent Stem Cells: a Promising Cancer Vaccine, *Stem Cell Rev Rep* 16(6) (2020) 1049-1061.
- [43] A.S. Lee, C. Tang, M.S. Rao, I.L. Weissman, J.C. Wu, Tumorigenicity as a clinical hurdle for pluripotent stem cell therapies, *Nat Med* 19(8) (2013) 998-1004.
- [44] M. Stadtfeld, M. Nagaya, J. Utikal, G. Weir, K. Hochedlinger, Induced pluripotent stem cells generated without viral integration, *Science* 322(5903) (2008) 945-9.
- [45] W. Zakrzewski, M. Dobrzyński, M. Szymonowicz, Z. Rybak, Stem cells: past, present, and future, *Stem Cell Research & Therapy* 10(1) (2019) 68.
- [46] J.S. Ryu, E.J. Jeong, J.Y. Kim, S.J. Park, W.S. Ju, C.H. Kim, J.S. Kim, Y.K. Choo, Application of Mesenchymal Stem Cells in Inflammatory and Fibrotic Diseases, *Int J Mol Sci* 21(21) (2020).
- [47] N. Guimarães-Camboa, P. Cattaneo, Y. Sun, T. Moore-Morris, Y. Gu, N.D. Dalton, E. Rockenstein, E. Masliah, K.L. Peterson, W.B. Stallcup, J. Chen, S.M. Evans, Pericytes of Multiple Organs Do Not Behave as Mesenchymal Stem Cells In Vivo, *Cell Stem Cell* 20(3) (2017) 345-359.e5.
- [48] A.I. Caplan, Mesenchymal Stem Cells: Time to Change the Name!, *Stem cells translational medicine* 6(6) (2017) 1445-1451.
- [49] W. Jiang, J. Xu, Immune modulation by mesenchymal stem cells, *Cell Prolif* 53(1) (2020) e12712.
- [50] M.F. Pittenger, D.E. Discher, B.M. Péault, D.G. Phinney, J.M. Hare, A.I. Caplan, Mesenchymal stem cell perspective: cell biology to clinical progress, *NPJ Regen Med* 4 (2019) 22.
- [51] D.E. Rodríguez-Fuentes, L.E. Fernández-Garza, J.A. Samia-Meza, S.A. Barrera-Barrera, A.I. Caplan, H.A. Barrera-Saldaña, Mesenchymal Stem Cells Current Clinical Applications: A Systematic Review, *Archives of Medical Research* 52(1) (2021) 93-101.
- [52] R.M. Samsonraj, M. Raghunath, V. Nurcombe, J.H. Hui, A.J. van Wijnen, S.M. Cool, Concise Review: Multifaceted Characterization of Human Mesenchymal Stem Cells for Use in Regenerative Medicine, *Stem Cells Transl Med* 6(12) (2017) 2173-2185.

- [53] A.Y. Clark, K.E. Martin, J.R. Garcia, C.T. Johnson, H.S. Theriault, W.M. Han, D.W. Zhou, E.A. Botchwey, A.J. Garcia, Integrin-specific hydrogels modulate transplanted human bone marrow-derived mesenchymal stem cell survival, engraftment, and reparative activities, *Nature Communications* 11(1) (2020).
- [54] H. Donnelly, M. Salmeron-Sanchez, M.J. Dalby, Designing stem cell niches for differentiation and self-renewal, *Journal of the Royal Society, Interface* 15(145) (2018).
- [55] J.K. Viridi, P. Pethe, Biomaterials Regulate Mechanosensors YAP/TAZ in Stem Cell Growth and Differentiation, *Tissue Eng Regen Med* (2020).
- [56] Y. Xing, S. Naik, Under pressure: Stem cell-niche interactions coordinate tissue adaptation to inflammation, *Curr Opin Cell Biol* 67 (2020) 64-70.
- [57] S. Chen, M. Lewallen, T. Xie, Adhesion in the stem cell niche: biological roles and regulation, *Development* 140(2) (2013) 255-65.
- [58] G. Kocer, P. Jonkheijm, About Chemical Strategies to Fabricate Cell-Instructive Biointerfaces with Static and Dynamic Complexity, *Adv Healthc Mater* 7(14) (2018) e1701192.
- [59] E. Pinney, M. Zimber, A. Schenone, M. Montes-Camacho, F. Ziegler, G.K. Naughton, Human Embryonic-like ECM (hECM) Stimulates Proliferation and Differentiation in Stem Cells While Killing Cancer Cells, *Int J Stem Cells* 4(1) (2011) 70-5.
- [60] J.K. Mouw, G. Ou, V.M. Weaver, Extracellular matrix assembly: a multiscale deconstruction, *Nat Rev Mol Cell Biol* 15(12) (2014) 771-85.
- [61] W. Li, Z. Yan, J. Ren, X. Qu, Manipulating cell fate: dynamic control of cell behaviors on functional platforms, *Chem Soc Rev* 47(23) (2018) 8639-8684.
- [62] C. Bonnans, J. Chou, Z. Werb, Remodelling the extracellular matrix in development and disease, *Nat Rev Mol Cell Biol* 15(12) (2014) 786-801.
- [63] S.W. Lane, D.A. Williams, F.M. Watt, Modulating the stem cell niche for tissue regeneration, *Nat Biotechnol* 32(8) (2014) 795-803.
- [64] C. Cimmino, L. Rossano, P.A. Netti, M. Ventre, Spatio-Temporal Control of Cell Adhesion: Toward Programmable Platforms to Manipulate Cell Functions and Fate, *Front Bioeng Biotechnol* 6 (2018) 190.
- [65] M. d'Angelo, E. Benedetti, M.G. Tupone, M. Catanesi, V. Castelli, A. Antonosante, A. Cimini, The Role of Stiffness in Cell Reprogramming: A Potential Role for Biomaterials in Inducing Tissue Regeneration, *Cells* 8(9) (2019) 25.
- [66] F.M. Watt, W.T. Huck, Role of the extracellular matrix in regulating stem cell fate, *Nat Rev Mol Cell Biol* 14(8) (2013) 467-73.
- [67] M.F. Brizzi, G. Tarone, P. Defilippi, Extracellular matrix, integrins, and growth factors as tailors of the stem cell niche, *Curr Opin Cell Biol* 24(5) (2012) 645-51.
- [68] S.L. Bellis, Advantages of RGD peptides for directing cell association with biomaterials, *Biomaterials* 32(18) (2011) 4205-10.

- [69] U. Hersel, C. Dahmen, H. Kessler, RGD modified polymers: biomaterials for stimulated cell adhesion and beyond, *Biomaterials* 24(24) (2003) 4385-415.
- [70] A.S. Rowlands, P.A. George, J.J. Cooper-White, Directing osteogenic and myogenic differentiation of MSCs: interplay of stiffness and adhesive ligand presentation, *Am J Physiol Cell Physiol* 295(4) (2008) C1037-44.
- [71] M.B. Rahmany, M. Van Dyke, Biomimetic approaches to modulate cellular adhesion in biomaterials: A review, *Acta Biomater* 9(3) (2013) 5431-7.
- [72] M. Nieberler, U. Reuning, F. Reichart, J. Notni, H.J. Wester, M. Schwaiger, M. Weinmüller, A. Räder, K. Steiger, H. Kessler, Exploring the Role of RGD-Recognizing Integrins in Cancer, *Cancers (Basel)* 9(9) (2017).
- [73] B. Geiger, K.M. Yamada, Molecular architecture and function of matrix adhesions, *Cold Spring Harb Perspect Biol* 3(5) (2011).
- [74] A. Tomar, D.D. Schlaepfer, Focal adhesion kinase: switching between GAPs and GEFs in the regulation of cell motility, *Curr Opin Cell Biol* 21(5) (2009) 676-83.
- [75] B. Geiger, J.P. Spatz, A.D. Bershadsky, Environmental sensing through focal adhesions, *Nat Rev Mol Cell Biol* 10(1) (2009) 21-33.
- [76] C. De Pascalis, S. Etienne-Manneville, Single and collective cell migration: the mechanics of adhesions, *Mol Biol Cell* 28(14) (2017) 1833-1846.
- [77] S.P. Palecek, J.C. Loftus, M.H. Ginsberg, D.A. Lauffenburger, A.F. Horwitz, Integrin-ligand binding properties govern cell migration speed through cell-substratum adhesiveness, *Nature* 385(6616) (1997) 537-40.
- [78] B. Trappmann, J.E. Gautrot, J.T. Connelly, D.G.T. Strange, Y. Li, M.L. Oyen, M.A. Cohen Stuart, H. Boehm, B. Li, V. Vogel, J.P. Spatz, F.M. Watt, W.T.S. Huck, Extracellular-matrix tethering regulates stem-cell fate, *Nat. Mater.* 11(7) (2012) 642-649.
- [79] R. McBeath, D.M. Pirone, C.M. Nelson, K. Bhadriraju, C.S. Chen, Cell shape, cytoskeletal tension, and RhoA regulate stem cell lineage commitment, *Dev Cell* 6(4) (2004) 483-95.
- [80] H. Zhang, X. Zheng, W. Ahmed, Y. Yao, J. Bai, Y. Chen, C. Gao, Design and Applications of Cell-Selective Surfaces and Interfaces, *Biomacromolecules* 19(6) (2018) 1746-1763.
- [81] N. Huettner, T.R. Dargaville, A. Forget, Discovering Cell-Adhesion Peptides in Tissue Engineering: Beyond RGD, *Trends Biotechnol* 36(4) (2018) 372-383.
- [82] X. Lin, K. Takahashi, Y. Liu, P.O. Zamora, Enhancement of cell attachment and tissue integration by a IKVAV containing multi-domain peptide, *Biochim Biophys Acta* 1760(9) (2006) 1403-10.
- [83] J.E. Frith, R.J. Mills, J.E. Hudson, J.J. Cooper-White, Tailored integrin-extracellular matrix interactions to direct human mesenchymal stem cell differentiation, *Stem Cells Dev* 21(13) (2012) 2442-56.

- [84] K.A. Kilian, M. Mrksich, Directing stem cell fate by controlling the affinity and density of ligand-receptor interactions at the biomaterials interface, *Angew Chem Int Ed Engl* 51(20) (2012) 4891-5.
- [85] I. Bilem, L. Plawinski, P. Chevallier, C. Ayela, E.D. Sone, G. Laroche, M.C. Durrieu, The spatial patterning of RGD and BMP-2 mimetic peptides at the subcellular scale modulates human mesenchymal stem cells osteogenesis, *J Biomed Mater Res A* 106(4) (2018) 959-970.
- [86] B.T. Houseman, M. Mrksich, The microenvironment of immobilized Arg-Gly-Asp peptides is an important determinant of cell adhesion, *Biomaterials* 22(9) (2001) 943-55.
- [87] G. Kocer, P. Jonkheijm, Guiding hMSC Adhesion and Differentiation on Supported Lipid Bilayers, *Adv Healthc Mater* 6(3) (2017).
- [88] A. Lagunas, I. Tsintzou, Y. Vida, D. Collado, E. Pérez-Inestrosa, C. Rodríguez Pereira, J. Magalhaes, J.A. Andrades, J. Samitier, Tailoring RGD local surface density at the nanoscale toward adult stem cell chondrogenic commitment, *Nano Research* 10(6) (2016) 1959-1971.
- [89] P.L. Benitez, S. Mascharak, A.C. Proctor, S.C. Heilshorn, Use of protein-engineered fabrics to identify design rules for integrin ligand clustering in biomaterials, *Integr Biol (Camb)* 8(1) (2016) 50-61.
- [90] S. Min, Y.S. Jeon, H.J. Jung, C. Khatua, N. Li, G. Bae, H. Choi, H. Hong, J.E. Shin, M.J. Ko, H.S. Ko, I. Jun, H.E. Fu, S.H. Kim, R. Thangam, J.J. Song, V.P. Dravid, Y.K. Kim, H. Kang, Independent Tuning of Nano-Ligand Frequency and Sequences Regulates the Adhesion and Differentiation of Stem Cells, *Adv Mater* 32(40) (2020) e2004300.
- [91] L.R. Anderson, T.W. Owens, M.J. Naylor, Structural and mechanical functions of integrins, *Biophys Rev* 6(2) (2014) 203-213.
- [92] M.A. Rubtsov, M.S. Syrkina, G. Aliev, RGD-based Therapy: Principles of Selectivity, *Curr Pharm Des* 22(7) (2016) 932-52.
- [93] E. Koivunen, B. Wang, E. Ruoslahti, Isolation of a highly specific ligand for the alpha 5 beta 1 integrin from a phage display library, *J Cell Biol* 124(3) (1994) 373-80.
- [94] Y. Kikkawa, K. Hozumi, F. Katagiri, M. Nomizu, H.K. Kleinman, J.E. Koblinski, Laminin-111-derived peptides and cancer, *Cell Adh Migr* 7(1) (2013) 150-256.
- [95] H. Li, J. Frith, J.J. Cooper-White, Modulation of stem cell adhesion and morphology via facile control over surface presentation of cell adhesion molecules, *Biomacromolecules* 15(1) (2014) 43-52.
- [96] M. Mehta, C.M. Madl, S. Lee, G.N. Duda, D.J. Mooney, The collagen I mimetic peptide DGEA enhances an osteogenic phenotype in mesenchymal stem cells when presented from cell-encapsulating hydrogels, *J Biomed Mater Res A* 103(11) (2015) 3516-25.

- [97] R.A. Marklein, J.A. Burdick, Controlling stem cell fate with material design, *Adv Mater* 22(2) (2010) 175-89.
- [98] M.M. Martino, M. Mochizuki, D.A. Rothenfluh, S.A. Rempel, J.A. Hubbell, T.H. Barker, Controlling integrin specificity and stem cell differentiation in 2D and 3D environments through regulation of fibronectin domain stability, *Biomaterials* 30(6) (2009) 1089-1097.
- [99] I. Bilem, P. Chevallier, L. Plawinski, E.D. Sone, M.C. Durrieu, G. Laroche, RGD and BMP-2 mimetic peptide crosstalk enhances osteogenic commitment of human bone marrow stem cells, *Acta Biomater* 36 (2016) 132-42.
- [100] F. Martini, A. Pellati, E. Mazzoni, S. Salati, G. Caruso, D. Contartese, M. De Mattei, Bone Morphogenetic Protein-2 Signaling in the Osteogenic Differentiation of Human Bone Marrow Mesenchymal Stem Cells Induced by Pulsed Electromagnetic Fields, *International journal of molecular sciences* 21(6) (2020) 2104.
- [101] M.J. Kim, B. Lee, K. Yang, J. Park, S. Jeon, S.H. Um, D.I. Kim, S.G. Im, S.W. Cho, BMP-2 peptide-functionalized nanopatterned substrates for enhanced osteogenic differentiation of human mesenchymal stem cells, *Biomaterials* 34(30) (2013) 7236-46.
- [102] F. Posa, A.L. Grab, V. Martin, D. Hose, A. Seckinger, G. Mori, S. Vukicevic, E.A. Cavalcanti-Adam, Copresentation of BMP-6 and RGD Ligands Enhances Cell Adhesion and BMP-Mediated Signaling, *Cells* 8(12) (2019).
- [103] T. Ebisawa, K. Tada, I. Kitajima, K. Tojo, T.K. Sampath, M. Kawabata, K. Miyazono, T. Imamura, Characterization of bone morphogenetic protein-6 signaling pathways in osteoblast differentiation, *J Cell Sci* 112 (Pt 20) (1999) 3519-27.
- [104] P. Gentile, A.M. Ferreira, J.T. Callaghan, C.A. Miller, J. Atkinson, C. Freeman, P.V. Hatton, Multilayer Nanoscale Encapsulation of Biofunctional Peptides to Enhance Bone Tissue Regeneration In Vivo, *Advanced Healthcare Materials* 6(8) (2017).
- [105] J.W. Lee, Y.J. Park, S.J. Lee, S.K. Lee, K.Y. Lee, The effect of spacer arm length of an adhesion ligand coupled to an alginate gel on the control of fibroblast phenotype, *Biomaterials* 31(21) (2010) 5545-51.
- [106] J.W. Lee, H. Kim, K.Y. Lee, Effect of spacer arm length between adhesion ligand and alginate hydrogel on stem cell differentiation, *Carbohydr Polym* 139 (2016) 82-9.
- [107] Q. Chen, S. Yu, D. Zhang, W. Zhang, H. Zhang, J. Zou, Z. Mao, Y. Yuan, C. Gao, R. Liu, Impact of Antifouling PEG Layer on the Performance of Functional Peptides in Regulating Cell Behaviors, *J Am Chem Soc* 141(42) (2019) 16772-16780.
- [108] Z. Karagöz, L. Rijns, P.Y.W. Dankers, M. van Griensven, A. Carlier, Towards understanding the messengers of extracellular space: Computational models of outside-in integrin reaction networks, *Computational and Structural Biotechnology Journal* 19 (2021) 303-314.

- [109] S. Huveneers, E.H. Danen, Adhesion signaling - crosstalk between integrins, Src and Rho, *J Cell Sci* 122(Pt 8) (2009) 1059-69.
- [110] J.Z. Kechagia, J. Ivaska, P. Roca-Cusachs, Integrins as biomechanical sensors of the microenvironment, *Nat Rev Mol Cell Biol* 20(8) (2019) 457-473.
- [111] X. Wang, C. Yan, K. Ye, Y. He, Z. Li, J. Ding, Effect of RGD nanospacing on differentiation of stem cells, *Biomaterials* 34(12) (2013) 2865-74.
- [112] F. Martino, A.R. Perestrelo, V. Vinarský, S. Pagliari, G. Forte, Cellular Mechanotransduction: From Tension to Function, *Front Physiol* 9 (2018) 824.
- [113] X. Wang, K. Ye, Z.H. Li, C. Yan, J.D. Ding, Adhesion, proliferation, and differentiation of mesenchymal stem cells on RGD nanopatterns of varied nanospacings, *Organogenesis* 9(4) (2013) 280-286.
- [114] T. Satav, J. Huskens, P. Jonkheijm, Effects of Variations in Ligand Density on Cell Signaling, *Small* 11(39) (2015) 5184-99.
- [115] S. Sankaran, E. Cavatorta, J. Huskens, P. Jonkheijm, Cell Adhesion on RGD-Displaying Knottins with Varying Numbers of Tryptophan Amino Acids to Tune the Affinity for Assembly on Cucurbit[8]uril Surfaces, *Langmuir* 33(35) (2017) 8813-8820.
- [116] S. Vafaei, S.R. Tabaei, N.J. Cho, Optimizing the Performance of Supported Lipid Bilayers as Cell Culture Platforms Based on Extracellular Matrix Functionalization, *ACS Omega* 2(6) (2017) 2395-2404.
- [117] X. Jiang, D.A. Bruzewicz, A.P. Wong, M. Piel, G.M. Whitesides, Directing cell migration with asymmetric micropatterns, *Proceedings of the National Academy of Sciences of the United States of America* 102(4) (2005) 975-978.
- [118] R. Inaba, A. Khademhosseini, H. Suzuki, J. Fukuda, Electrochemical desorption of self-assembled monolayers for engineering cellular tissues, *Biomaterials* 30(21) (2009) 3573-9.
- [119] H.J. Kwon, G.S. Lee, H. Chun, Electrical stimulation drives chondrogenesis of mesenchymal stem cells in the absence of exogenous growth factors, *Scientific Reports* 6(1) (2016) 39302.
- [120] L. Glennon-Alty, R. Williams, S. Dixon, P. Murray, Induction of mesenchymal stem cell chondrogenesis by polyacrylate substrates, *Acta Biomater* 9(4) (2013) 6041-51.
- [121] C. Rodriguez-Pereira, A. Lagunas, I. Casanellas, Y. Vida, E. Perez-Inestrosa, J.A. Andrades, J. Becerra, J. Samitier, F.J. Blanco, J. Magalhaes, RGD-Dendrimer-Poly(L-lactic) Acid Nanopatterned Substrates for the Early Chondrogenesis of Human Mesenchymal Stromal Cells Derived from Osteoarthritic and Healthy Donors, *Materials (Basel)* 13(10) (2020).
- [122] W. Luo, E.W. Chan, M.N. Yousaf, Tailored electroactive and quantitative ligand density microarrays applied to stem cell differentiation, *J Am Chem Soc* 132(8) (2010) 2614-21.

- [123] J.E. Frith, R.J. Mills, J.J. Cooper-White, Lateral spacing of adhesion peptides influences human mesenchymal stem cell behaviour, *J Cell Sci* 125(Pt 2) (2012) 317-27.
- [124] P.P. Han, J.E. Frith, G.A. Gomez, A.S. Yap, G.M. O'Neill, J.J. Cooper-White, Five Piconewtons: The Difference between Osteogenic and Adipogenic Fate Choice in Human Mesenchymal Stem Cells, *Acs Nano* 13(10) (2019) 11129-11143.
- [125] Y. Ma, X.H. Tian, L. Liu, J.M. Pan, G.Q. Pan, Dynamic Synthetic Biointerfaces: From Reversible Chemical Interactions to Tunable Biological Effects, *Accounts Chem. Res.* 52(6) (2019) 1611-1622.
- [126] J.N. Roberts, J.K. Sahoo, L.E. McNamara, K.V. Burgess, J. Yang, E.V. Alakpa, H.J. Anderson, J. Hay, L.A. Turner, S.J. Yarwood, M. Zelzer, R.O. Oreffo, R.V. Ulijn, M.J. Dalby, Dynamic Surfaces for the Study of Mesenchymal Stem Cell Growth through Adhesion Regulation, *ACS Nano* 10(7) (2016) 6667-79.
- [127] T.T. Lee, J.R. Garcia, J.I. Paez, A. Singh, E.A. Phelps, S. Weis, Z. Shafiq, A. Shekaran, A. Del Campo, A.J. Garcia, Light-triggered in vivo activation of adhesive peptides regulates cell adhesion, inflammation and vascularization of biomaterials, *Nat Mater* 14(3) (2015) 352-60.
- [128] Q. An, J. Brinkmann, J. Huskens, S. Krabbenborg, J. de Boer, P. Jonkheijm, A supramolecular system for the electrochemically controlled release of cells, *Angew Chem Int Ed Engl* 51(49) (2012) 12233-7.
- [129] L. Liu, X. Tian, Y. Ma, Y. Duan, X. Zhao, G. Pan, A Versatile Dynamic Mussel-Inspired Biointerface: From Specific Cell Behavior Modulation to Selective Cell Isolation, *Angew Chem Int Ed Engl* 57(26) (2018) 7878-7882.
- [130] H. Kang, H.J. Jung, D.S.H. Wong, S.K. Kim, S. Lin, K.F. Chan, L. Zhang, G. Li, V.P. Dravid, L. Bian, Remote Control of Heterodimeric Magnetic Nanoswitch Regulates the Adhesion and Differentiation of Stem Cells, *Journal of the American Chemical Society* 140(18) (2018) 5909-5913.
- [131] W. Du, D.T. Zhang, X.M. Wang, T.C. Ren, C.Y. Gao, Mediating the Migration of Mesenchymal Stem Cells by Dynamically Changing the Density of Cell-selective Peptides Immobilized on beta-Cyclodextrin-modified Cell-resisting Polymer Brushes, *Chin. J. Polym. Sci.* 38(2) (2020) 126-136.
- [132] L.B. Zhang, Z.J. Wang, J. Das, M. Labib, S. Ahmed, E.H. Sargent, S.O. Kelley, Potential-Responsive Surfaces for Manipulation of Cell Adhesion, Release, and Differentiation, *Angewandte Chemie-International Edition* 58(41) (2019) 14519-14523.
- [133] D.S.H. Wong, J.N. Li, X.H. Yan, B. Wang, R. Li, L. Zhang, L.M. Bian, Magnetically Tuning Tether Mobility of Integrin Ligand Regulates Adhesion, Spreading, and Differentiation of Stem Cells, *Nano Letters* 17(3) (2017) 1685-1695.
- [134] H. Kang, D.S.H. Wong, X.H. Yan, H.J. Jung, S. Kim, S. Lin, K.C. Wei, G. Li, V.P. Dravid, L.M. Bian, Remote Control of Multimodal Nanoscale Ligand

Oscillations Regulates Stem Cell Adhesion and Differentiation, *Acs Nano* 11(10) (2017) 9636-9649.

[135] X. Wang, C. Yao, W. Weng, K. Cheng, Q. Wang, Visible-Light-Responsive Surfaces for Efficient, Noninvasive Cell Sheet Harvesting, *ACS Appl Mater Interfaces* 9(34) (2017) 28250-28259.

[136] S.H. Yoon, M.R. Mofrad, Cell adhesion and detachment on gold surfaces modified with a thiol-functionalized RGD peptide, *Biomaterials* 32(30) (2011) 7286-96.

[137] M. Wirkner, J.M. Alonso, V. Maus, M. Salierno, T.T. Lee, A.J. García, A. del Campo, Triggered cell release from materials using bioadhesive photocleavable linkers, *Adv Mater* 23(34) (2011) 3907-10.

[138] J. Jin, Y. Xing, Y. Xi, X. Liu, T. Zhou, X. Ma, Z. Yang, S. Wang, D. Liu, A triggered DNA hydrogel cover to envelop and release single cells, *Adv Mater* 25(34) (2013) 4714-7.

[139] J. Yang, L.E. McNamara, N. Gadegaard, E.V. Alakpa, K.V. Burgess, R.M. Meek, M.J. Dalby, Nanotopographical induction of osteogenesis through adhesion, bone morphogenic protein cosignaling, and regulation of microRNAs, *ACS Nano* 8(10) (2014) 9941-53.

[140] C.A. DeForest, D.A. Tirrell, A photoreversible protein-patterning approach for guiding stem cell fate in three-dimensional gels, *Nat. Mater.* 14(5) (2015) 523-531.

[141] Z.Z. Ming, X. Ruan, C.Y. Bao, Q.N. Lin, Y. Yang, L.Y. Zhu, Micropatterned Protein for Cell Adhesion through Phototriggered Charge Change in a Polyvinylpyrrolidone Hydrogel, *Advanced Functional Materials* 27(25) (2017).

[142] S. De Martino, S. Cavalli, P.A. Netti, Photoactive Interfaces for Spatio-Temporal Guidance of Mesenchymal Stem Cell Fate, *Adv Healthc Mater* 9(13) (2020) e2000470.

[143] S.G. Parker, Y. Yang, S. Ciampi, B. Gupta, K. Kimpton, F.M. Mansfeld, M. Kavallaris, K. Gaus, J.J. Gooding, A photoelectrochemical platform for the capture and release of rare single cells, *Nat Commun* 9(1) (2018) 2288.

[144] J. Nakanishi, Y. Kikuchi, T. Takarada, H. Nakayama, K. Yamaguchi, M. Maeda, Spatiotemporal control of cell adhesion on a self-assembled monolayer having a photocleavable protecting group, *Anal Chim Acta* 578(1) (2006) 100-4.

[145] G.C. Gurtner, S. Werner, Y. Barrandon, M.T. Longaker, Wound repair and regeneration, *Nature* 453(7193) (2008) 314-21.

[146] L. Liu, X.H. Tian, Y. Ma, Y.Q. Duan, X. Zhao, G.Q. Pan, A Versatile Dynamic Mussel-Inspired Biointerface: From Specific Cell Behavior Modulation to Selective Cell Isolation, *Angewandte Chemie-International Edition* 57(26) (2018) 7878-7882.

[147] L. Zwi-Dantsis, B. Wang, C. Marijon, S. Zonetti, A. Ferrini, L. Massi, D.J. Stuckey, C.M. Terracciano, M.M. Stevens, Remote Magnetic Nanoparticle Manipulation Enables the Dynamic Patterning of Cardiac Tissues, *Advanced Materials* 32(6) (2020) 1904598.

- [148] Y. Kim, H. Choi, J.E. Shin, G. Bae, R. Thangam, H. Kang, Remote active control of nanoengineered materials for dynamic nanobiomedical engineering, *View* 1(4) (2020).
- [149] S. Min, M.J. Ko, H.J. Jung, W. Kim, S.B. Han, Y. Kim, G. Bae, S. Lee, R. Thangam, H. Choi, N. Li, J.E. Shin, Y.S. Jeon, H.S. Park, Y.J. Kim, U.K. Sukumar, J.J. Song, S.K. Park, S.H. Yu, Y.C. Kang, K.B. Lee, Q. Wei, D.H. Kim, S.M. Han, R. Paulmurugan, Y.K. Kim, H. Kang, Remote Control of Time-Regulated Stretching of Ligand-Presenting Nanocoils In Situ Regulates the Cyclic Adhesion and Differentiation of Stem Cells, *Adv Mater* 33(11) (2021) e2008353.
- [150] C. Khatua, S. Min, H.J. Jung, J.E. Shin, N. Li, I. Jun, H.W. Liu, G. Bae, H. Choi, M.J. Ko, Y.S. Jeon, Y.J. Kim, J. Lee, M. Ko, G. Shim, H. Shin, S. Lee, S. Chung, Y.K. Kim, J.J. Song, V.P. Dravid, H. Kang, In Situ Magnetic Control of Macroscale Nanoligand Density Regulates the Adhesion and Differentiation of Stem Cells, *Nano Lett* 20(6) (2020) 4188-4196.
- [151] D.S. Wang, F. Schellenberger, J.T. Pham, H.J. Butt, S. Wu, Orthogonal photo-switching of supramolecular patterned surfaces, *Chemical Communications* 54(27) (2018) 3403-3406.
- [152] T. Bai, A. Sinclair, F. Sun, P. Jain, H.C. Hung, P. Zhang, J.R. Ella-Menye, W.G. Liu, S.Y. Jiang, Harnessing isomerization-mediated manipulation of nonspecific cell/matrix interactions to reversibly trigger and suspend stem cell differentiation, *Chem. Sci.* 7(1) (2016) 333-338.
- [153] G. Xu, S. Li, C. Liu, S. Wu, Photoswitchable Adhesives Using Azobenzene-Containing Materials, *Chem Asian J* 15(5) (2020) 547-554.
- [154] L. Albert, O. Vázquez, Photoswitchable peptides for spatiotemporal control of biological functions, *Chem Commun (Camb)* 55(69) (2019) 10192-10213.
- [155] C.H. Yu, N.B. Rafiq, F. Cao, Y. Zhou, A. Krishnasamy, K.H. Biswas, A. Ravasio, Z. Chen, Y.H. Wang, K. Kawachi, G.E. Jones, M.P. Sheetz, Integrin-beta3 clusters recruit clathrin-mediated endocytic machinery in the absence of traction force, *Nat Commun* 6 (2015) 8672.
- [156] E. Ruoslahti, RGD and other recognition sequences for integrins, *Annu Rev Cell Dev Biol* 12 (1996) 697-715.
- [157] R. Freeman, N. Stephanopoulos, Z. Alvarez, J.A. Lewis, S. Sur, C.M. Serrano, J. Boekhoven, S.S. Lee, S.I. Stupp, Instructing cells with programmable peptide DNA hybrids, *Nat Commun* 8 (2017) 15982.
- [158] L.C. Bahlmann, A. Fokina, M.S. Shoichet, Dynamic bioengineered hydrogels as scaffolds for advanced stem cell and organoid culture, *MRS Communications* 7(3) (2017) 472-486.
- [159] J. Lee, A.A. Abdeen, Y. Li, S. Goonetilleke, K.A. Kilian, Gradient and Dynamic Hydrogel Materials to Probe Dynamics in Cancer Stem Cell Phenotypes, *ACS Applied Bio Materials* 4(1) (2021) 711-720.

[160] M. Tanaka, M. Nakahata, P. Linke, S. Kaufmann, Stimuli-responsive hydrogels as a model of the dynamic cellular microenvironment, *Polymer Journal* 52(8) (2020) 861-870.

[161] K. Zhang, R. Deng, Y. Sun, L. Zhang, J. Li, Reversible control of cell membrane receptor function using DNA nano-spring multivalent ligands, *Chem Sci* 8(10) (2017) 7098-7105.

Chapter 3

DNA modified MSN-films as versatile biointerfaces to study stem cell adhesion processes

Xingzhen Zhang and Sabine van Rijt

Department of Instructive Biomaterials Engineering, MERLN Institute for Technology Inspired Regenerative Medicine, Maastricht University, Maastricht, the Netherlands.

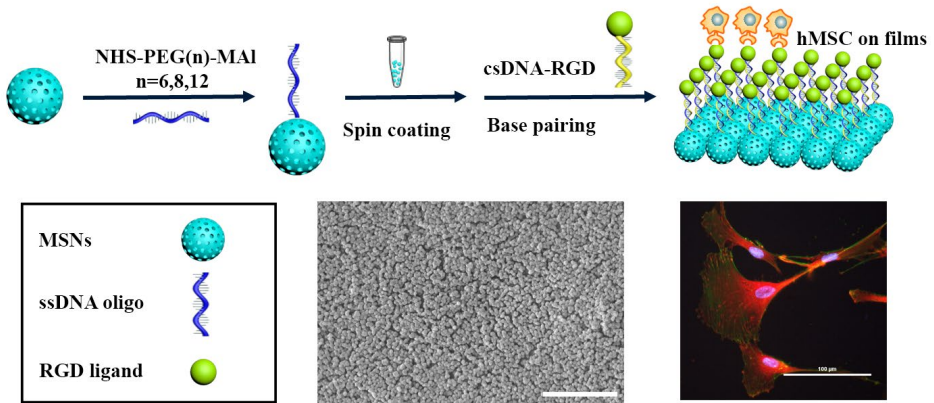
Abstract

A significant bottleneck in the clinical translation of stem cells remains eliciting the desired stem cell behavior once transplanted in the body. In their natural environment, stem cell fate is regulated by their interaction with extracellular matrix (ECM), mainly through integrin-mediated cell adhesion. 2D biointerfaces that selectively present ECM-derived ligands can be used as valuable tools to study and improve our understanding on how stem cells interact with their environment. Here we developed a new type of biointerface based on mesoporous silica nanoparticles (MSN) which are interesting nanomaterials for biointerface engineering because they allow close control over surface physicochemical properties. To create the platform, DNA functionalized MSN (MSN-ssDNA) with varying PEG linker length were developed. Cell adhesion tripeptide RGD was conjugated to a complementary DNA strand, which could specifically bind to MSN-ssDNA to create MSN-dsDNA-RGD films. We showed that MSN-dsDNA-RGD films could promote hMSCs adhesion and spreading, whereas MSN-dsDNA films without RGD resulted in poor cell spreading with round morphology, and low cell adhesion. In addition, we showed that cell adhesion to the films is PEG length-dependent. The design of the platform allows easy incorporation of other and multiple ECM ligands, as well as soluble cues, making MSN-ssDNA based biointerfaces a novel tool to study ligand–stem cell interactions.

Keywords

stem cell, cell adhesion, biointerface, mesoporous silica nanoparticle, DNA, ligand presentation

Graphical abstract



1. Introduction

Stem cells are characterized by an inherent ability to self-renew and the potential to differentiate into specialized cells [1]. Due to their regenerative capacities, stem cells are heavily researched in the regenerative medicine field [2]. However, an ongoing challenge in their clinical translation is control over their behavior once transplanted. *In vivo*, stem cells live in a complex extracellular microenvironment (ECM), which is termed the *stem cell niche* [3]. Stem cells can sense and respond to multiple physical and chemical cues present in their ECM [4]. The ECM is a complex assembly of multiple structural proteins (e.g. collagen and fibronectin), glycoproteins, and polysaccharides and embedded growth factors [5]. It has been reported that the ECM plays a crucial role in regulating stem cell adhesion, proliferation and differentiation, but the mechanisms of which are still poorly understood [6].

Stem cells interact with their ECM mainly via integrin receptor-mediated adhesion [7]. Integrin receptors are heterodimeric transmembrane proteins, which can recognize and recruit multiple ECM proteins to form focal adhesions between the stem cell's cytoskeleton and the ECM [8]. Integrin-mediated interactions not only provide stem cells anchoring points but also directs their fate such as stem cell differentiation and self-renewal. Previous studies have shown that large adhesions, high cell spreading and increased cytoskeletal tension could facilitate osteogenic differentiation, whereas weaker cell adhesions resulted in enhanced stem cell self-renewal [9, 10]. Hence, integrin-mediated stem cell adhesion processes are an important field of study to understand, predict and control stem cell behaviors [11]. A better understanding of how stem cells interact and respond to ECM presented ligands will help researchers rationally design better performing bioactive materials.

2D biointerfaces that offer high control over ligand presentation are popular material-based tools to study ligand-stem cell interactions. 2D biointerfaces have been used to improve our understanding on stem cell adhesion processes and subsequent stem cell fate [12, 13]. Numerous biointerfaces have been engineered, where ECM-derived adhesive motifs such as Arg-Gly-Asp (RGD) peptide are often used to allow stem cell adhesion to the biointerfaces [14, 15]. Using such interfaces, the importance of adhesive motif type, density, and spacing have been investigated [16, 17]. Diverse chemical strategies have been employed to fabricate biointerfaces, where the most reported strategies are based on self-assembled monolayers (SAMs) on glass or metal substrates [18, 19]. In these approaches,

functionalized molecules bind to the metal or silica surface and spontaneously organize to form SAMs. Nanoparticles represent an alternative to this approach and can also be used to generate biointerfaces. The unique physiochemical properties of nanoparticles, such as controlled synthesis, high surface area as well as flexible surface modification in the nanoscale, make them interesting materials to create biointerfaces where close control over surface properties are important. In addition, compared to covalent SAM based approaches, nanoparticles could be used to create interfaces with different surface morphologies [20-22]. Various types of nanoparticles such as gold nanoparticles and nanomagnets have been used to create biointerfaces [23, 24]. For example, RGD functionalized gold nanoparticles were successfully micropatterned over a glass substrate via lithography technology to manipulate cell adhesion [25].

Mesoporous silica nanoparticles (MSN) have promising characteristics to develop 2D biointerfaces, which include high surface area, mesoporous structure and high control over their size and shape. MSN can be further surface and core functionalized, making them incredibly flexible platforms for post-functionalization. In addition, their porous structure gives the possibility for controlled delivery of cargo such as growth factors. So far, MSN have been extensively used for drug delivery and bio-imaging applications [26]. However, their application as nanoparticle based films is much less widely explored. In our previous work we have demonstrated that stable homogeneous MSN based films can be created using spin coating and can be used for biomolecule delivery to steer stem cell differentiation [27]. In this work, we aim to develop a new type of biointerface based on MSN films that is able to specifically and flexibly present ECM ligands to study stem cell–ligand interactions. To create the flexible platform, a single strand DNA (ssDNA) functionalized MSN (MSN-ssDNA) were developed where ssDNA was used to introduce RGD to the MSN films. DNA is a promising engineering material to create biointerfaces, as DNA duplex hybridization via Watson-Crick base-pairing is highly specific. DNA based platforms have high flexibility in their use, as highlighted in one recent study where different adhesion peptides, or both growth factors and bioactive peptides could be tethered in one single system, simultaneously. Moreover, DNA could also be exploited for dynamic ligand presentation to study the importance of integrin-binding ligand dynamics on cell behaviors [28-30]. Although here we study RGD mediated cell adhesion, our method of RGD incorporation using DNA hybridization allows facile substitution of other or even multiple ECM ligands.

To specifically present ECM ligands, polyethylene glycol (PEG) was used as an antifouling linker between RGD and MSN surface to prevent unspecific binding. In previous studies, PEG has been extensively utilized as an antifouling linker to couple bioactive motifs to substrates to prevent nonspecific cell adhesion interference [31, 32]. However, few studies have investigated how PEG chain length influences cell adhesion processes. Thus, the effect of PEG linker length with 6, 8 or 12 repeating units (PEG6, PEG8 and PEG12) on specific bone marrow derived human mesenchymal stromal cells (hMSC) adhesion on MSN films was also assessed in this work. Here, PEG linker modified MSN (MSN-L) were coupled to a single strand DNA (MSN-L-ssDNA) and RGD was introduced by conjugating RGD to a complementary DNA strand (csDNA-RGD). The presence of ssDNA on films and its ability to specifically bind csDNA-RGD was verified by a surface hybridization assay. Finally, we investigated hMSCs adhesion on different films with and without RGD as a function of PEG linker length. Here we show that MSN films using PEG12 as linkers can be used as flexible 2D biointerfaces to study ligand–stem cell interactions.

2. Results

2.1. DNA can be successfully surface grafted to MSN using various PEG linkers.

To create the DNA modified MSN, MSN were first surface functionalized with an amine (MSN-NH₂) or thiol (MSN-SH) functional group to allow functionalization with ssDNA. Two functionalization routes were tested to determine which route would allow the best graft ratios of ssDNA to the MSN. The presence of the amine or thiol groups on MSN was verified by 5/6-Carboxyfluorescein succinimidyl ester (FITC-NHS) or ATTO 647-maleimide labeling, where the fluorescence intensity of amine/thiol surface modified MSN was significantly higher compared to non-modified MSN (Figure S1). The synthesis of DNA modified MSN was performed in two steps (Figure 1a and Figure S2a). First, MSN-NH₂ or MSN-SH were modified with a maleimide-polyethylene glycol-succinimidyl ester linker (Mal-PEG-NHS) to form MSN-L. In the second step, amine or thiol functionalized ssDNA was grafted onto the PEG linker modified MSN (MSN-L) using the same conjugation chemistry. The amount of immobilized ssDNA on MSN surface was quantified using Nanodrop Microvolume Spectrophotometer. Higher DNA graft ratios were observed with MSN-NH₂ compared to MSN-SH (Figure S2b). Thus in our further studies MSN-NH₂ was used for ssDNA attachment. Three lengths of the PEG linker ($n=6, 8$ and 12) were conjugated to MSN-NH₂, designated as MSN-L₆-ssDNA, MSN-L₈-ssDNA,

MSN-L₁₂-ssDNA to determine the effect of PEG linker length to promote specific RGD- stem cell interactions.

The MSN-NH₂, MSN-L and MSN-L-ssDNA were further characterized using transmission electron microscope (TEM) and dynamic light scattering (DLS). TEM images showed that MSN-NH₂ displayed spherical-shaped morphology with uniform porous structure (Figure 1b). MSN modification with PEG linkers and ssDNA resulted in MSN with a spherical morphology but less visible porous structure likely due to the ssDNA surface modification (Figure S2c). The particle size of MSN-L and MSN-L-ssDNA estimated from the TEM images was around 75 nm, which was slightly higher than that of MSN-NH₂ (70 nm). DLS measurements showed that the hydrodynamic diameter of MSN-NH₂ was around 200 nm, which did not significantly change after PEG and DNA modification (Table 1 and Table S2). All prepared MSN were monodisperse with a polydispersity index (PDI) of 0.13 for MSN-NH₂, 0.18 for MSN-L₆-ssDNA, 0.16 for MSN-L₈-ssDNA, and 0.21 for MSN-L₁₂-ssDNA. The surface charge of MSN-NH₂ at pH 7.2 was -18.4 mV, which became more negative after PEG and ssDNA modification (Figure 1c and Table 1). In addition, the zeta potential of MSN-ssDNA was similar for all three nanoparticles irrespective of PEG length. The amount of immobilized ssDNA on MSN surface using different PEG linkers was further quantified using Nanodrop Microvolume Spectrophotometer. As shown in Figure 1d, the conjugation efficiency of ssDNA to MSN was similar for all three PEG linkers. In summary, MSN surface could be successfully modified with PEG chains of different lengths and ssDNA via a two-step synthesis approach.

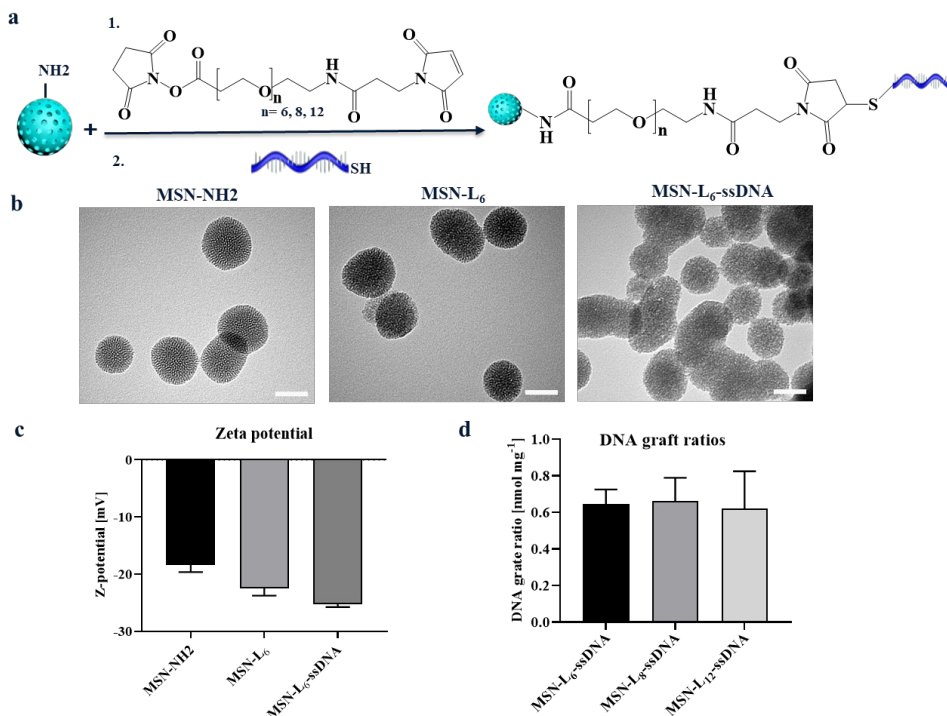


Figure 1. Synthesis and characterization of MSN-L-ssDNA. a) Schematic illustration of MSN-L-ssDNA synthesis using PEG linkers with different chain lengths ($n = 6, 8$ or 12). b) TEM images show that MSN-NH₂, MSN-L₆ and MSN-L₆-ssDNA have a spherical shape and mesoporous structure. DNA surface modification resulted in a less visible porous structure. Scale bar represents 50 nm. c) Zeta potential determined by DLS. d) DNA graft ratios using different PEG linker lengths.

Table 1. Physical characterization of the synthesized MSN.

Items	Hydrodynamic diameter [nm] ^{a)}	PDI	Zeta potential [mV] b)
MSN-NH ₂	231.87 ± 0.23	0.13 ± 0.13	-18.4 ± 1.23
MSN-L ₆ -ssDNA	241.33 ± 1.11	0.18 ± 0.01	-25.27 ± 0.50
MSN-L ₈ -ssDNA	210.40 ± 2.45	0.16 ± 0.03	-25.73 ± 0.51
MSN-L ₁₂ -ssDNA	235.37 ± 2.76	0.21 ± 0.01	-24.87 ± 0.58

a) Size measurements were carried out in absolute ethanol at a concentration of 0.5 mg/ml; b) Zeta potential measurements were conducted in HEPES buffer (pH 7.2, 25 mM) at 0.1 mg/ml concentration.

2.2. Development of stable and homogeneous MSN-ssDNA films using spin coating

To prepare DNA-modified MSN based films, the synthesized MSN-L₆-ssDNA, MSN-L₈-ssDNA and MSN-L₁₂-ssDNA were dispersed in water and then spin coated over plasma-pretreated glass coverslips. The coating quality and surface morphology of MSN-L-ssDNA films were characterized using SEM. All three MSN-L-ssDNA could be homogeneously spin coated to form a continuous layer of nanoparticles over the glass substrate (Figure 2a and Figure S3a-c). In addition, an optical image of MSN-L₆-ssDNA films revealed that the nanoparticles completely covered the glass substrate. 3D laser scanning revealed a film thickness of around 200 nm for MSN-L₆-ssDNA in the center, middle and edge of the film (Figure 2b), indicating that the film was homogeneously covered and that 2-3 layers of nanoparticles deposited over the glass substrate. As surface wettability is known to influence cell adhesion and can be varied by surface chemical composition, we measured the water contact angle (WCA) on the different substrates [17]. As shown in Figure 2c and Figure S4, the WCA measured on nanoparticles coated glass was lower than that measured on plasma treated glass, which indicated an increase in surface hydrophilicity due to hydrophilic PEG linker and DNA modification. No significant difference in WCA was observed as a function of PEG chain length. Next, MSN-L₁₂-ssDNA film stability was evaluated by immersing films prepared from fluorescently labeled MSN in PBS (pH 7.4) and cell culture media for 1, 7 and 14 days. DNA modified MSN films were stable over the 14 day incubation in both PBS and culture media (Table S3). In conclusion, we could develop homogeneous and stable MSN-L-ssDNA films using spin coating. Finally, MSN-L₁₂-ssDNA film stability under cell culture conditions was investigated after 1 and 5 days of culture using ATTO647 labeled MSN-L₁₂-ssDNA particles and flow cytometry analysis (Figure S5). After 5 days of culture, no peak shift was observed compared to hMSCs cultured on control glass substrates, indicating that limited MSNs were taken up by hMSCs, and that the films were stable under cell culture conditions.

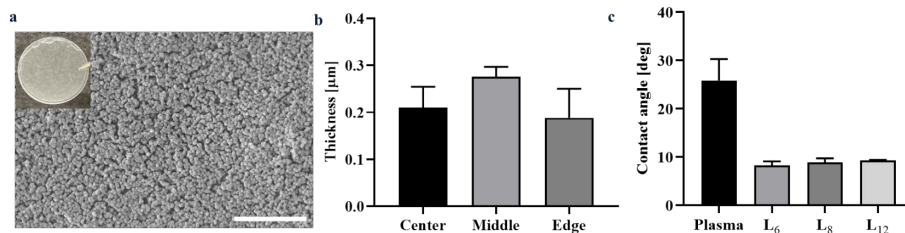


Figure 2. Characterization of MSN-ssDNA spin-coated films. a) SEM image and optical image (insert) shows homogenous surface structure of MSN-L₆-ssDNA films. Scale bar is 2 μm. b) MSN-L₆-ssDNA film thickness measured at different positions of the coverslip by 3D laser scanning microscopy. c) Water contact angle of glass surfaces before and after coating with different MSN-L-ssDNA.

2.3. *csDNA-RGD conjugation and hybridization assay*

To allow RGD binding to MSN-L-ssDNA, RGD was conjugated to a complementary strand DNA (csDNA) that was able to hybridize with the tethered ssDNA on the MSN. For this, commercially available 5'-amine modified DNA was conjugated to an NHS-PEG₆-maleimide cross-linker, yielding a csDNA-PEG₆-Mal conjugate. Then this conjugate was immediately reacted with cysteine modified RGD (RGDC) overnight (Figure 3a). Both csDNA-PEG₆-Mal and csDNA-RGD conjugate were characterized using Liquid Chromatography Electrospray ionization Mass Spectrometry (LC-ESI-MS). The calculated Molecular Weight (Mw) is the theoretical average mass of the conjugates. The measured masses of conjugates were determined by deconvolution of the acquired mass spectrum (Thermo BioPharma Finder software) (Figure S6). The measured MW of csDNA-RGD was 7247.5 g mol⁻¹ and matched with the calculated Mw of 7248.2 g mol⁻¹, verifying the successful synthesis of the conjugate. Next, a hybridization assay was performed to verify the ability and specificity of DNA duplex binding to MSN-L-ssDNA. For this, complementary DNA strands labeled with FAM (csDNA-FAM) were used to quantify the amount of specific DNA binding, while FAM labeled mismatched DNA strands (msDNA-FAM) which are unable to bind to the MSN-L-ssDNA, were used as control to examine nonspecific adsorption of DNA onto the MSN-L-ssDNA. The hybridization experiments were done both on MSN in suspension and on MSN films. A high fluorescent signal was detected when exposing MSN-L₆-ssDNA in suspension to the csDNA-FAM, while no measurable signal was detected after

exposure to msDNA-FAM, demonstrating the hybridization was successful and selective (Figure 3b). Next, we further quantified RGD density on the films, as surface RGD density plays a crucial role in regulating cell adhesion [33]. For this, MSN-L-ssDNA with different PEG linkers were synthesized and exposed to csDNA-FAM. After hybridization, nanoparticles were collected by centrifugation and re-suspended in water. Then RGD amount was calculated based on csDNA-FAM fluorescent intensity. The hybridized RGD amount for 1 mg of nanoparticles of MSN-L₆-ssDNA, MSN-L₈-ssDNA and MSN-L₁₂-ssDNA was 0.41 nmol, 0.32 nmol and 0.37 nmol, respectively. As 1 mg of nanoparticles were applied for glass spin coating and the surface area of glass coverslip is 4.84 cm², the final RGD densities on different MSN films showed a similar surface RGD density, with 85.52 pmol cm⁻² for MSN-L₆-ssDNA, 66.97 pmol cm⁻² for MSN-L₈-ssDNA, and 77.45 pmol cm⁻² for MSN-L₁₂-ssDNA.

To further measure DNA hybridization on the films, MSN-ssDNA films with different PEG chain lengths were prepared and then exposed to csDNA-FAM in hybridization buffer. Similarly, high fluorescent signals were observed when MSN-L-ssDNA films were exposed to csDNA-FAM, and significantly lower fluorescent signal was observed after exposure to msDNA-FAM, demonstrating that the DNA duplex hybridization on films was also possible and specific (Figure 3c). In addition, DNA hybridization efficiency on the surface was PEG linker length dependent as evidenced by fluorescent intensity, with L₁₂ showing significantly higher fluorescence compared to films made with L₆.

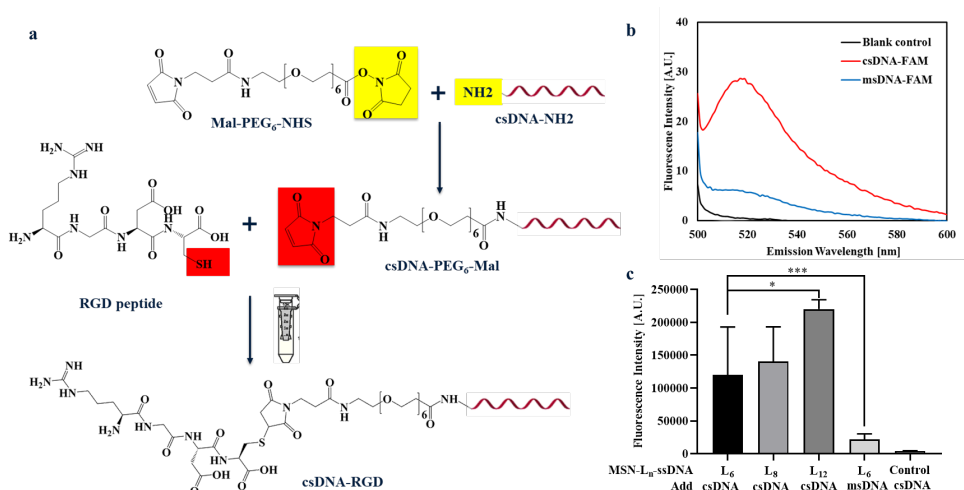


Figure 3. Synthesis of csDNA-RGD conjugate and DNA duplex hybridization. a) Schematic illustration of synthesis of csDNA-RGD conjugate. Bifunctional PEG₆ linker first reacts with amine group of DNA to form the Mal-DNA conjugate. This solution then reacts with thiol group of RGDC peptide to form csDNA-RGD. b) Hybridization of FAM labeled complementary strand DNA (csDNA-FAM) to MSN-L₆-ssDNA in suspension (red line), compared to exposure of MSN-L₆-ssDNA to FAM labeled mismatch strand DNA (msDNA-FAM), showing specific hybridization. The blank control is MSN-L-ssDNA not exposed to DNA-FAM. c) Hybridization of csDNA-FAM on MSN-L-ssDNA films. Hybridization efficiency was determined by fluorescence intensity. Control groups are MSN-L₆-ssDNA films exposed to msDNA-FAM and MSN films exposed to csDNA-FAM. Data are expressed as the mean \pm SD (n=3). *p < 0.05; **p < 0.01; ***p < 0.001.

2.4. hMSC attachment to MSN-L-ssDNA films

The ability of hMSCs to attach to the developed MSN-L-ssDNA surfaces was assessed by DAPI staining of the cell nucleus, and cell numbers were determined after 4 and 24 h on RGD presenting (RGD(+)) and non RGD (RGD(-)) presenting MSN films using CellProfiler. RGD presentation on RGD(+) films was initialized by hybridization of csDNA-RGD with surface-tethered ssDNA (MSN-L-dsDNA-RGD), where csDNA without RGD was used for surface hybridization as a control group (MSN-L-dsDNA; RGD(-)). MSN-L-ssDNA films were prepared using the three different PEG spacers (MSN-L₆-ssDNA, MSN-L₈-ssDNA, MSN-L₁₂-ssDNA) to investigate if PEG length influences hMSCs attachment. Incorporation of RGD onto MSN surfaces with L₈ and L₁₂ linkers resulted in significantly higher attached cell numbers after 4 h, which increased after 1 day, compared to surfaces without RGD (Figure 4). In contrast, there was no significant difference in cell attachment for RGD negative versus RGD positive MSN-L₆-dsDNA films after 4 or 24 h. This indicates that PEG chain length influences RGD presentation to the cells. Overall, L₁₂ as a spacer showed the best results, as evidenced by very low cell attachment on MSN-L₁₂-dsDNA (RGD(-)) surface and significantly enhanced cell attachment on films with RGD present (RGD(+); Figure 4).

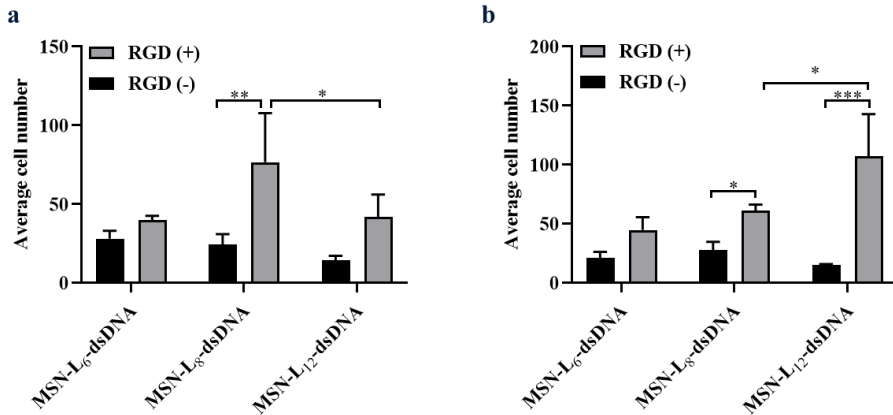


Figure 4. hMSCs attachment to MSN-L-dsDNA surfaces. Statistical results of attached cell number on MSN-L₆-dsDNA-RGD, MSN-L₈-dsDNA-RGD, MSN-L₁₂-dsDNA-RGD films compared to MSN-L-dsDNA films after a) 4 h and b) 1 day culture. The attached cell number on MSN-L-dsDNA films was quantified using CellProfiler with custom-made pipelines. Data are expressed as the mean \pm SD (n=3). *p < 0.05; **p < 0.01; ***p < 0.001.

2.5. PEG linker length affects cell morphology

Next, we studied hMSCs spreading and morphology on fabricated MSN films with and without presented RGD. After 4 and 24 h of cell culture on the films, hMSCs were fixed and stained with DAPI and phalloidin to visualize the nuclei and cytoskeletal F-actin organization, respectively, and imaged using fluorescence microscopy (Figure 5). hMSCs poorly adhered to MSN-L-dsDNA surface (without RGD present) and adhered cells exhibited a round shape with no stress fibers formed also after 24 h of incubation (Figure 5). In contrast, hMSCs significantly spread more on MSN-L-dsDNA-RGD surfaces already after 4 h and developed a highly stretched morphology with more prominent actin stress fibers after 24 h of incubation. Cell area, form factor (form factor approaches 1 for highly circular cells), and compactness (higher values indicate more irregular shaped cells) of attached hMSCs was further calculated and analyzed using Cell Profiler. The image analysis pipeline using Cell Profiler is shown in the supplementary data (Figure S7). Quantitative analysis showed that hMSCs grown on RGD presenting films (MSN-L-dsDNA-RGD; RGD(+)) exhibited a significantly larger cell area compared to hMSCs cultured on MSN films which did not present RGD (MSN-L-

dsDNA; RGD(-)), irrespective of PEG linker length (Figure 5b). In addition, the morphology of hMSCs cultured on films with RGD was overall more elongated and irregular, as evidenced by a significantly larger cell compactness and smaller cell shape factor value in comparison to that of hMSCs cultured on films without RGD (Figure 5c and d). Furthermore, hMSCs cultured on MSN-L₁₂-dsDNA-RGD surface had a similar cell area in comparison to hMSCs cultured on MSN-L₆-dsDNA-RGD surface, but showed a significantly larger compactness and significantly lower form factor. This indicates that hMSCs on MSN-L₁₂-dsDNA-RGD films were more irregular and elongated in shape compared to hMSCs on MSN-L₆-dsDNA-RGD surfaces. In summary, enhanced cell adhesion and spreading could be achieved by incorporation of RGD onto the MSN films via DNA hybridization, and efficacy of RGD functionality was affected by the chain length of the PEG linker. Overall, MSN-L₁₂-dsDNA-RGD films demonstrated highest cell number attachment and induced highest hMSC spreading.

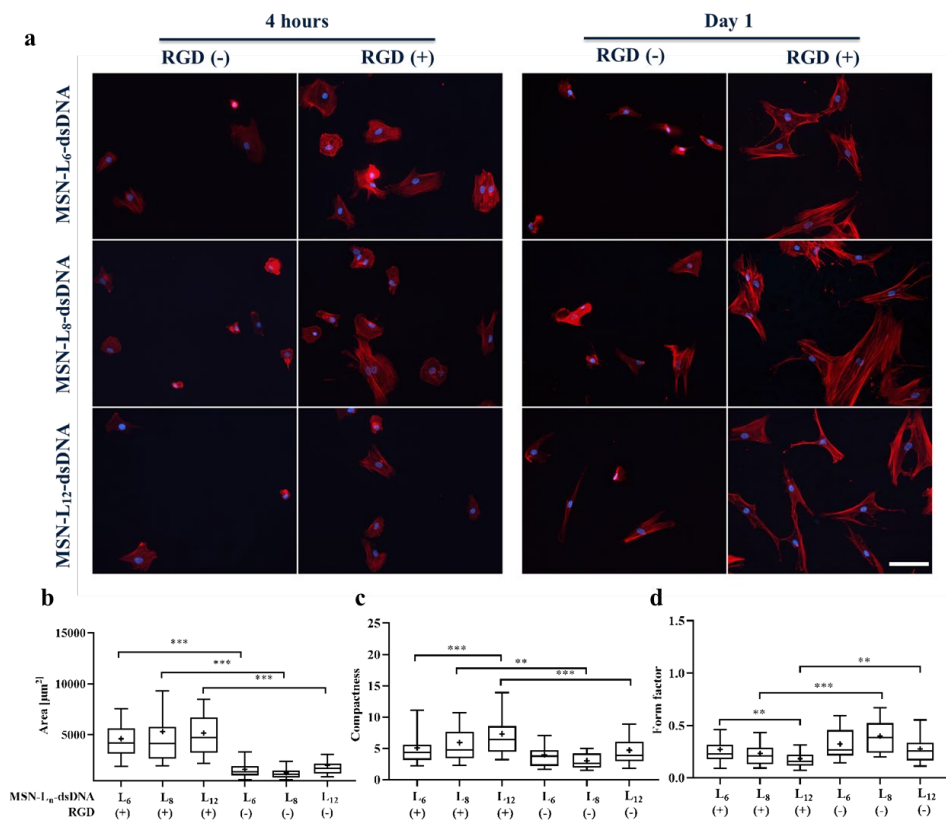


Figure 5. a) Representative fluorescence micrographs showing distinct morphology of hMSCs grown on MSN-L-dsDNA films with and without RGD for 4 h and 1 day. Cells are stained for actin (red) and nuclei (blue). Scale bar represents 100 μm . Box plots showing the b) cell area, c) compactness and d) form factor of hMSCs grown on MSN-L-dsDNA surfaces with and without RGD for 1 day (n=22-147, 3-9 images). * $p < 0.05$; ** $p < 0.01$; *** $p < 0.001$.

2.6. PEG linker length affects focal adhesion of hMSCs

Next, we assessed the ability of hMSCs to form focal adhesions after 1 and 3 days of culture on MSN-L-dsDNA films with varying PEG linker length by staining for vinculin, which is an important adaptor protein of focal adhesions [34]. Moreover, cytoskeletal F-actin reorganization was also studied by performing phalloidin staining. After 1 day of culture, limited vinculin expression was observed in any of the samples, and hMSCs showed an elongated stretched morphology. In accordance with our previous observations, more stretched morphology was observed for hMSCs cultured on L₈ and L₁₂ films. After 3 days of culture, hMSCs cultured on MSN-L₁₂-dsDNA-RGD and MSN-L₈-dsDNA-RGD films showed high vinculin expression, more focal points and presented more prominent elongated and aligned actin cytoskeleton organization compared to cells cultured on MSN-L₆-dsDNA-RGD surfaces (Figure 6a-b). Quantitative analysis showed that hMSCs grown on MSN-L₁₂-dsDNA-RGD films exhibited largest area and longest length of vinculin-containing FAs compared to hMSCs cultured on L₆ and L₈ films. (Figure 6e-f). This indicated MSN films created with longer PEG chains resulted in a more robust and strong focal adhesion of hMSCs.

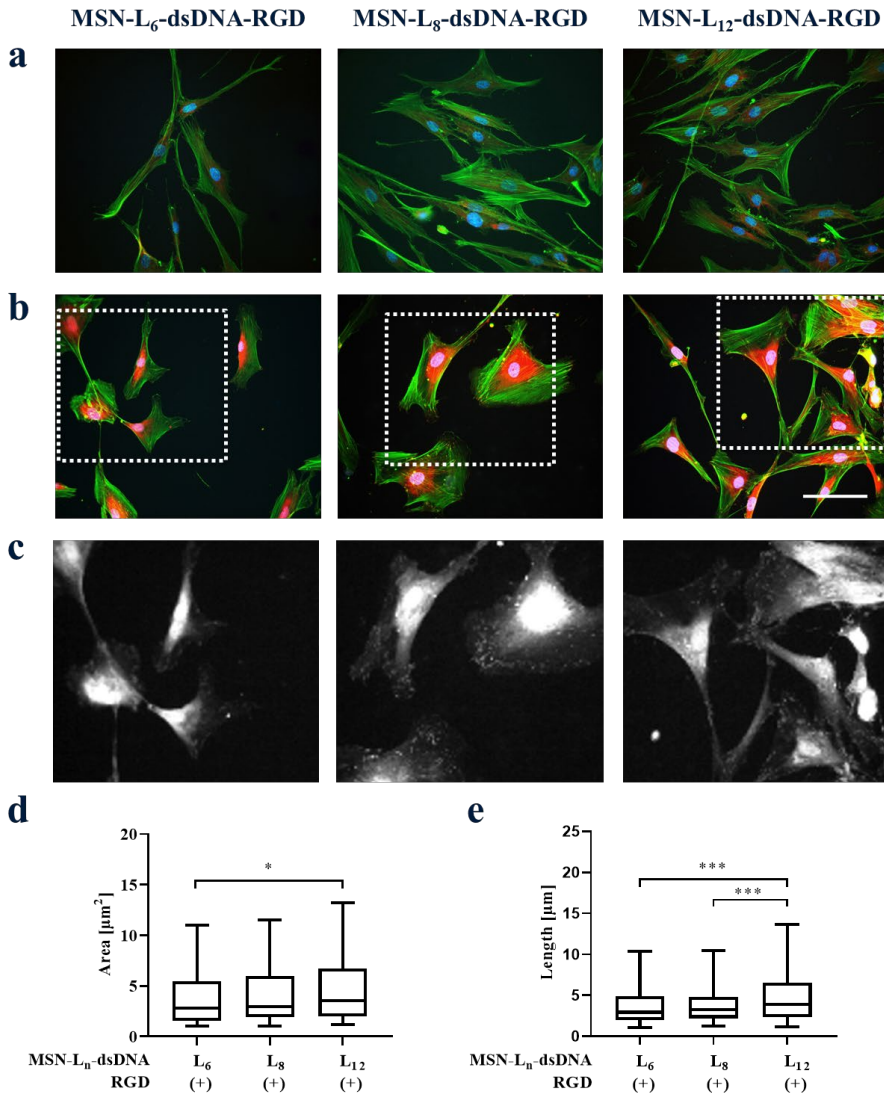


Figure 6. Representative fluorescence microscopy images of hMSCs cultured on MSN-L-dsDNA-RGD films showing focal adhesions after a) 1 and b) 3 days of culture. hMSCs were stained for focal adhesion protein vinculin (red), actin (green) and nuclei (blue). Scale bar represents 100 μm and applies to all fluorescence microscopy images. c) Magnified images from the inserts of b, and vinculin expression in white, clearly show formation of focal adhesions for hMSCs cultured on MSN-L₈-dsDNA-RGD and MSN-L₁₂-dsDNA-RGD. d) Area and e) length of focal adhesions after 3 days (n = 200).

hMSC focal adhesion to MSN-L₁₂-dsDNA-RGD films was also compared to hMSC adhesion to glass substrates after 1, 3 and 5 days of culture (Figure 7). After 1 day of culture, no evident differences could be observed in vinculin expression for hMSCs cultured on MSN-L₁₂-dsDNA-RGD films compared to hMSCs cultured on control glass substrates. After 3 and 5 days of culture, small-dot like spherical vinculin localization of hMSCs on MSN-L₁₂-dsDNA-RGD films was observed, indicating that MSN-L₁₂-dsDNA-RGD films could facilitate formation of strong focal adhesions as a function of RGD presence on the films.

Finally, we performed a live-dead assay using calcein AM and Ethidium homodimer 1 (EthD-1) to evaluate cell viability of hMSCs cultured on MSN-L₁₂-dsDNA-RGD films after 1 and 5 days of culture. Calcein AM is itself non-fluorescent and only fluoresces green after transportation through the cell membrane and hydrolysis of the acetomethoxy group by intracellular esterases in live active cells. EthD-1 binds to DNA and can only stain dead cells due to their damaged plasma membranes. Most of hMSCs on both MSN-L₁₂-dsDNA-RGD films and glass substrates were stained green after 5 days of culture and only very few red cells could be seen in the images (Figure S8). This indicated that the MSN films are biocompatible and support hMSC adhesion also after 5 days of culture. In addition, a relative higher cell density of green-stained cells was observed on MSN-L₁₂-dsDNA-RGD films compared to glass control substrates both after 1 and 5 days.

To further investigate the biocompatibility of MSN films, PrestoBlue™ metabolic activity assay was performed for hMSCs cultured on MSN-L₁₂-dsDNA-RGD films after 1 and 5 days. PrestoBlue™ analysis (Figure S9) showed that hMSCs cultured on films exhibited a higher metabolic activity compared with the glass control after 5 days, further confirming that the developed MSN films were able to support cell proliferation and maintenance of metabolic activity. These observations supported the results of focal adhesion and confirmed a good stability and biocompatibility for MSN-L₁₂-dsDNA-RGD films.

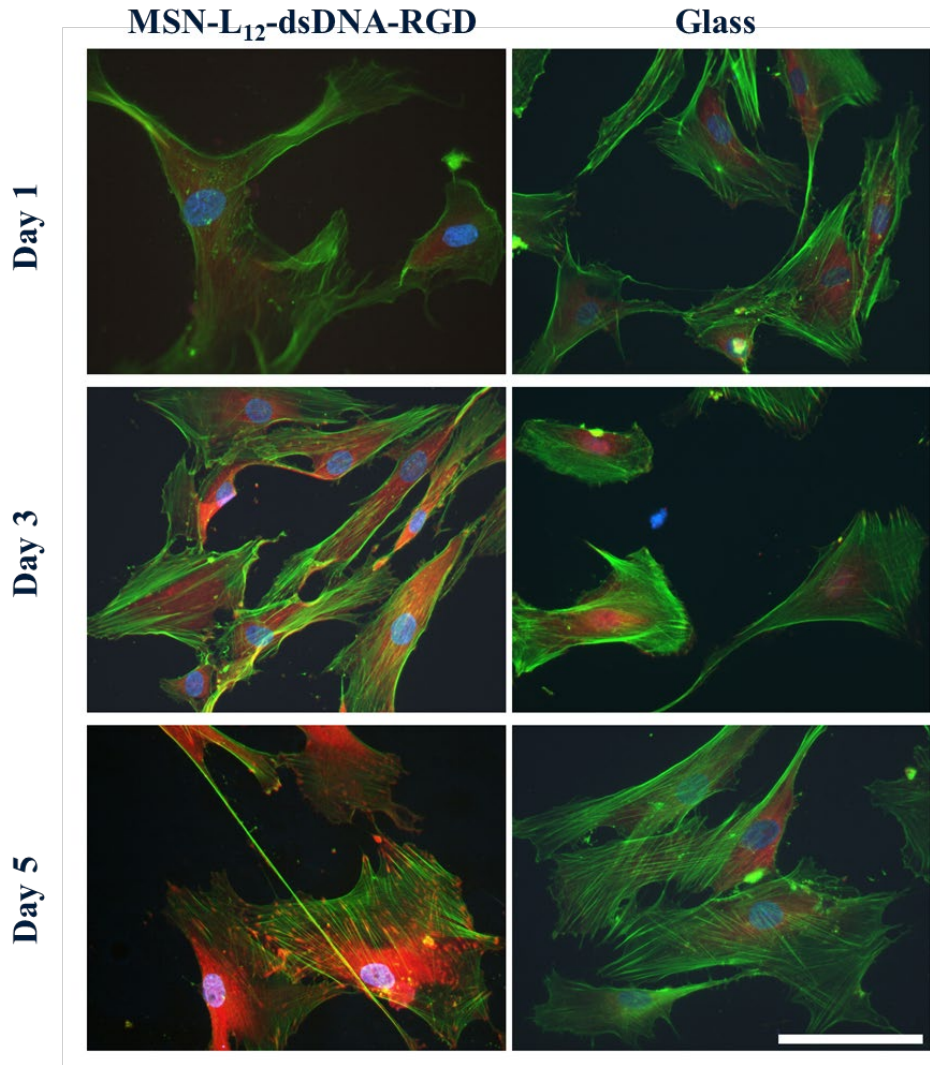


Figure 7. Fluorescence microscopy images of hMSCs cultured on MSN-PEG12-dsDNA-RGD films showing focal adhesions after 1, 3 and 5 days. hMSCs cultured on glass surface were used as negative control. Cells were stained for focal adhesion protein vinculin (red), actin (green) and nuclei (blue). Scale bar represents 100 μm and applies to all images.

3. Discussion

Here we developed a new type of biointerface based on DNA modified silica nanoparticles, which were spin coated to create a homogeneous and stable film. The developed biointerface enables selective incorporation of ligands using a DNA hybridization strategy and allows us to study specific stem cell–ligand interactions. Although here we used RGD as a ligand to study stem cell adhesion, many other ligands can also be easily incorporated onto the surface by peptide-DNA conjugation and subsequent DNA hybridization.

To optimize DNA modification of MSN, we compared two different coupling routes using MSN surface functionalized with amines or thiols (MSN-NH₂ or MSN-SH) as starting materials. Although in both these routes we used N-hydroxysuccinimide ester groups and maleimide coupling reactions, we showed that the reaction sequence influences the final DNA conjugation efficiency. This can be explained by hydrolytic degradation of the NHS ester in aqueous solutions, which is a competing reaction with NHS-NH₂ conjugation. The maleimide group is known to be more stable in aqueous solutions which can explain why the DNA grafting to MSN-NH₂ was more successful in our reactions. Our DNA grafting ratios on to MSN-NH₂ were 0.6 $\mu\text{mol g}^{-1}$, which is similar to a previous reported study [35]. Here, optimal DNA grafting per MSN was chosen, however, DNA grafting ratios to the MSN can be modulated by modulating amine functionalization on MSN starting material.

Using spin coating, homogenous and stable films made from MSN modified with PEG and DNA could be created. Spin coating is a relatively simple technique compared to lithography techniques, which have been used to create nanoparticle based biointerfaces thus far. Conjugation of adhesion tripeptide RGD to complementary DNA was possible though the use of a bifunctional PEG linker. Hybridization of the DNA-RGD conjugate to the MSN-DNA films through Watson-Crick base-pairing allowed us to create RGD presenting films. Since RGD density is a key parameter to control stem cells adhesion, we further calculated RGD amount on the films. Our results show we can achieve a higher RGD density of 85.52 pmol cm^{-2} compared to other substrates reported in the literature [36]. For example, self-assembled adamantane-terminated polystyrene-*b*-poly(ethylene oxide) (PS-PEO-Ada) films have been employed to nanopattern RGD by noncovalently conjugating β -cyclodextrin (β -CD) modified peptide onto surface

through inclusion complexing interactions between β -CDs and adamantine. In this study, the calculated highest RGD density was at 42.45 pmol cm⁻² [37].

It is also important to note that all MSN films have similarly high RGD densities, which means all MSN surface could provide adequate adhesive sites for cell binding and the observed difference in cell adhesion is because of the chain effects. Moreover, although in the current approach MSN surface was fully grafted, this can be modified to control RGD density on the films.

To investigate the effect of PEG length on hMSC ability to specifically adhere to our films, we used PEG linkers at varying chain length (PEG6, PEG8, PEG12) creating three different MSN-ssDNA films. We could see a clear effect on hMSC attachment, compactness, and form factor, depending on PEG linker length, where MSN films using PEG12 linker showed the most promising features for studying hMSC-RGD interactions. Specifically, low non-specific cell attachment was observed on RGD negative MSN-L₁₂-dsDNA surfaces, whereas high cell numbers were observed on the representative RGD positive films. This effect was also observed, although to a lesser extent on MSN-L₈-dsDNA films, and interestingly, there was no significant difference in cell number on RGD positive versus RGD negative MSN-L₆-dsDNA films. Adhered cells on MSN-L₁₂-dsDNA-RGD films also showed significantly enhanced hMSCs attachment, spreading and focal adhesion, with a significantly more elongated morphology compared to hMSC adhered to MSN-L₆-dsDNA-RGD films. This is an important feature as previous studies have shown that the morphology, intracellular cytoskeletal organization, formation and maturation of focal adhesion of stem cells are linked to stem cell differentiation [38]. These data demonstrate that PEG linker length have a clear effect on the number of hMSCs that adhere but also on their morphology, where longer chain lengths appear to allow better cell adhesion with a more spread morphology. Since there was no significant difference in surface immobilization RGD densities on the MSN films, we speculate this enhanced effect was related to the PEG length and the ability to improve RGD presentation and accessibility to hMSCs. However, we cannot exclude that the longer PEG length also alters other properties that can regulate cell adhesion processes such as the interfacial stiffness and surface roughness [39]. Our findings are in line with a previous study by Lee et al. who reported that an increase in spacer arm length led to enhanced cell spreading and proliferation in both 2D and 3D culturing systems due to an enhancing accessibility of the RGD peptides to cells with a longer chain [40]. Moreover, Chen et al. reported that a short spacer (OEG4) led to unspecific cell

adhesion [41]. In contrast, in a study by the Mrksich group, it was demonstrated that increasing the length of the oligo(ethylene glycol) groups can also result in decreased cell adhesion and spreading [42]. However, in this study another system based on SAMs was used to present the RGD to the cells. The authors discuss that longer PEG linkers could lead to crowding, resulting in the RGD being less accessible with increasing PEG length. This indicates that the optimal PEG linker length is also highly dependent on the composition and structure of the substrate. Regardless, our and previous findings by others clearly demonstrate that the linker length is an important parameter that needs to be optimized in any system to ensure proper cell adhesion.

Our study further shows that MSN-L₁₂-dsDNA-RGD films can be used as a platform to study ligand induced cell attachment, adhesion and spreading of hMSCs. Encouraged by these findings, we continued to explore if MSN-L₁₂-dsDNA-RGD films can support the formation of focal adhesion and a long-term growth of hMSCs. We found that MSN-L₁₂-dsDNA-RGD films could induce a pronounced vinculin expression in hMSCs and showed high cell viability also after 5 days of culture. As far as we are aware, this is the first report of using DNA modified MSNs and spin coating to develop a biointerface to study specific stem-cell ligand interactions.

4. Conclusions

In conclusion, we show that MSN modified with PEG and ssDNA can be spin coated to create homogenous, stable and biocompatible films, which can be used as a novel and versatile 2D biointerface to study ligand-induced stem cell adhesion processes. Stem cell–ligand interactions play an important role in regulating stem cell behavior such as adhesion, migration and differentiation [43]. Thus, biointerfaces with the capability to present ECM-derived ligand specifically and flexibly such as the one developed here, are important tools in the field of regenerative medicine to improve our understanding on how stem cell–ligand interactions contribute to regenerative processes. Using the developed MSN-ssDNA films, we investigated the impact of immobilization PEG chain length on RGD functionality and hMSCs adhesion. We demonstrated that an appropriate PEG chain length is required to achieve optimal RGD presentation and subsequent hMSC adhesion. This information can help material engineers to optimize their biomaterial design. As an example here we used RGD, however, since DNA hybridization is highly flexible and tunable, one powerful advantage of our design is

that different types of ligands or growth factors can easily be introduced into the platform to study the effect of ligand nature on stem cell processes [44]. Moreover, the programmability of DNA will also allow the design of more advanced biointerfaces where multiple ligands can be introduced at the same time, to probe, for example, the effect of ligand crosstalk. In addition, since soluble bioactive factors can be easily loaded in the mesopores of MSN, this system also allows for the simultaneous study of soluble factors as well as immobilized ligands in regulating stem cell processes. Finally, the MSN surface and size can be easily tuned to modify ligand density on the surface. As such, we envisage that this platform can be used in the future to study a wide variety of ligand induced stem cell processes.

5. Experimental Section

5.1. Materials

If not noted differently, all chemicals were purchased from Sigma Aldrich GmbH (Germany). All oligonucleotides were custom-synthesized by Integrated DNA Technologies (Leuven, Belgium). DNA sequences are shown in Table S1. RGDC peptides were purchased from Sanbio (The Netherlands). Absolute ethanol, paraformaldehyde (PFA), bovine serum albumin (BSA), Triton X-100 was purchased from VWR (US). Minimum essential medium alpha GlutaMAX (α MEM), Alexa Fluor™ 488 Phalloidin, Alexa Fluor™ 647 Phalloidin, Calcein AM was purchased from Fisher Scientific (The Netherlands). Recombinant Alexa Fluor® 647 Anti-Vinculin antibody was purchased from Abcam (1:200).

5.2. Synthesis of MSN-NH₂ and MSN-SH

MSN were synthesized based on a sol-gel co-condensation process as reported previously [45-48]. Here, two types of MSN were prepared: MSN with amine surface functionalization (MSN-NH₂) and thiol surface functionalization (MSN-SH). To synthesize MSN with amine/thiol surface functionalization, a mixture of 1.73 g tetraethyl orthosilicate (TEOS) and 14.3 g triethanolamine (TEA) was heated to 90 °C under static conditions for 20 min (Solution 1). Solution 2 was prepared by adding 100 mg of ammonium fluoride (NH₄F), 2.41 ml of cetyltrimethylammonium chloride (CTAC) to 22 ml of bi-distilled water (DIW) and heated to 60 °C for 10 min. Next, Solution 2 was quickly added to solution 1, and the mixture was stirred vigorously for 20 min, after which 138.2 mg TEOS was added to the mixture in four equal portions every 3 min, and stirred for 30 min. In the next, a mixture of 19.3 mg

TEOS with either 20.5 mg 3-Aminopropyl triethoxysilane (APTES, in the case of MSN-NH₂) or 20.5 mg 3-mercaptopropyl triethylsilane (MPTES, in the case of MSN-SH) was added and stirred overnight at room temperature. The following day, particles were collected by centrifugation and washed once with ethanol, and then redispersed in an ethanolic ammonium nitrate solution. Then, the mixture was refluxed at 90°C for 45 min. Afterwards, MSN were collected by centrifugation, washed once with ethanol, redispersed in 100 ml of a hydrochloric acid solution (HCl 37% in DIW), and refluxed again at 90°C for 45 min. Finally, MSN were collected, re-dissolved in ethanol and kept at -20°C for future use.

5.3. Validation of chemical groups of MSN MSN-NH₂ and MSN-SH

To confirm the successful surface functionalization of MSN, the respective chemical groups were labeled with fluorescent dyes. ATTO 647-maleimide and FITC-NHS were used to label thiol groups and amino groups, respectively. The labeling experiment was conducted by adding 0.5 µl of ATTO 647 solution (5 mg/ml in DMF, in the case of MSN-SH) or 20 µl of FITC-NHS (6.3 mg/ml in absolute ethanol, in the case of MSN-NH₂) to 1 ml of MSN solution (1 mg/ml in absolute ethanol). The mixture was stirred overnight in the dark. The next day, MSNs were centrifuged and washed with absolute ethanol. Then, MSN were resuspended in absolute ethanol at a concentration of 10 mg/ml and the fluorescence were measured using a CIARIOstar spectrophotometer (BMG LABTECH, Germany).

5.4. Synthesis of MSN-ssDNA

According to the manufacturer's instruction, ssDNA-SH was dissolved in TE buffer with a final concentration of 50 µM (10 mM Tris, 0.1 mM EDTA, pH 7.5) at and activated by adding tris(2-carboxyethyl)phosphine (TCEP) (5mM), and stored at -20°C until use. ssDNA-SH was purified using Microspin™ G-25 Columns (Merck). ssDNA-NH₂ was dissolved in nuclease free water to a final stocking concentration of 50 µM and stored at -20°C until use.

Stock solutions of three PEG linkers (Mal-PEG6-NHS, Mal-PEG8-NHS, Mal-PEG12-NHS) were prepared by dissolving 100 mg of linker in a proper volume of dimethyl sulfoxide (DMSO) to a final concentration of 5 mM. The stocking solution was aliquoted and stored at -20°C until use.

For conjugation of single-strand DNA onto MSN, two synthetic routes were applied, either using ssDNA-SH and MSN-NH₂, or ssDNA-NH₂ and MSN-SH. In

the case of first route, ssDNA-SH was conjugated onto MSN-NH₂ using Mal-PEG6-NHS cross linking. To this end, 2 mg of MSN were collected and resuspended in 920 μ l of PBS buffer (pH 8.3). After sonification, 80 μ l of Mal-PEG6-NHS stocking solution was added and the mixture was stirred for 4 h. Then, the solution was centrifuged and washed with water to remove excess PEG linkers. The obtained MSN-L₆ were then redissolved in 200 μ L of TE buffer (pH 7.4) and reacted with freshly activated ssDNA overnight. Finally, ssDNA-SH modified MSN were obtained by centrifugation, followed by washing, and then redispersed in water for storage at -20 °C. The unbind ssDNA in suspension and washing solution was collected and combined to quantify the amount of immobilized DNA on the particle surface using NanoDrop Microvolume Spectrophotometer. The second synthesis route was performed in a reversible way. In brief, MSN-SH was reacted with Mal-PEG6-NHS in TE buffer (pH 7.4) overnight to yield NHS-functionalized particles. Following centrifugation and washing, the particles were dispersed in PBS buffer (pH 8.3) and mixed with ssDNA-NH₂ for 4 h at room temperature.

Since it was observed that synthetic route 1 showed a higher DNA conjugation efficiency, MSN-L₈-ssDNA, MSN-L₁₂-ssDNA were prepared following the exactly same protocol of synthetic route 1, except using Mal-PEG8-NHS and Mal-PEG12-NHS instead of Mal-PEG6-NHS.

5.5. TEM and DLS Measurement of Nanoparticles

The hydrodynamic particle size, PDI and zeta potential of MSN and MSN-L-ssDNA were analyzed using Malvern Zetasizer Nano (Malvern Panalytical, UK). For size measurements, nanoparticles were suspended in absolute ethanol at a concentration of 0.5 mg/ml. For zeta potential measurements, nanoparticles were suspended in HEPES buffer (pH 7.2, 25 mM) at 0.1 mg/ml concentration. The morphologies of MSN and ssDNA modified MSN were selectively examined by TEM (JEM-100CX II, Japan). The nanoparticles that suspended in absolute ethanol were dropped onto a copper grid and air-dried at RT overnight before TEM imaging. At least 5 nanoparticles from the captured TEM images were used to determine nanoparticle size using Image J.

5.6. Preparation and characterization of MSN films

MSN films were created using spin coating. Immediately prior to spin coating, coverslips with a diameter of 22 mm were surface-cleaned and activated with O₂

plasma treatment (Plasma Cleaner, Diener Electronics Femto PCCE) at 0.4 bar, 5 sscm O₂, 70 W, 10 min. Nanoparticles were collected by centrifugation and redispersed in bi-distilled water at a concentration of 40 mg ml⁻¹. 25 µl of the nanoparticle suspension was pipetted centrally on a coverslip and spun at on the tabletop of spin coater (800 rpm for 10 seconds and then 2050 rpm for another 10 seconds). All DNA modified MSN-films were stored dry at 4°C for future use. To characterize the films, 3D laser scanning microscopy (Keyence VR-3000 3D Profilometer, Keyence, Japan) was used to assess film thickness. For this, three locations from each sample (center of sample, between center and edge, and edge of sample) of three samples were used for analysis. For each location, a scratch line was made using a peptide tip. Then the vertical distance (film thickness) between the scratch (lowest point) to area with coating (highest point) was measured. SEM (Teneo, FEI, US) imaging was used to analyze the surface properties of the films and assess the coating quality. For SEM analysis, spin-coated MSN-L-ssDNA films were sputtered with a 2-nm layer of iridium and imaged at 25000 x and 10000 x magnification. WCA of substrates was measured by a sessile drop technique at room temperature using a contact angle goniometer (Drop shape Analyzer DSA25, Kruss, Germany). For this, spin coated coverslips were fixed on a stage of the goniometer. A droplet of 5 µl water dropped onto the films and the values were read after 1 minute. To investigate the film stability, the thiol-core and amine-surface functionalized MSN was first synthesized and labeled with ATTO 488-mal in the core by stirring overnight [49]. After that, ATTO 488 labeled MSN was further modified with ssDNA and ATTO 488 labeled MSN-ssDNA films was prepared by spin coating. Then, the films were incubated in 2 ml of PBS or cell culture medium at RT. 100 µl aliquots of the supernatant were collected after 1 d and 7 d, and 14 d of incubation. The released amount of MSN-ssDNA from films was analysed using a CLARIOstar spectrophotometer (BMG Labtech, Germany). To investigate cellular uptake of nanoparticles from the MSN-ssDNA films, hMSCs were seeded on spin-coated coverslips with ATTO 647 core-labelled MSN-ssDNA. Uncoated coverslips were used as negative control. Cellular uptake was measured after 1 and 5 days using fluorescence-activated cell sorting (FACS, Accuri B6 flow cytometer, BD Biosciences, US).

5.7. Synthesis and characterization of csDNA-RGD conjugate

The conjugation was carried out according to a previous study [50]. In brief, a stock solution of csDNA-NH₂ was prepared by dissolving 1000 nmol of dry-delivered

csDNA-NH₂ in 1 ml of nuclease-free water. To synthesize DNA-linker composites (DNA-PEG₆-L), 100 μ l of csDNA-NH₂ stock (20 nmol) was mixed with 40 μ l of the linker solution (166 mM in DMSO). The reaction was conducted in 1 ml of KH₂PO₄ buffer (100 mM, pH 7.2) for 1 h at RT. Then DNA-PEG₆-L was purified and concentrated by centrifugation using Amicon Ultra Centrifugal Filter (Merck). Concentrated DNA-PEG₆-L was diluted in 1 ml of KH₂PO₄ buffer (100 mM, pH 7.2) and mixed with 50 μ l of RGDC solution (5 mg/ml in nuclease-free water). The mixture was incubated at room temperature overnight. The next day, csDNA-RGD conjugate was purified by centrifugation, dissolved in a solution of ULC/MS grade water (Biosolve) and ULC/MS grade acetonitrile (Biosolve) (50:50) and analyzed using LC-ESI-MS.

5.8. DNA hybridization

Hybridization assay was performed in suspension and on the films using FAM labeled csDNA and characterized using a Cary Eclipse Fluorescence Spectrophotometer and CLARIOstar spectrophotometer, respectively. For DNA hybridization in suspension, 250 μ l of MSN-L₆-ssDNA suspension (2 mg mL⁻¹, in H₂O) were mixed with 30 μ l of FAM labeled csDNA (csDNA-FAM, 100 μ M, in water) or FAM labeled msDNA (msDNA-FAM, 100 μ M, in water), and allowed to incubate at RT in dark for 6 h in hybridization buffer (20 mM Tris, 37.5 mM MgCl₂, pH 8.0). Afterwards, the hybridized MSN-L₆-dsDNA-FAM were collected by centrifugation and the pellet was dispersed in nuclease-free water, and the fluorescence intensity was detected using Cary Eclipse Fluorescence Spectrophotometer.

Hybridization on films was also analyzed. To this end, spin coated MSN-L-ssDNA films (MSN-L₆-ssDNA films, MSN-L₈-ssDNA films, MSN-L₁₂-ssDNA films) were placed in 6-well plate and immersed in 2 ml of hybridization buffer containing csDNA-FAM (5 nmol), and incubated at 4°C in Dark for 30 min. After hybridization, the films were washed with hybridization buffer and the fluorescence intensity was measured using CLARIOstar spectrophotometer (BMG Labtech, Germany). To quantify the amount of DNA which absorbed unspecifically onto film surface, MSN films in the absence of ssDNA were prepared and exposed to csDNA-FAM. In addition, msDNA-FAM was added to MSN-L₆-ssDNA films to determine the specific of DNA duplex binding. The same protocol was applied for hybridization of MSN-L-ssDNA films and csDNA-RGD.

5.9. hMSC *in vitro* cell culture

hMSCs were obtained from one donor with informed consent and cultured in α MEM medium supplemented with 10% (v/v) fetal bovine serum (FBS), 0.2 mM ascorbic-acid-2-phosphate (ASAP), and incubated in a humidified incubator in an atmosphere of 5% CO₂ at 37°C. All the experiments of hMSCs were conducted using cells before passage 6. Cell seeding densities varied depending on individual experiment and detailed information could be found in each experimental section.

5.10. Cell morphology staining

Cell attachment to surfaces was evaluated by staining hMSCs for F-actin and nuclei using Alexa Fluor™ 647 Phalloidin and 4',6 diamidino-2-phenylindole (DAPI) on the MSN films. After surface hybridization with csDNA or csDNA-RGD, hMSCs were seeded onto the films at a density of 3000 cells cm⁻² and 2000 cells cm⁻² for culturing 4 h and 1 day, respectively. After 4 h and 1 day of culturing, the cells were fixed with 4% PFA for 10 min. After rinsing with PBS three times, the cells were permeabilized with Triton X-100 (0,2% (vol/vol) in PBS) for 10 min, washed three times with PBS and blocked with blocking buffer (10% (w/v) BSA in PBS) for 5 min at RT. Afterwards, the cells were stained with Alexa Fluor™ 647 Phalloidin (1:100 in PBS) overnight at 4°C, followed by DAPI staining (1:100 in PBS) for 10 min. Then the films were rinsed thoroughly in PBS, mounted on a glass slide with mounting media (Dako), and imaged using a Nikon Eclipse Ti-E microscope (Nikon Instruments Europe BV, the Netherlands) at 10x (to image DAPI) and 20x objectives (to image DAPI and Phalloidin). Images were further processed to analyze attached cell number and cell morphology using CellProfiler software [20, 27]. The attached cell number was determined by applying Otsu adaptive thresholding method on the DAPI channel. The average cell number refers to the mean number of cell nuclei from three different images captured using a 10x objective. The cell morphology was analyzed by applying Otsu adaptive thresholding method on both DAPI and Phalloidin channel. To quantify morphological parameters, F-actin staining from each cell of at least 20 cells from 3-9 different images captured with a 20x objective was used. The morphological parameters including cell spreading area (the number of pixels occupied), compactness (squared distance of the object pixels from the centroid divided by the area) [20], and form factors (numbers closer to 1 describes rounder cells) were quantified [27].

5.11. Focal adhesion using vinculin staining

Cell focal adhesion on MSN-L-dsDNA-RGD films was determined by immunohistochemical staining of the focal adhesion protein vinculin. Briefly, cells cultured on MSN-L-dsDNA-RGD films and glass substrate were fixed 4% PFA for 10 min, permeabilized with Triton X-100 (0.2% (vol/vol) in PBS) for 10 min and then blocked with blocking buffer (4% (w/v) BSA and 0.05% (v/v) Tween in PBS) for 1 h at RT. Then the cells were incubated with Alexa Fluor® 647 Anti-Vinculin antibody (1:200 in blocking buffer) overnight at 4°C, followed by washing three times with PBS. To visualize actin bundles and nuclei, cells were further stained with Alexa Fluor™ 488 Phalloidin (1:40 in PBS) for 1 h at RT and DAPI ((1:100 in PBS) for 15 min at RT, respectively. After washing three times, the cells were mounted Dako®. To determine focal adhesions, 3-6 images from different samples were taken with a Nikon Eclipse Ti-E microscope (Nikon Instruments Europe BV, the Netherlands) using 40x objective. Images were further processed to quantify the length and area of vinculin-containing FAs using NIS-Elements AR Analysis 5.30 with custom-made pipelines.

5.12. Live/dead staining

The cell viability of hMSCs cultured on MSN-L-dsDNA-RGD films was evaluated by live/ dead staining. In order to obtain similar cell numbers at the time of measurement, seeding densities were varied for different time points as: 2000 cells cm⁻² for 1 day and 1000 cells cm⁻² for 5 days. After 1 and 5 days, the cells were washed once with PBS and incubated with a staining solution containing 1 µM of calcein-AM and 2 µM of Ethidium homodimer at 37 C for 30 minutes. After washing once with PBS, the cells were imaged immediately with a Nikon Eclipse Ti-E microscope (Nikon Instruments Europe BV, the Netherlands).

5.13. Assessment of cytocompatibility of MSN films

Cytocompatibility of MSN films was evaluated with metabolic activity assay [51]. Briefly, cells were seeded on MSN-L-dsDNA-RGD films and glass substrate at a density of 2000 cells cm⁻². At day 1 and day 5, cell culture medium was removed and the coverslips with cells (n=3) were washed with PBS, followed by the addition of 2 ml of 10% PrestoBlue™ (Fisher Scientific) in culture medium to each well. After 40 min of incubation at 37° C in the dark, 100 µL of solution was transferred to a black 96-well plate with clear bottom and fluorescence was measured on a microplate reader (BMG Labtech CLARIOstar, Germany) at 590 nm.

5.14. Statistical analysis

All data was statistically analyzed using one-way analysis of variance (ANOVA) followed by a Turkey's multiple comparison post hoc test. All data was expressed as the mean \pm standard deviation. For all figures the following p-values apply: *p < 0.05; **p < 0.01; ***p < 0.001. A difference with a p value less than 0.05 was considered statistically significant.

Authorship contribution statement

Xingzhen Zhang: Conceptualization, Methodology, Validation, Formal analysis, Investigation, Writing–original draft, Visualization. Sabine van Rijt: Conceptualization, Writing–review & editing, Supervision, Project administration.

Conflict of Interest

The authors declare no conflict of interest.

Acknowledgements

We acknowledge China Scholarship Council (grant number 201806220082) for financial support. We thank Ronny Mohren for technical assistance with ESI MS. We thank Denis van Beurden for technical assistance with SEM imaging and Eva Gubbins for technical assistance with the profilometer.

Supporting Information

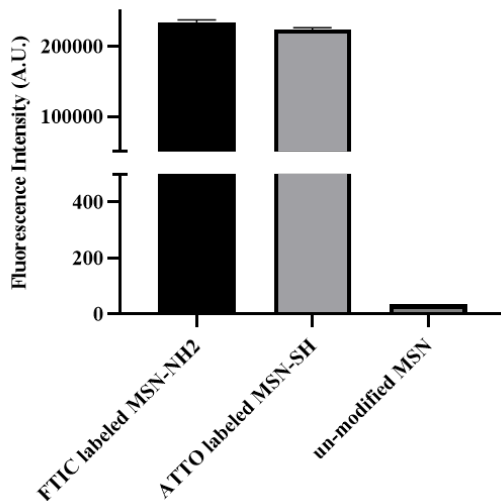


Figure S1. Fluorescence intensity (a.u.) of FITC-NHS labeled MSN-NH2 and ATTO 647-labeled MSN-SH. Un-modified MSN used as control.

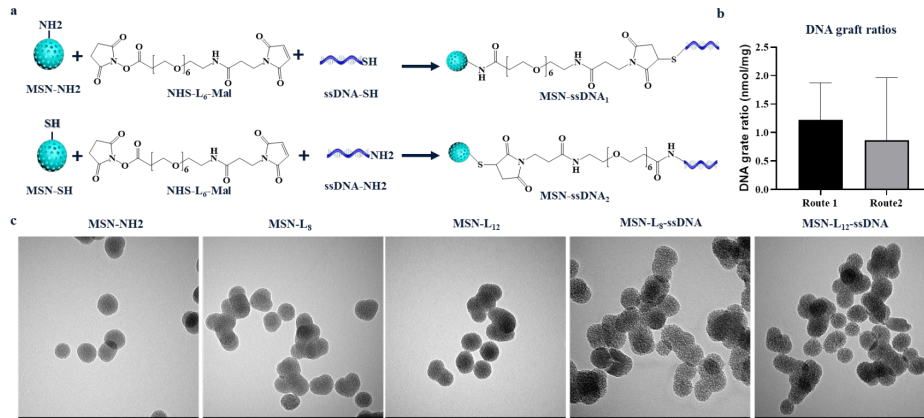


Figure S2. Optimization of ssDNA conjugation to MSN. a) Schematic illustration of two synthesis routes of MSN-ssDNA using NHS-PEG₆-Mal as a linker. b) DNA graft ratios of MSN following two synthesis routes. c) TEM images of MSN-NH₂, MSN-L₈, MSN-L₁₂, MSN-L₈-ssDNA, MSN-L₁₂-ssDNA, scale bar represents 100 nm.

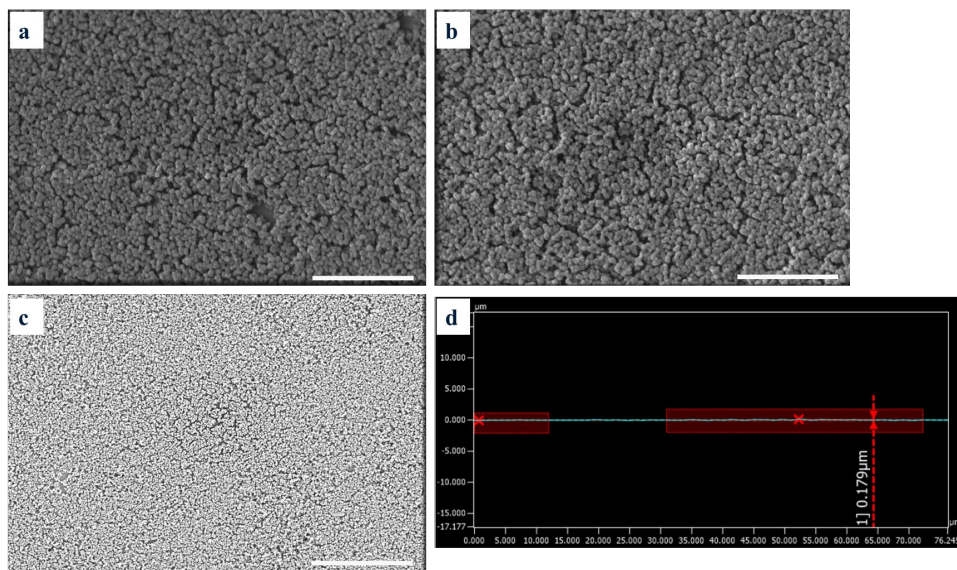


Figure S3. SEM image of spin-coated a) MSN-L₈-ssDNA films and b) MSN-L₁₂-ssDNA films. Scale bar = 2 μm. c) A low magnification SEM image of MSN-L₆-ssDNA film. Scale bar = 5 μm. d) A representative 3D laser scanning microscopy image showing the smooth surface profile of the MSN film. The arrow indicates the film thickness, which is the vertical distance between the highest point (the left red cross) and lowest point (the right red cross) of the surface. Details of measurements were shown in the experimental section.

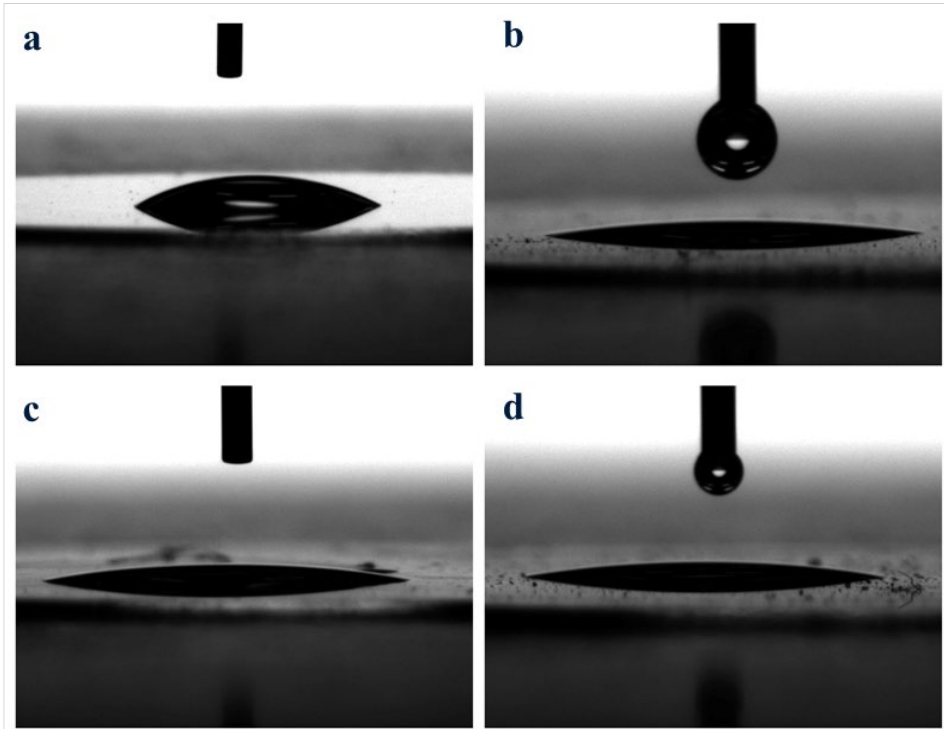


Figure S4. The contact angle measurement of a) uncoated glass surfaces, glass coated with b) MSN-L₆-ssDNA, c) MSN-L₈-ssDNA and d) MSN-L₁₂-ssDNA.

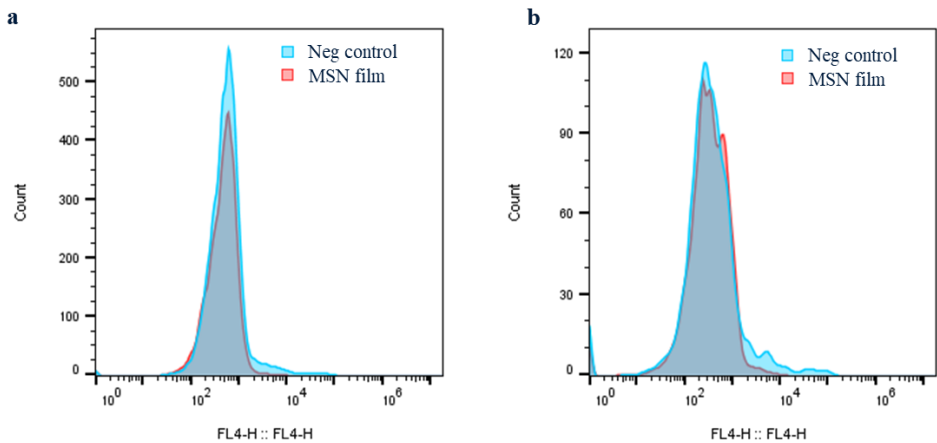


Figure S5 Histograms of total take of nanoparticles by hMSCs from glass cover slips (neg control), ATTO 674 labelled MSN-L12-ssDNA films after a) 1 and b) 5 days of culture.

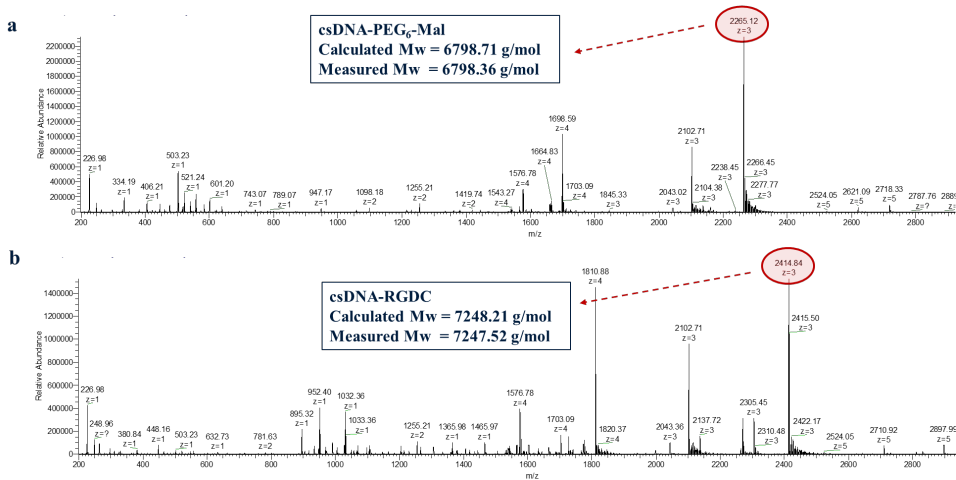


Figure S6. Mass spectrum of csDNA-PEG₆-Mal and csDNA-RGDC conjugates. The m/z values for the major isotopic species are indicated. The m/z value of most evident peak was used to do deconvolution.

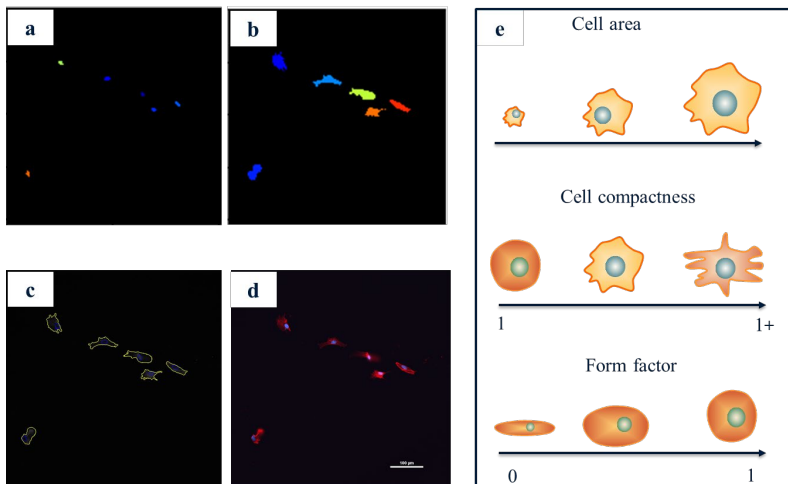


Figure S7. Image analysis workflow with CellProfiler including a) identification of objectives based on nuclei staining, b) identification of cells based on phalloidin staining, c) overlay of objectives and cells. d) An example fluorescent microscopy image showing DAPI (blue) and phalloidin (red) staining that were used for analysis. Scale bar represents 100 μm and applies to images a-d. e) Schematic illustrations of the morphological parameters including spreading area, compactness and form factor.

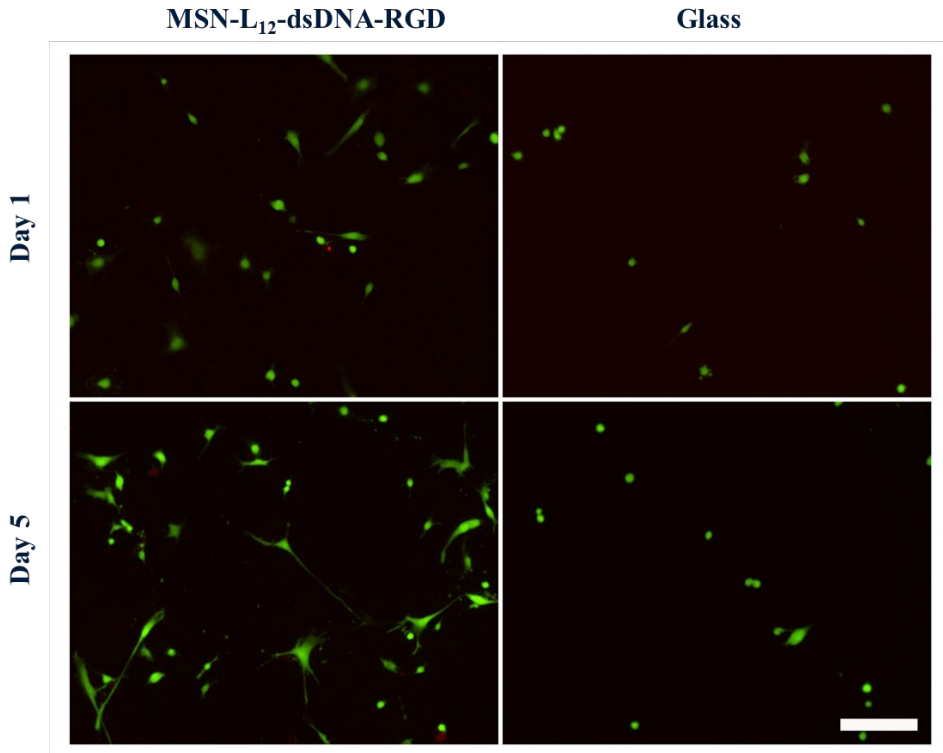


Figure S8. Live/dead staining of hMSCs cultured on MSN-L₁₂-dsDNA-RGD films (left) and glass substrate (right). Scale bar represents 200 μ m.

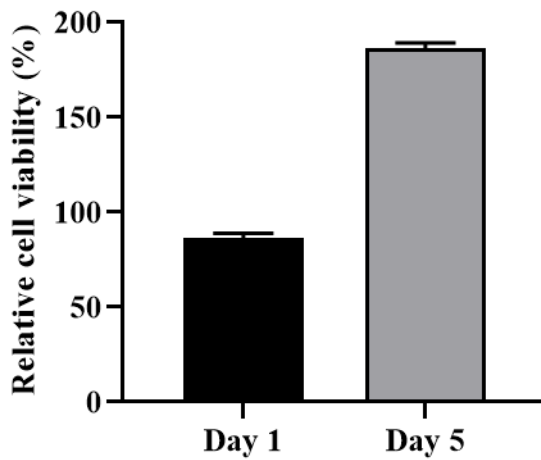


Figure S9. The viability of hMSCs cultured for 1 and 5 days on MSN-L₁₂-dsDNA-RGD films. Cell viability values were expressed as the percentage of fluorescence intensity relative to the glass controls.

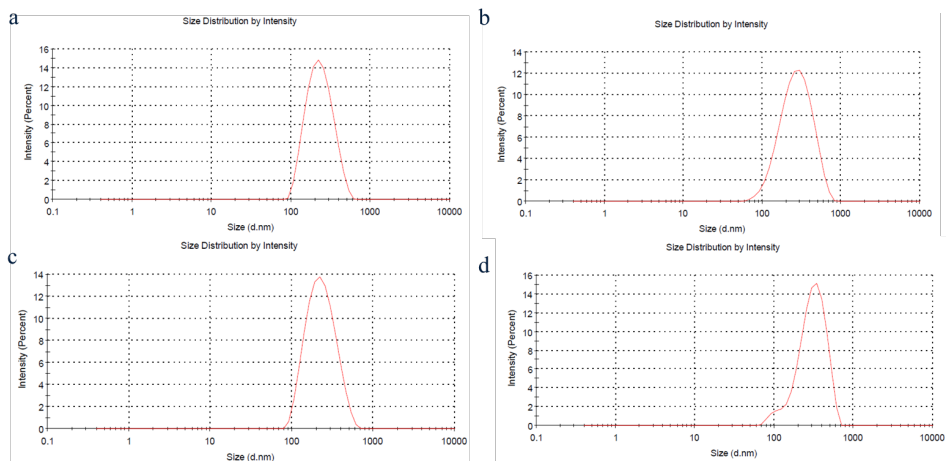


Figure S10. Representative size distribution plots of a) MSN-NH₂, b) MSN-L₆-ssDNA, c) MSN-L₈-ssDNA, and d) MSN-L₁₂-ssDNA. Details of measurements are shown in the Experimental Section.

Table S1. List of DNA sequences used in this study.

DNA name	Sequence and modification
ssDNA-SH	5'- /5ThioMC6-D/ TT ATA CAT CTA TTC GTG TGA -3'
ssDNA-NH ₂	5'- /5AmMC6/CC CTA GAG TGA GTC GTA TGA -3'
csDNA-NH ₂	5'- /5AmMC6/TC ACA CGA ATA GAT GTA TAA -3'
csDNA-FAM	5'- /56-FAM/TC ACA CGA ATA GAT GTA TAA -3'
msDNA-FAM	5'- /56-FAM/TA GAT CTC ACT CAC CAT ACT -3'

Table S2. Physical characterization of the synthesized MSN-L_n.

Items	Hydrodynamic diameter [nm]	PDI	Zeta potential [mV]
MSN-L ₆	196.80 ± 1.28	0.15 ± 0.02	-22.50 ±1.25
MSN-L ₈	199.40 ± 1.37	0.09 ± 0.01	-21.43 ± 0.57
MSN-L ₁₂	225.57 ± 0.85	0.17 ± 0.02	-21.40 ± 0.35

Table S3. Stability of MSN-L₁₂-ssDNA films. Fluorescent intensity measured in the supernatant of incubated MSN-L₁₂-ssDNA films with ATTO 488 fluorescently labelled MSNs after 1, 7 and 14 days incubation in PBS and cell culture medium. Values shown as mean ± SD.

Time [days]	Release from films in PBS [%]	Release from films in cell culture medium [%]
1	0.01 ± 0.0000088	0.01 ± 0.0000166
7	0.02 ± 0.0000641	0.02 ± 0.0000406
14	0.02±0.0001286	0.04 ± 0.0006325

References

- [1] W. Zakrzewski, M. Dobrzyński, M. Szymonowicz, Z. Rybak, Stem cells: past, present, and future, *Stem Cell Research & Therapy* 10(1) (2019) 68.
- [2] H. Wang, X. Luo, J. Leighton, Extracellular Matrix and Integrins in Embryonic Stem Cell Differentiation, *Biochem Insights* 8(Suppl 2) (2015) 15-21.
- [3] H. Donnelly, M. Salmeron-Sanchez, M.J. Dalby, Designing stem cell niches for differentiation and self-renewal, *Journal of the Royal Society, Interface* 15(145) (2018).
- [4] F. Gattazzo, A. Urciuolo, P. Bonaldo, Extracellular matrix: a dynamic microenvironment for stem cell niche, *Biochim Biophys Acta* 1840(8) (2014) 2506-19.
- [5] J.K. Mouw, G. Ou, V.M. Weaver, Extracellular matrix assembly: a multiscale deconstruction, *Nat Rev Mol Cell Biol* 15(12) (2014) 771-85.
- [6] X. Zhang, S. van Rijt, 2D biointerfaces to study stem cell-ligand interactions, *Acta Biomater* 131 (2021) 80-96.
- [7] D.S.H. Wong, J.N. Li, X.H. Yan, B. Wang, R. Li, L. Zhang, L.M. Bian, Magnetically Tuning Tether Mobility of Integrin Ligand Regulates Adhesion, Spreading, and Differentiation of Stem Cells, *Nano Letters* 17(3) (2017) 1685-1695.
- [8] S. Sankaran, E. Cavatorta, J. Huskens, P. Jonkheijm, Cell Adhesion on RGD-Displaying Knottins with Varying Numbers of Tryptophan Amino Acids to Tune the Affinity for Assembly on Cucurbit[8]uril Surfaces, *Langmuir* 33(35) (2017) 8813-8820.
- [9] J.N. Roberts, J.K. Sahoo, L.E. McNamara, K.V. Burgess, J.L. Yang, E.V. Alakpa, H.J. Anderson, J. Hay, L.A. Turner, S.J. Yarwood, M. Zelzer, R.O.C. Oreffo, R.V. Ulijn, M.J. Dalby, Dynamic Surfaces for the Study of Mesenchymal Stem Cell Growth through Adhesion Regulation, *ACS Nano* 10(7) (2016) 6667-6679.
- [10] B. Trappmann, J.E. Gautrot, J.T. Connelly, D.G.T. Strange, Y. Li, M.L. Oyen, M.A. Cohen Stuart, H. Boehm, B. Li, V. Vogel, J.P. Spatz, F.M. Watt, W.T.S. Huck, Extracellular-matrix tethering regulates stem-cell fate, *Nat. Mater.* 11(7) (2012) 642-649.
- [11] S.J. Ellis, G. Tanentzapf, Integrin-mediated adhesion and stem-cell-niche interactions, *Cell Tissue Res* 339(1) (2010) 121-30.
- [12] G. Kocer, P. Jonkheijm, About Chemical Strategies to Fabricate Cell-Instructive Biointerfaces with Static and Dynamic Complexity, *Adv Healthc Mater* 7(14) (2018) e1701192.
- [13] Y. Yang, X. Wang, Y. Wang, X. Hu, N. Kawazoe, Y. Yang, G. Chen, Influence of Cell Spreading Area on the Osteogenic Commitment and Phenotype Maintenance of Mesenchymal Stem Cells, *Scientific Reports* 9(1) (2019) 6891.

- [14] J.E. Frith, R.J. Mills, J.J. Cooper-White, Lateral spacing of adhesion peptides influences human mesenchymal stem cell behaviour, *J Cell Sci* 125(Pt 2) (2012) 317-27.
- [15] T. Satav, J. Huskens, P. Jonkheijm, Effects of Variations in Ligand Density on Cell Signaling, *Small* 11(39) (2015) 5184-99.
- [16] J. Li, Y. Chen, N. Kawazoe, G. Chen, Ligand density-dependent influence of arginine–glycine–aspartate functionalized gold nanoparticles on osteogenic and adipogenic differentiation of mesenchymal stem cells, *Nano Research* 11(3) (2018) 1247-1261.
- [17] A. Lagunas, I. Tsintzou, Y. Vida, D. Collado, E. Pérez-Inestrosa, C. Rodríguez Pereira, J. Magalhaes, J.A. Andrades, J. Samitier, Tailoring RGD local surface density at the nanoscale toward adult stem cell chondrogenic commitment, *Nano Research* 10(6) (2016) 1959-1971.
- [18] J. Robertus, W.R. Browne, B.L. Feringa, Dynamic control over cell adhesive properties using molecular-based surface engineering strategies, *Chem Soc Rev* 39(1) (2010) 354-78.
- [19] P. Neiryck, J. Brinkmann, Q. An, D.W. van der Schaft, L.G. Milroy, P. Jonkheijm, L. Brunsveld, Supramolecular control of cell adhesion via ferrocene-cucurbit[7]uril host-guest binding on gold surfaces, *Chem Commun (Camb)* 49(35) (2013) 3679-81.
- [20] P. Sutthavas, P. Habibovic, S.H. van Rijt, The shape-effect of calcium phosphate nanoparticle based films on their osteogenic properties, *Biomaterials Science* 9(5) (2021) 1754-1766.
- [21] Y. Hou, L. Yu, W. Xie, L.C. Camacho, M. Zhang, Z. Chu, Q. Wei, R. Haag, Surface Roughness and Substrate Stiffness Synergize To Drive Cellular Mechanoresponse, *Nano Letters* 20(1) (2020) 748-757.
- [22] Y. Hou, W. Xie, L. Yu, L.C. Camacho, C. Nie, M. Zhang, R. Haag, Q. Wei, Surface Roughness Gradients Reveal Topography-Specific Mechanosensitive Responses in Human Mesenchymal Stem Cells, *Small* 16(10) (2020) 1905422.
- [23] H. Kang, H.J. Jung, D.S.H. Wong, S.K. Kim, S. Lin, K.F. Chan, L. Zhang, G. Li, V.P. Dravid, L. Bian, Remote Control of Heterodimeric Magnetic Nanoswitch Regulates the Adhesion and Differentiation of Stem Cells, *Journal of the American Chemical Society* 140(18) (2018) 5909-5913.
- [24] T.-M. Liu, J. Conde, T. Lipiński, A. Bednarkiewicz, C.-C. Huang, Revisiting the classification of NIR-absorbing/emitting nanomaterials for in vivo bioapplications, *NPG Asia Materials* 8(8) (2016) e295-e295.
- [25] M. Zhu, G. Baffou, N. Meyerbröker, J. Polleux, Micropatterning Thermoplasmonic Gold Nanoarrays To Manipulate Cell Adhesion, *ACS Nano* 6(8) (2012) 7227-7233.

- [26] L. Chen, X. Zhou, C. He, Mesoporous silica nanoparticles for tissue-engineering applications, *Wiley Interdiscip Rev Nanomed Nanobiotechnol* 11(6) (2019) e1573.
- [27] L. Andree, D. Barata, P. Sutthavas, P. Habibovic, S. van Rijt, Guiding mesenchymal stem cell differentiation using mesoporous silica nanoparticle-based films, *Acta Biomater* 96 (2019) 557-567.
- [28] C. Wolf-Brandstetter, V. Hänchen, B. Schwenzer, N. Aeckerle, H. Schliephake, D. Scharnweber, Application of Lateral and Distance Spacers in an Oligonucleotide Based Immobilization System for Bioactive Molecules onto Titanium Implants, *ACS Applied Materials & Interfaces* 8(6) (2016) 3755-3764.
- [29] L. Yu, Y. Hou, W. Xie, J.L.C. Camacho, C. Cheng, A. Holle, J. Young, B. Trappmann, W. Zhao, M.F. Melzig, E.A. Cavalcanti-Adam, C. Zhao, J.P. Spatz, Q. Wei, R. Haag, Ligand Diffusion Enables Force-Independent Cell Adhesion via Activating $\alpha 5\beta 1$ Integrin and Initiating Rac and RhoA Signaling, *Advanced Materials* 32(29) (2020) 2002566.
- [30] L. Yu, Y. Hou, W. Xie, J.L. Cuellar-Camacho, Q. Wei, R. Haag, Self-Strengthening Adhesive Force Promotes Cell Mechanotransduction, *Advanced Materials* 32(52) (2020) 2006986.
- [31] B. Cao, Z. Li, R. Peng, J. Ding, Effects of cell–cell contact and oxygen tension on chondrogenic differentiation of stem cells, *Biomaterials* 64 (2015) 21-32.
- [32] K. Ye, X. Wang, L. Cao, S. Li, Z. Li, L. Yu, J. Ding, Matrix Stiffness and Nanoscale Spatial Organization of Cell-Adhesive Ligands Direct Stem Cell Fate, *Nano Letters* 15(7) (2015) 4720-4729.
- [33] X. Wang, C. Yan, K. Ye, Y. He, Z. Li, J. Ding, Effect of RGD nanospacing on differentiation of stem cells, *Biomaterials* 34(12) (2013) 2865-74.
- [34] J.D. Humphries, P. Wang, C. Streuli, B. Geiger, M.J. Humphries, C. Ballestrem, Vinculin controls focal adhesion formation by direct interactions with talin and actin, *The Journal of cell biology* 179(5) (2007) 1043-1057.
- [35] P. Sun, A. Leidner, S. Weigel, P.G. Weidler, S. Heissler, T. Scharnweber, C.M. Niemeyer, Biopebble Containers: DNA-Directed Surface Assembly of Mesoporous Silica Nanoparticles for Cell Studies, *Small* 15(20) (2019) e1900083.
- [36] A. Lagunas, J. Comelles, E. Martínez, E. Prats-Alfonso, G.A. Acosta, F. Albericio, J. Samitier, Cell adhesion and focal contact formation on linear RGD molecular gradients: study of non-linear concentration dependence effects, *Nanomedicine* 8(4) (2012) 432-9.
- [37] H. Li, J. Frith, J.J. Cooper-White, Modulation of stem cell adhesion and morphology via facile control over surface presentation of cell adhesion molecules, *Biomacromolecules* 15(1) (2014) 43-52.
- [38] J.E. Frith, R.J. Mills, J.E. Hudson, J.J. Cooper-White, Tailored integrin-extracellular matrix interactions to direct human mesenchymal stem cell differentiation, *Stem cells and development* 21(13) (2012) 2442-2456.

- [39] Q. Sun, Y. Hou, Z. Chu, Q. Wei, Soft overcomes the hard: Flexible materials adapt to cell adhesion to promote cell mechanotransduction, *Bioactive Materials* 10 (2022) 397-404.
- [40] J.W. Lee, Y.J. Park, S.J. Lee, S.K. Lee, K.Y. Lee, The effect of spacer arm length of an adhesion ligand coupled to an alginate gel on the control of fibroblast phenotype, *Biomaterials* 31(21) (2010) 5545-51.
- [41] Q. Chen, S. Yu, D. Zhang, W. Zhang, H. Zhang, J. Zou, Z. Mao, Y. Yuan, C. Gao, R. Liu, Impact of Antifouling PEG Layer on the Performance of Functional Peptides in Regulating Cell Behaviors, *J Am Chem Soc* 141(42) (2019) 16772-16780.
- [42] B.T. Houseman, M. Mrksich, The microenvironment of immobilized Arg-Gly-Asp peptides is an important determinant of cell adhesion, *Biomaterials* 22(9) (2001) 943-55.
- [43] K.A. Kilian, M. Mrksich, Directing stem cell fate by controlling the affinity and density of ligand-receptor interactions at the biomaterials interface, *Angew Chem Int Ed Engl* 51(20) (2012) 4891-5.
- [44] R. Hager, A. Arnold, E. Sevcsik, G.J. Schütz, S. Howorka, Tunable DNA Hybridization Enables Spatially and Temporally Controlled Surface-Anchoring of Biomolecular Cargo, *Langmuir* 34(49) (2018) 15021-15027.
- [45] V. Cauda, A. Schlossbauer, J. Kecht, A. Zürner, T. Bein, Multiple Core-Shell Functionalized Colloidal Mesoporous Silica Nanoparticles, *Journal of the American Chemical Society* 131(32) (2009) 11361-11370.
- [46] L. Haddick, W. Zhang, S. Reinhard, K. Möller, H. Engelke, E. Wagner, T. Bein, Particle-Size-Dependent Delivery of Antitumoral miRNA Using Targeted Mesoporous Silica Nanoparticles, *Pharmaceutics* 12(6) (2020).
- [47] I. Slowing, B.G. Trewyn, V.S. Lin, Effect of surface functionalization of MCM-41-type mesoporous silica nanoparticles on the endocytosis by human cancer cells, *J Am Chem Soc* 128(46) (2006) 14792-3.
- [48] H.-J. Liu, P. Xu, Smart Mesoporous Silica Nanoparticles for Protein Delivery, *Nanomaterials* 9(4) (2019).
- [49] A. Zengin, J.P.O. Castro, P. Habibovic, S.H. van Rijt, Injectable, self-healing mesoporous silica nanocomposite hydrogels with improved mechanical properties, *Nanoscale* 13(2) (2021) 1144-1154.
- [50] B.A. Williams, J.C. Chaput, Synthesis of peptide-oligonucleotide conjugates using a heterobifunctional crosslinker, *Curr Protoc Nucleic Acid Chem* Chapter 4 (2010) Unit4 41.
- [51] Y. Zhang, J. Li, M. Soleimani, F. Giacomini, H. Friedrich, R. Truckenmüller, P. Habibovic, Biodegradable Elastic Sponge from Nanofibrous Biphasic Calcium Phosphate Ceramic as an Advanced Material for Regenerative Medicine, *Advanced Functional Materials* 31(40) (2021) 2102911.

Chapter 4

Development of mesoporous silica nanoparticle based films with tunable arginine-glycine-aspartate peptides global density and clustering levels to study stem cell adhesion and differentiation

Xingzhen Zhang¹, Zeynep Karagöz², Sangita Swapnasrita², Pamela Habibovic¹, Aurélie Carlier², and Sabine van Rijt^{1*}

¹Department of Instructive Biomaterials Engineering, MERLN Institute for Technology Inspired Regenerative Medicine, Maastricht University, Maastricht, the Netherlands.

²Department of Cell Biology-Inspired Tissue Engineering, MERLN Institute for Technology-Inspired Regenerative Medicine, Maastricht University, the Netherlands

Abstract

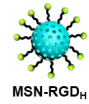
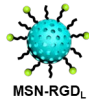
Stem cell adhesion is mediated via the binding of integrin receptors to adhesion motifs present in the extracellular matrix (ECM). Spatial organization of adhesion ligands plays an important role in stem cell integrin-mediated adhesion. In this study, we developed a series of biointerfaces using RGD functionalized mesoporous silica nanoparticles (MSN-RGD) to study the effect of RGD adhesion ligand global density (ligand coverage over the surface), spacing, and RGD clustering levels on stem cell adhesion and differentiation. To prepare the biointerface, MSN were chemically functionalized with RGD peptides via an antifouling PEG linker. The RGD surface functionalization ratio could be controlled to create MSN with high and low RGD ligand clustering levels. MSN films with varying RGD global densities could be created by blending different ratios of MSN-RGD and non-RGD functionalized MSN together. A computational simulation study was performed to analyze nanoparticle distribution and RGD spacing on the resulting surfaces to determine experimental conditions. Enhanced cell adhesion and spreading was observed when RGD global density increased from 1.06 nmol cm⁻² to 5.32 nmol cm⁻² using highly-clustered RGD MSN based films. Higher RGD ligand clustering levels led to larger cell spreading and increased formation of focal adhesions. Moreover, a higher RGD ligand clustering level promoted the expression of alkaline phosphatase in hMSCs. Overall, these findings indicate that both RGD global density and clustering levels are crucial variables to regulate stem cell behaviors. This study provides important information about ligand-integrin interactions, which could be implemented into biomaterial design to achieve optimal performance of adhesive functional peptides.

Keywords

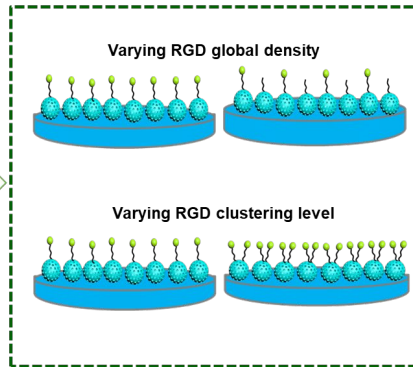
global ligand density, ligand clustering level, biointerfaces, mesoporous silica nanoparticles, mesenchymal stem cell adhesion, RGD

Graphical abstract

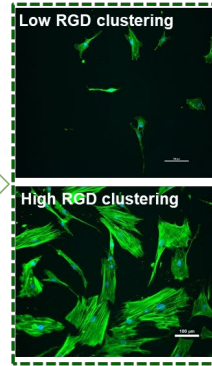
Toolbox



MSN based biofilms



Stem cell adhesion



1. Introduction

Stem cells are unspecialized cells, characterized by an inherent ability to self-renew and the potential to differentiate into specialised cells[1]. In our body, stem cells play a vital role in tissue development, tissue homeostasis, and wound repair throughout life [2, 3]. Stem cell behavior such as self-renewal and differentiation is finely regulated by multifactorial cues provided by the extracellular matrix (ECM) [4]. The native ECM is an insoluble matrix containing intrinsic mechanical and biochemical cues that influence stem cell functions including adhesion, migration, and differentiation [5, 6]. In particular, the ECM provides instructive biochemical cues by presenting adhesive ligands, which are clustered and organized at the nanoscale and interact with stem cells to dictate cell behaviour [7].

Due to their inherent regenerative capabilities, stem cells have tremendous therapeutic potential for regenerating or repairing tissues and organs damaged by aging, cancer, and other diseases in the field of tissue engineering and regenerative medicine [8]. One of the major strategies in this field is to develop engineered biomaterials which can mimic the native ECM to elicit certain stem cell behaviour [9]. Ideally, the engineered biomaterials should not only provide essential structural and mechanical support but also contain biological and biochemical cues that can actively interact with cells to guide stem cell-mediated regenerative processes [10, 11]. In particular, designing bioactive materials able to drive specific cellular behaviors, is gaining more attention in the past few decades. One popular approach is to functionalize materials with tripeptide arginine-glycine-aspartate (RGD), which is a cell-adhesive ligand and can bind to integrin receptors on cellular membranes to enhance stem cell adhesion and integration with the materials [12-14]. Integrin receptors are heterodimeric transmembrane proteins (containing α and β -integrin subunits) and are around 10 nm in size [15, 16]. RGD sequence has been known to bind to several different integrin dimers, i.e., $\alpha_v \beta_1$, $\alpha_v \beta_3$, $\alpha_v \beta_5$, $\alpha_v \beta_6$, $\alpha_v \beta_8$, $\alpha_5 \beta_1$, $\alpha_8 \beta_1$, and $\alpha_{11b} \beta_3$, and is found in multiple ECM proteins such as fibronectins and vitronectin [17]. Integrin-mediated cell focal adhesion (bundles of clustered integrins) and organization of cytoskeletal actin play a vital role in regulating various intracellular signaling pathways and subsequent cell properties [18, 19]. Hence, understanding integrin-mediated stem cell adhesion in the context of tissue regeneration is important in order to rationally design functional biomaterials able to control stem cell behavior.

2D biointerfaces that offer high control over ligand presentation are popular material-based tools to study receptor-ligand interactions [20]. So far, numerous 2D biointerfaces have been created to study the effect of ligand presenting patterns on integrin-mediated signalling [21, 22]. A traditional way to create a biointerface is to decorate a non-fouling surface with monovalent adhesive ligands, which randomly bind to integrin receptors. In this instance, control over the surface bioactivity can be achieved by tuning the ligand global density present at the interface [23, 24]. However, this random distribution of ligands only promotes integrin occupancy, not integrin clustering [25]. Cell adhesion requires both integrin occupancy and integrin clustering [26]. Integrin clustering is initiated by integrin dimerization and can be promoted by presenting ligands in a clustered format. Ligand clustering refers to incorporating multiple adhesive ligands within a small area and is an important factor that influences cell adhesion, spreading, and migration. For example, a surface with locally clustered ligands was generated by grouping several RGD ligands into isolated nano-sized areas. It was shown that RGD ligand clustering could promote integrin clustering and facilitate the formation of adhesion complexes [27]. While ligand clustering is known to enhance integrin activation, it is rare to investigate the effect of RGD global densities and clustering on stem cell behaviour [28-30].

In this study, we aimed to create a new type of biointerface, which allows us to control both the global density and local clustering level of RGD on the surface to a high extent. To create the biointerfaces, we propose a novel strategy based on mesoporous silica nanoparticles (MSN). MSNs have been widely explored for various biomedical applications due to their favorable properties such as tunable morphology, good biocompatibility, porous structures and easy surface functionalization. In addition, previously we have shown that we could create homogenous and stable MSN films using a simple spin coating technique to specifically incorporate ligands onto the surfaces [31]. Importantly, MSN have a high surface area, which implies a high potential to graft densely clustered ligands at the nanoscale, and allows us to change the ligand clustering level with a high degree of control [32]. Here, MSN were functionalized with RGD peptides through a PEG linker, which was used to resist protein absorption to the surface and prevent unspecific cell binding. Systematic variation in surface RGD global density has been achieved by blending different ratios of RGD-modified MSN (MSN-RGD) with non-modified MSN (MSN-PEG) for spin coating, and the distribution of RGD on these resultant surfaces was analyzed by a computational simulation study. To

vary the RGD ligand clustering level, MSN-RGD_H (high-clustered RGD) and MSN-RGD_L (low-clustered RGD) were synthesized. First, the effect of global ligand density on human mesenchymal stromal cells (hMSCs) morphology and adhesion was studied. Then we investigated the effect of the nanocluster level of RGD on hMSCs focal adhesion and differentiation.

2. Results

2.1. Synthesis and characterization of MSN-PEG and MSN-RGD and preparation of MSN films

Synthesis of amine surface-functionalized mesoporous silica nanoparticles (MSN_{NH2}) was performed via hydrolysis and condensation of silica precursors in the presence of a micelle template, followed by surface grafting using 3-aminopropyl triethoxysilane (APTES), as we have reported recently [33]. The presence of the amine group on MSN was validated by labeling with 5/6-Carboxyfluorescein succinimidyl ester (FITC-NHS, able to bind to amine groups). The fluorescent intensity of amine surface-modified MSN was significantly higher compared to non-modified MSN (Fig. S1). RGD functionalization was carried out via a two-step synthesis approach (Fig. 1a). In the first step, the amine group was reacted with a heterobifunctional maleimide-PEG12-succinimidyl ester crosslinker (Mal-PEG12-NHS) to form MSN-PEG_{mal}. Here a PEG linker with 12 repeating units was selected as an anti-fouling spacer based on our earlier study showing that this length enables optimal RGD presentation [31]. In the second step, cysteine-modified RGD peptide was conjugated to MSN-PEG_{mal}, yielding RGD modified MSN (MSN-RGD). A FAM-tagged version of the RGD peptide (RGD-FAM) was used to monitor functionalization quantitatively (Fig. 1b). By changing the RGD-FAM/MSN-PEG_{mal} ratios from 0.32 $\mu\text{mol mg}^{-1}$ to 0.16 $\mu\text{mol mg}^{-1}$, MSN with high-clustered RGD (MSN-RGD_H, 29.1 nmol mg^{-1}) and low-clustered RGD (MSN-RGD_L, 14.5 nmol mg^{-1}) could be obtained, respectively (Fig. 1b). MSN control nanoparticles functionalized with a PEG-CH₃ linker (MSN-PEG) were synthesized by grafting a mono-functional m-dPEG-12-NHS ester linker to MSN_{NH2} (Fig. 1a).

Successful surface MSN amination and subsequent modification with PEG and RGD were further validated using zeta potential measurements. MSN_{NH2} had a positive surface charge of +24.9 mV due to the presence of amine group on the surfaces, which became negative after PEG (-38.0 mV) and RGD modification (-31.4 mV) (Fig. 1c). Transmission electron microscopy (TEM) was employed to characterize the nanoparticle shape and morphology, and to monitor changes in

size over the subsequent surface modifications with PEG and RGD. MSN_{NH₂} displayed an evenly round-shaped morphology with a uniform porous structure and had an average particle size of around 75 nm as estimated from TEM images. The particle morphology and size were similar after surface modification with PEG and RGD (Fig. 1d and e).

To create uniform films, concentrated nanoparticles were spin-coated over plasma-pretreated glass coverslips, as we reported previously [34]. The global RGD density was varied by spin coating mixtures of 10, 25 and 50 % MSN-RGD_H with MSN-PEG nanoparticles, which were designated as 10% MSN-RGD_H, 25% MSN-RGD_H and 50% MSN-RGD_H, respectively (Table 1). In addition, spin coating parameters including applied solvent and spin speed were optimized for the different nanoparticle compositions. An increased content of ethanol in water solution resulted in improved coating homogeneity for MSN-RGD_H films (Fig S2a). As a result, an increased amount of ethanol was used as solvent for spin coating as the percentages of MSN-RGD increased. Uniform and homogenous films were obtained for all formulations (Fig S2b). The coating quality and surface roughness of MSN films were characterized using SEM and profilometer, respectively. The SEM images showed that a homogenous coating with continuous layers of nanoparticles spread over the glass substrate could be achieved with the different nanoparticle compositions (Fig. S3). In addition, a 3D laser scanning image of MSN film made from 50% MSN-RGD_H revealed a smooth surface profile (Fig. S4a). The developed MSN films had a thickness of around 300 nm, indicating that the film was homogeneously covered and that 3-4 layers of nanoparticles deposited over the glass substrate (Figure S4b). All MSN films showed a low surface roughness with Ra around 0.10 μm. No significant differences in roughness and thickness were found among MSN films that were made of different nanoparticle compositions (Figure S4c). The water contact angle (WCA) decreased from 60.5° for glass surface to 20.5° after coating with 50% MSN-RGD_H (Fig.1g and Fig. S5), which further confirmed the successful creation of nanoparticle films. As surface wettability is known to influence cell adhesion[35]³⁵ and can be varied by surface chemical composition, we measured the WCA on the different MSN films. No significant difference in WCA was observed among surfaces prepared using 50%, 25% and 10% MSN-RGD_H (Fig 1g).

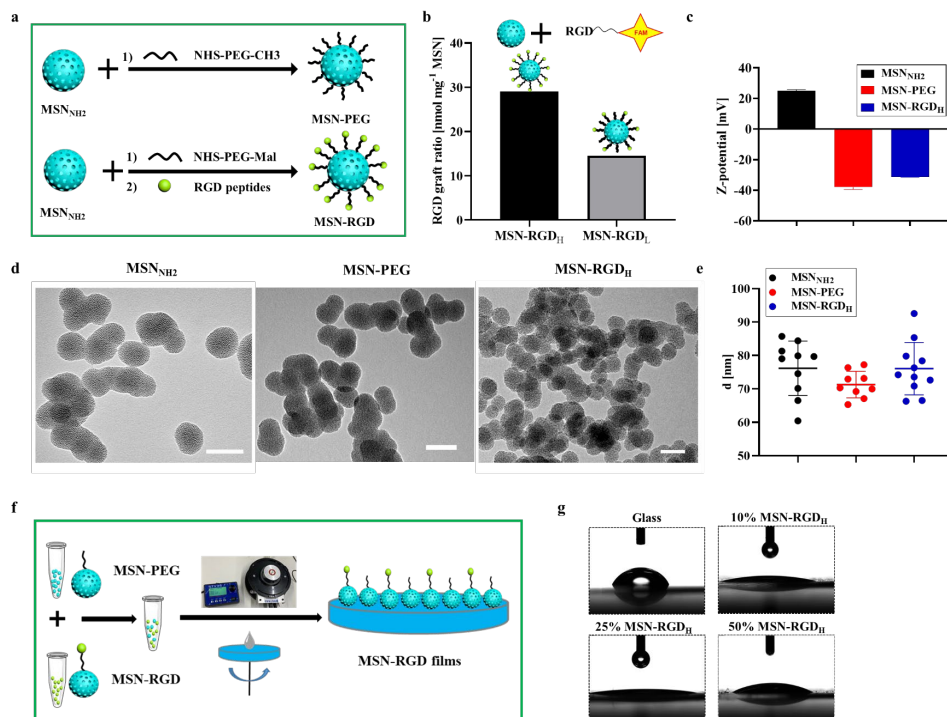


Figure 1. Synthesis and characterization of MSN-RGD. a) A schematic illustration of surface functionalization of MSN_{NH₂} with PEG linkers and RGD peptides. b) Quantification of RGD surface functionalization of MSN_{NH₂} using FAM fluorescently labeled RGD. c) Zeta surface potential as measured by DLS in water showing change of surface charge after PEG and RGD surface functionalization. d) TEM images of MSN_{NH₂}, MSN-PEG and MSN-RGD_H showing as-synthesized nanoparticles have a spherical shape. The scale bar is 100 μ m. e) Particle size of MSN_{NH₂}, MSN-PEG and MSN-RGD_H as determined by TEM. f) Schematic illustration of the preparation of MSN films with different surface RGD densities by spin coating of pre-mixed nanoparticles. g) Water contact angle of glass surfaces before and after coating with nanoparticles containing 10%, 25% and 50% MSN-RGD_H.

Table 1. wt% composition of nanoparticles used for preparation of MSN films with varying global densities and clustering levels.

Formulations	wt% MSN- RGD _H	wt% MSN- RGD _L	wt% MSN- PEG	RGD global density [nmol cm ⁻²]
10% MSN- RGD _H	10	–	90	1.06
25% MSN- RGD _H	25	–	75	2.66
50% MSN- RGD _H	50	–	50	5.32
50% MSN- RGD _L	–	50	50	2.66
100% MSN- RGD _L	–	100	0	5.32

2.2. Computational calculation of RGD distribution on MSN films

Computational simulations were performed to quantitatively assess nanoparticle distribution over the 2D surfaces to aid the selection of MSN-RGD variables for our experimental study. In these simulations, the random localization of the nanoparticles on the glass substrate were analyzed. We first made random distributions of 10%, 25%, 50% and 75% of MSN-RGD particles (MSN with a diameter of 70 nm and an RGD ligand attached to it) on a 2000 × 2000 nm grid (a 100% distribution implies 2000/70 × 2000/70 particles). We have also assumed mean field approximation on the nanoparticle surface, i.e., the exact localisation of the RGD ligand is not included in this study. A representative example of nanoparticles random distribution on surfaces is shown in Figure 2a. The pairwise distance between RGD ligands (note: distance from surface-to-surface is only considered because of the mean field approximation) was then calculated. For each MSN-RGD particle, only those MSN-RGD at a distance lower than 70 nm were defined as “neighbors”. Here 70 nm was selected as a cut-off value because

previous studies have shown that ligand spacing larger than ~ 70 nm resulted in immature focal adhesions (because integrins cannot cluster), whereas ligand spacing smaller than ~ 70 nm promoted maturation of focal adhesions [36-40]. We replicated the steps (randomization of distribution, assigning neighbors) 100 times in order to remove removing any random number generator bias (Figure S6) [41]. First, the ratio of RGD particles that had at least one “neighbor” over the total number of MSN-RGD particles on the surface (Figure 2b) was calculated. Interestingly, this ratio was 100% on surfaces made from 50% MSN-RGD, which meant every RGD modified nanoparticles had at least one neighbor of MSN-RGD within 70 nm distance on the surface. However the ratio for surfaces prepared with 10% RGD modified nanoparticles to have one “neighbor” is as high as 50% (Probability(RGD particle with RGD neighbor) = 1- probability(having no RGD neighbors) = $1-(0.9)^8 = 0.57$). To study the effect of the nanoparticle size on RGD ligand distribution at a certain RGD global density (25% RGD), we varied the diameter of nanoparticles (50, 70, 90, and 120 nm) and recalculated the ratio of the “clustered RGD” over the total number of MSN-RGD particles. This ratio decreased with a larger nanoparticle diameter (Figure S7). When the diameter was 50 nm, there were 12 “neighbors” that are within the cut-off distance of 70 nm at a global density of 25%, which gave a probability of $1-(0.75)^{20} \sim 0.9968$. As the diameter increased to 120 nm, the number of “neighbors” within 70 nm cut-off distance decreased to 8, and the chance of having at least one neighbor in the 8 neighbors = $1-(0.75)^8 \sim 0.89$. Additionally, we also plotted the average number of RGD “neighbors” of the RGD peptide-containing particles which had at least one other MSN-RGD within 70 nm distance over the total number of MSN-RGD particles based on 100 different surface coatings (Figure 2c) to calculate average aggregate size. On average, on 10% MSN-RGD surfaces, MSN-RGD aggregate consisted of 2 RGD particles, while aggregate size on 50% MSN-RGD surfaces MSN-RGD is approximately 5. Overall, as the fraction of RGD particles increased, the ratio of RGD particles that had at least one “neighbor” increased, and at a limit of 50% RGD-particle, the neighboring ratio reached a plateau of 100% with an aggregate size of 5 [42]. Therefore, 10% MSN-RGD, 25% MSN-RGD, and 50% MSN-RGD surfaces were selected as our experimental groups for cell adhesion study.

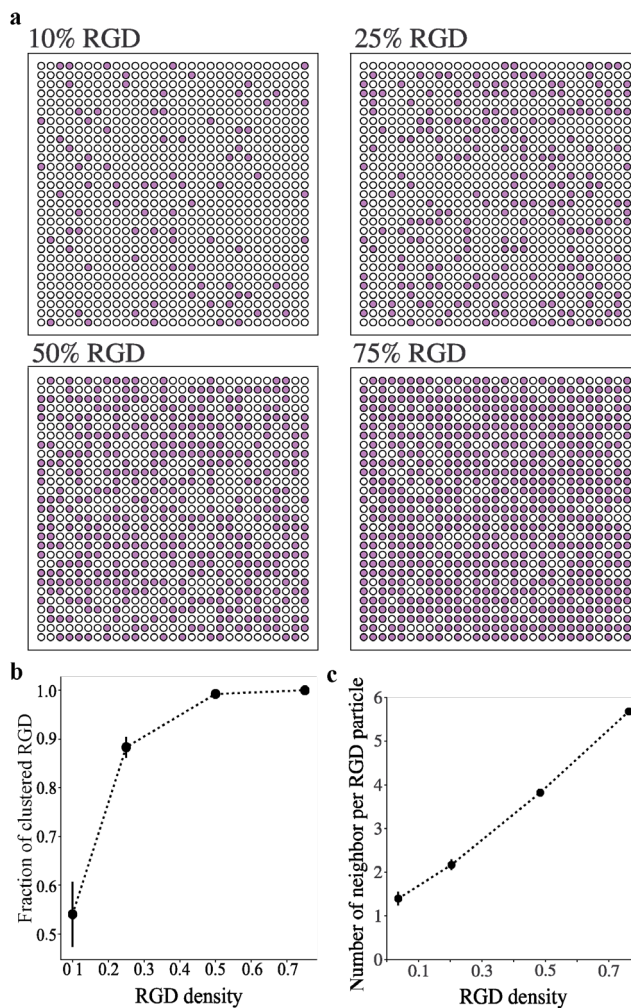


Figure 2. Computational calculation of spacing between adjacent MSN-RGD_H on a surface made from different ratios of MSN-RGD_H and MSN-PEG. a) Computational description of how RGD clusters distributed over a surface made from varied MSN-RGD portions (Magenta circle, RGD-functionalized nanoparticles; white circle, non-RGD-containing nanoparticles). b) Ratio of MSN-RGD particles which have at least one other MSN-RGD within 70 nm distance over the total number of MSN-RGD particles on the surface. c) Average number of neighboring MSN-RGD per nanoparticle on surfaces made from different weight percent of MSN-RGD.

2.3. The effect of RGD global density on hMSCs morphology and spreading on high-clustered MSN-RGD films

Cells need enough adhesion sites with defined inter-ligand spacing to be able to adhere. Several studies have highlighted the importance of ligand spacing on integrin-mediated cell adhesion processes [43-45]. However, very few studies report on the ligand global density range that is required for stem cell adhesion. Here, the effect of RGD global density (RGD coverage over the surface) on hMSCs spreading and morphology was assessed by seeding hMSCs on MSN films containing 10, 25 and 50% MSN-RGD_H. After 1 and 3 days, hMSCs were stained to visualize the nuclei and cytoskeletal F-actin organization, and imaged using fluorescence microscopy (Figure 3a). hMSCs cultured on 50% MSN-RGD_H surface (high global RGD density of 5.32 nmol cm⁻²) showed spread morphology with well-defined stress fibers (Figure 3a). In contrast, cells cultured on 10% MSN-RGD_H surface (low global RGD density of 1.06 nmol cm⁻²) were only stretched in one or two directions with limited formation of stress fibers. The attached cell number, cell spreading area, and form factor (form factor approaches 1 for highly circular cells) of adhered hMSCs were further analyzed using Cell Profiler. After 1 day of culture, the cell spreading area and the number of adhered hMSCs showed an increasing trend as RGD global density increased (Figure 3b and Figure S8a). After 3 days of culture, cells cultured on 50% MSN-RGD_H surface had a significantly higher area compared to hMSCs cultured on 10% and 25% MSN-RGD_H surfaces (Figure 3d). Moreover, the cell number on 50% MSN-RGD_H surface was significantly higher compared to the other two MSN films (Figure S8b). No significant differences in form factor were observed for the hMSCs cultured on the three different surfaces after 1 day of culture (Figure 3c). However, there was an increase in elongation of the cells (smaller form factor) cultured on 10% MSN-RGD_H surfaces, as compared to hMSCs cultured on surfaces with 50% MSN-RGD_H after 3 days of culture (Figure 3e).

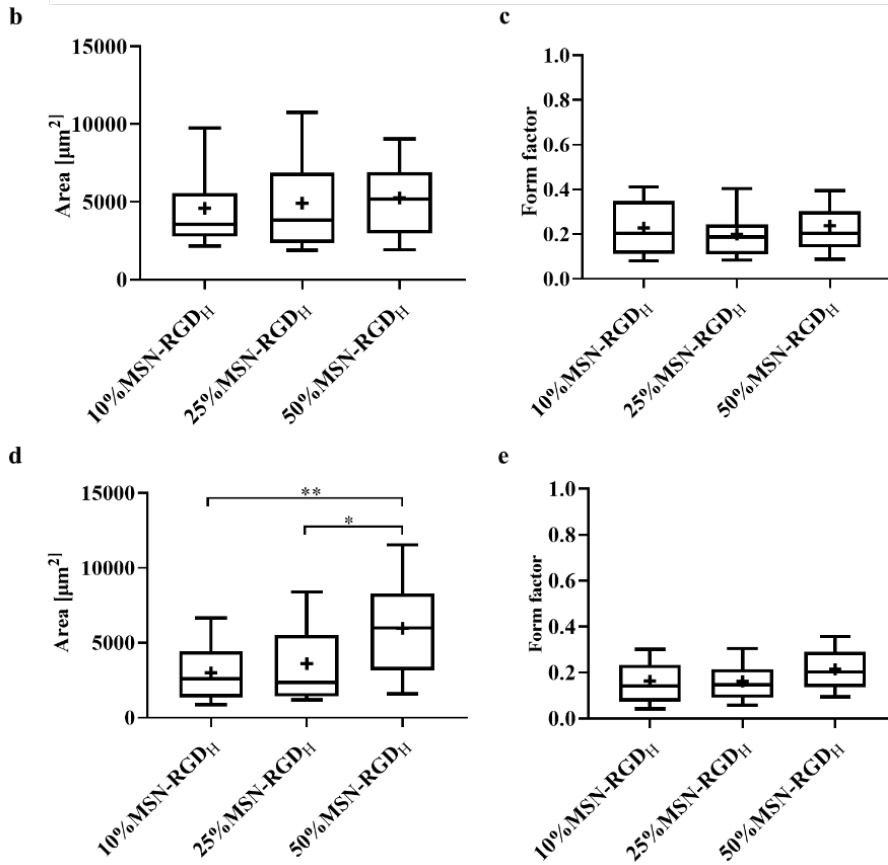
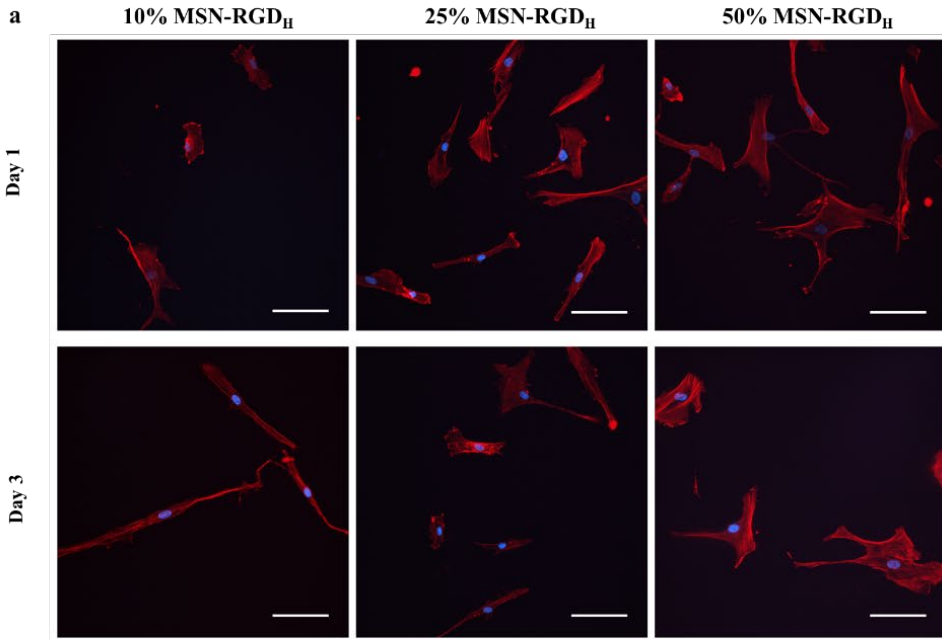


Figure 3. Effect of the global ligand density on hMSCs morphology. a) Representative fluorescent microscopy images showing distinct morphology of hMSCs grown on different MSN films composed of 10%, 25% and 50% of MSN-RGD_H for 1 day and 3 days. Cells were stained to visualize F-actins (red) and nuclei (blue). Scale bar is 100 μm . Box plots showing the b) cell area and c) form factor of hMSCs grown on three different MSN films for 1 day; d) cell area and e) form factor after 3 days of culture on films containing of 10%, 25% and 50% MSN-RGD_H. Data shown as the mean \pm SD from 4 biological replicates. * $p < 0.05$; ** $p < 0.01$; *** $p < 0.001$.

2.4. The effect of nanoscale RGD ligand clustering levels on hMSCs morphology and adhesion at varied RGD global densities

Next, we studied the effect of RGD ligand clustering levels at different global ligand densities on hMSCs morphology and spreading. While maintaining the global RGD density constant, two surfaces with a varied RGD cluster level were generated by using MSN-RGD_H or MSN-RGD_L blended together with MSN-PEG nanoparticles. Specifically, two types of MSN films were developed with the same global density of 2.66 nmol cm^{-2} , which consisted of 50% MSN-RGD_L mixed with 50% MSN-PEG and 25% MSN-RGD_H mixed with 75% MSN-PEG. A second set of MSN films were created that contained 5.32 nmol cm^{-2} RGD global density, which consisted of 50% MSN-RGD_H mixed with 50% MSN-PEG and 100% MSN-RGD_L. A schematic illustration of the RGD-nanoparticle distribution of the prepared surfaces is shown in Figure 4a. hMSCs were cultured on the four different MSN films for 3 days and then stained for filamentous actins (F-actins, green) and nuclei (blue). A distinct difference in the morphology of hMSCs was observed between 100% MSN-RGD_L and 50% MSN-RGD_H (Figure 4b). Overall, hMSCs adhered to surfaces with high global RGD density (100% MSN-RGD_L and 50% MSN-RGD_H) showed better-organized actin assembly and spreading morphology compared to cells cultured on surfaces with low global RGD density (50% MSN-RGD_L and 25% MSN-RGD_H), which had an elongated cell shape. Interestingly, although similar cell shape was observed on 50% MSN-RGD_H and 100% MSN-RGD_L surfaces, cells grown on highly-clustered RGD surface (50% MSN-RGD_H) were much larger in comparison to that on 100% MSN-RGD_L surface (Figure 4b).

Single cells were outlined using the Cell Profiler software to calculate cell spreading areas and form factor. The attached cell number of hMSCs cultured on

highly-clustered RGD surfaces (50% MSN-RGD_H) was significantly higher compared to hMSCs adhered to low-clustered RGD surfaces (50% MSN-RGD_L) (Figure 4c). In addition, hMSC spread out more when adhered on 50% MSN-RGD_H than on 50% MSN-RGD_L and 100% MSN-RGD_L surfaces (Figure 4d). There was a significant difference in cell spreading between 50% MSN-RGD_H and 100% MSN-RGD_L surfaces, suggesting a clustering effect on cell spreading. However, this difference was not observed between 25% MSN-RGD_H and 50% MSN-RGD_L surfaces. Together, these findings suggested that local ligand clustering level below 70 nm scale has an effect on cell morphology and spreading, and this effect is also global density-dependent.

Next, we calculated the effective distance on clustered surfaces to help to explain our observations of cell morphology and spreading. The effective distance in this study was defined as the average ligand distance between any two RGD particles and was calculated by sum of distances between any two RGD-nanoparticles divided by the total number of RGD nanoparticles on the substrates (Figure 5a). Higher effective distance would imply higher ligand interaction and as a result, higher cell spreading. When we simulated the coating on a surface with a size of 2000 x 2000 (unitless dimension), we observed a higher effective distance for high local density particles (MSN-RGD_H) than MSN-RGD_L, and this pattern didn't change with an altered global density of RGD on the interface (Figure 5b). To make sure our observation was not affected by the size of the surface we chose, we also studied the effect of surface size on the effective distance. We found that irrespective of the surface size, high local clustering particles always had a larger effective distance (Figure 5c). This simulation also explained our experimental observations, where an increased cell spreading area on 50% MSN-RGD_H in comparison to 100% MSN-RGD_L could be attributed to a higher effective distance on high RGD clustered particle coated surfaces.

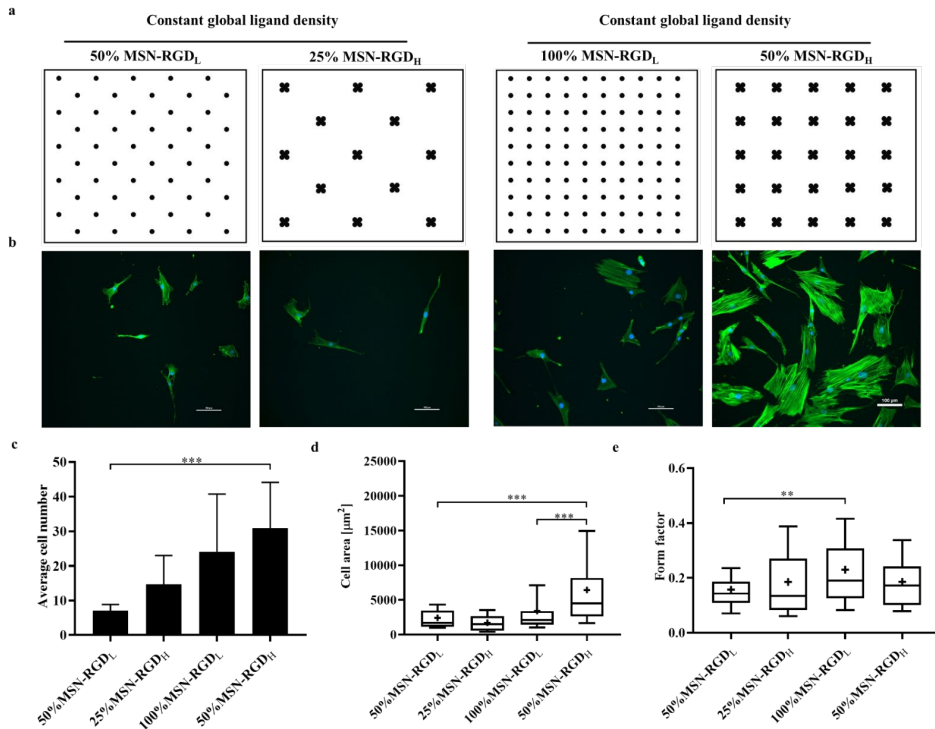


Figure 4. Effect of RGD global density and clustering on hMSCs morphology. a) A schematic illustration of the developed MSN films showing RGD local and global density. b) The morphology of hMSCs adherent to MSN films with different nanoscale RGD ligand clustering, while maintaining the same global RGD density after 3 days of culture. Cells stained for nuclei (DAPI; blue) and actin (phalloidin 488; green). Scale bar is 100 μm. c) Attached cell number on highly-clustered films compared to low-clustered films. Box plots showing the d) cell area and e) form factor of hMSCs grown on four different MSN films for 3 days. Data are expressed as the mean ± SD (n=18-97, 3-6 images from biological triplicates). *p < 0.05; **p < 0.01; ***p < 0.001.

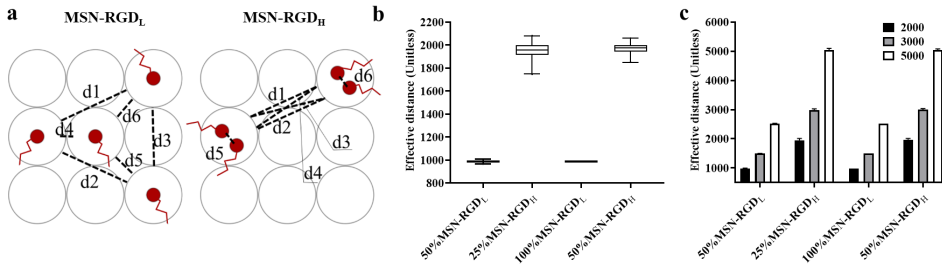


Figure 5. Characterization of effective distance. a) Schematic presentation of the calculation of the effective distance on high and low-clustered nanoparticle surfaces. In low local density (MSN-RGD_L) situation, the effective distance between the RGD particles is the average of all distances and is calculated as $(d1+d2+d3+d4+d5+d6)/6$. In high local density (MSN-RGD_H) situation, the effective distance becomes $(d1 + d2 + d3 + d4 + d5 + d6)/6$. We neglect $d5$ and $d6$ because of the mean field approximation. We can also approximate $d1 = d2 = d3 = d4$. So the effective distance becomes, $4 * d1/4 = d1$. b) Effective distance between MSN-RGD particles on surfaces with varied global and local densities. c) Effective distance on surfaces with varied surface sizes.

2.5. Focal adhesion

Focal adhesions (FAs) are key for cell anchorage and organization of the actin cytoskeleton [46]. Thus, we next studied how ligand clustering levels at varied global ligand densities influence the vinculin expression of hMSCs, which is a protein recruited from the cytoplasm to the focal adhesion complex [47, 48]. hMSCs were cultured on 100% MSN-RGD_L, 50% MSN-RGD_H, 50% MSN-RGD_L, and 25% MSN-RGD_H surfaces for 5 days, and then stained for vinculin (red), F-actin bundles (green), and nuclei (blue). In accordance with our previous observations, a more spread morphology with prominent actin cytoskeleton alignment could be observed for hMSCs cultured on 50% MSN-RGD_H (Figure 6a). Additionally, hMSCs on the 50% MSN-RGD_H substrates exhibited a higher vinculin expression, with larger and longer focal points formed compared to cells on the 100% MSN-RGD_L substrates (Figure 6a-c), suggesting that the presentation of RGD in a highly clustered format resulted in more efficient grouping of integrin receptors as compared the same surface global density of RGD with a low clustering level.

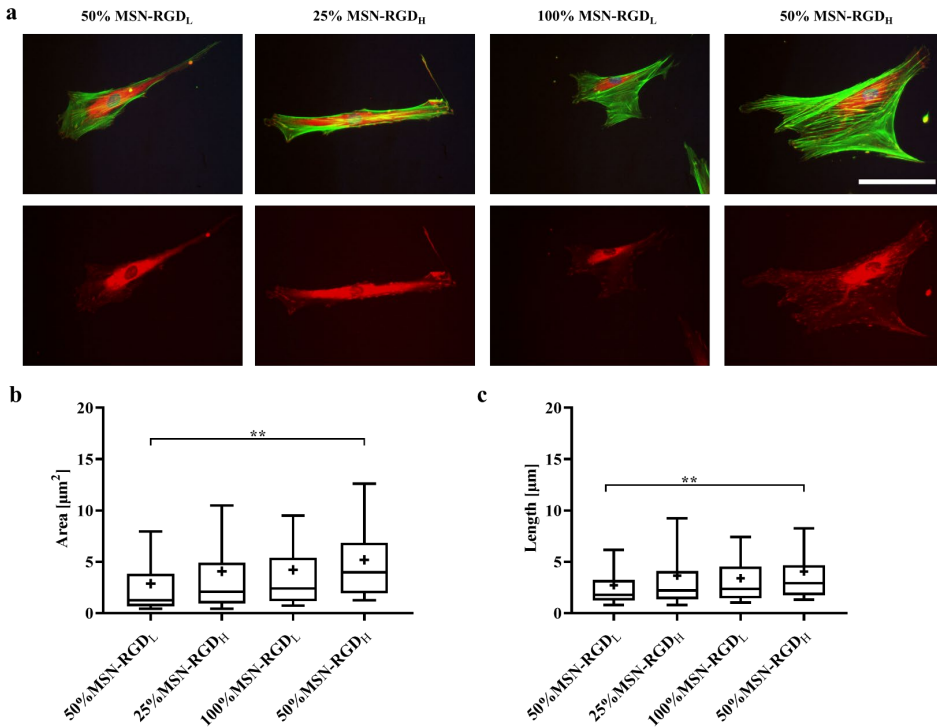


Figure 6. The effect of nanoscale ligand clustering levels on hMSCs focal adhesion points. a) Representative fluorescence microscopy images of hMSCs cultured on MSN films showing focal adhesions after 5 days of culture. hMSCs were stained for focal adhesion protein vinculin (red), actin (green) and nuclei (blue). The vinculin staining (red) was shown separately. Scale bar represents 100 μm and applies to all images. b) Area and c) length of focal adhesions after 5 days. Data is presented as mean \pm SD (n=89-104 from biological triplicates). *p < 0.05; **p < 0.01; ***p < 0.001.

2.6. The effect of RGD ligand clustering on ALP production in hMSCs

Cytoskeleton organization, cell spreading, and focal adhesion is known to influence stem cell differentiation [49]. To test if the difference in the initial cell focal adhesion on our biointerfaces could induce cell differentiation processes, hMSCs were cultured on 100% MSN-RGD_L, 50% MSN-RGD_H, 50% MSN-RGD_L, and 25% MSN-RGD_H surfaces either in basic or osteogenic medium (with 10 nM Dex supplementation) for 14 days. After 14 days of cell culture, alkaline phosphatase

(ALP) production in hMSCs was examined. ALP is one of the earliest markers of osteogenic differentiation and has been widely used for evaluating the osteogenic potential of hMSCs [50]. hMSCs cultured on glass slides in basic medium were used as control. In basic conditions, significantly higher ALP levels were observed for hMSCs cultured on 50% MSN-RGD_H films compared to negative control conditions (Fig. 7a), indicating that RGD ligand clustering at high RGD global density can promote osteogenic marker expression when no other osteogenic stimulants are present. Interestingly, this was not observed for lower clustered RGD surfaces with the same RGD density (100%MSN-RGD_L). Furthermore, this effect was more pronounced when hMSCs were cultured in osteogenic medium; ALP expression on 50% MSN-RGD_H film was 12.4 fold compared to 3.3 fold ALP increase for cells cultured on glass controls (Fig. 7b). Remarkably, hMSC cultured on surfaces that contained the same RGD density, but had lower RGD clustering (i.e. 100%MSN-RGD_L) did not show significantly increased ALP production compared to glass controls. These data indicate that RGD ligand clustering at high RGD density can play an important role in promoting osteogenic differentiation in hMSCs.

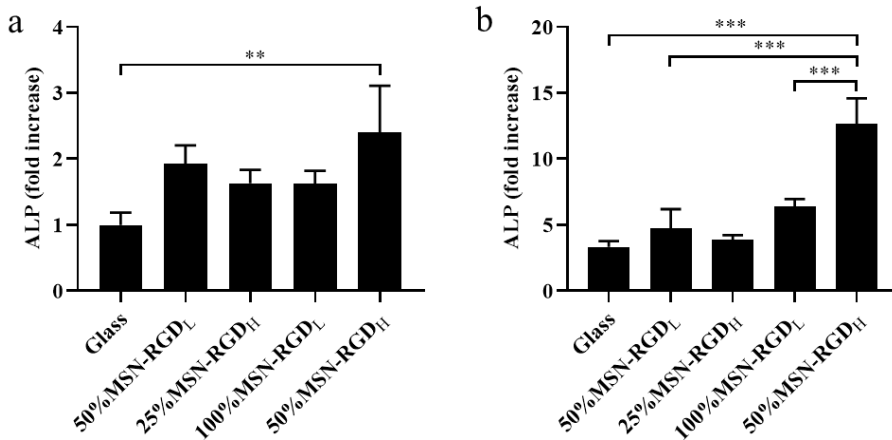


Figure 7. Effect of RGD ligand clustering and local density on hMSCs ALP production. ALP production of MSCs cultured on the four MSN films and glass for 14 days in a) basic medium and b) osteogenic medium. hMSCs cultured on glass in basic medium was negative control. Values are x-fold increases compared to the negative control. Data is shown as mean \pm SD of biological triplicates. * $p < 0.05$; ** $p < 0.01$; *** $p < 0.001$.

3. Discussion

In this study, we presented a novel strategy to create biointerfaces based on RGD-modified silica nanoparticles, which enables high control over RGD ligand clustering level and global density on 2D surfaces. Although several studies report on the importance of ligand clustering to promote (stem) cell adhesion processes, no previous study has looked into the effect of ligand clustering level on integrin-mediated adhesion and stem cell function. We fabricated four MSN films using high and low-clustered RGD on MSN surfaces to investigate the effect of RGD nanoscale clustering level and spacing on hMSCs adhesion and differentiation. We found that the RGD ligand clustering level regulates integrin-mediated stem cell adhesion and ALP expression.

In our approach, we used MSN to create a novel biointerface capable of presenting clustered ligands in a controlled way. MSN were successfully functionalized with RGD peptides using a PEG linker. Here, a PEG linker was used as an antifouling spacer to resist nonspecific protein adsorption and cell adhesion. As the PEG chain length could potentially influence its antifouling property and ligand functionality, it's also important to optimize the PEG spacer length in any system to ensure proper cell adhesion. In this work, PEG 12 was selected as an antifouling spacer based on our previous study where we showed that this PEG length was optimal to study specific hMSC-RGD interactions [31]. Our approach enabled tunable RGD functionalization by changing the ratios of MSN to RGD during synthesis. Using this method, we could control the RGD ligand clustering level on the silica nanoparticles to create high- and low- RGD clustered MSNs. However, considering the large surface area and nanometer size of MSN, our platform allows tailoring of the RGD ligand clustering level at the nanoscale. Indeed, our results showed that we can achieve a higher RGD ligand clustering level of $29.1 \text{ nmol mg}^{-1}$, compared to other substrates reported in the literature [27, 51]. In addition, the particle size could be easily tuned, which therefore enables precise control over the size of ligand islands. Another advantage of our novel interface is the simplicity of the preparation process. Previously, ligand immobilization and patterning on surfaces have been achieved using several distinct methods such as the nanolithography technique and covalently surface-grafting, which either relies on expensive and specialized equipment or involves aggressive and complex fabrication processes [25]. For example, traditional covalent immobilization of ligands to glass substrates often required piranha treatment to activate the hydroxyl groups of glass surfaces [52, 53]. In our

approach, using a simple blending and spin coating technique, homogenous MSN films made from different nanoparticle compositions could be created and therefore ensure easy modulation of ligand distribution.

To investigate what RGD global density range was required to stimulate cell adhesion when the ligands were highly clustered at the nanoscale, three MSN films with a varied RGD global density were generated. We observed enhanced cell adhesion and spreading as global RGD density increased. Specifically, hMSCs on high RGD density surfaces presented a more spread morphology with a better-organized actin cytoskeleton as compared to that on low RGD density surfaces. Cytoskeletal components such as actin have been reported to regulate stem cell differentiation, with a higher cytoskeleton tension leading to a greater osteogenic differentiation [54-56]. The increase of cell adhesion with the increase of RGD density is consistent with a previous study about cell adhesion of another cell type (C2C12 skeletal myoblasts) [57]. However, the surface RGD density that can induce proper cell adhesion in our system is $5.32 \text{ nmol cm}^{-2}$, which is much lower as compared to the published data of $1.2 \times 10^3 \text{ nmol cm}^{-2}$ as reported by other research group [58]. This difference could be in part explained by the high clustering of RGD ligands at the nanoscale in our system. Previously it has been shown that the presentation of integrin-binding ligands in a clustered format resulted in enhanced integrin clustering and the formation of focal complexes [59]. Furthermore, the different cell types could be another explanation, as it has been previously reported that the effect of local and global ligand density is distinct for different cell types [25].

To investigate the effect of RGD ligand clustering level on stem cell adhesion, we used MSN with varied RGD ligand clustering levels to create four different MSN films. We observed that when we kept global ligand densities the same, surfaces with more highly clustered RGD promoted cell adhesion. Specifically, highly clustered surfaces resulted in increased cell numbers, larger cell spreading, and larger and longer focal adhesion points as compared to lower clustered surfaces. Binding of integrins to ECM ligands induces a conformational change in the structure of the cytoplasmic tail of the integrin, which initiates integrin clustering and subsequent formation of focal complexes [59]. As such, the enhanced cell adhesion to the highly clustered surface may be related to a higher level of integrin clustering that was mediated by the clustered ligands [60]. The positive effect of ligand clustering on cell adhesion has also been reported

previously [61]. In this study, it was shown that even at the maximal density of 30,000 YGRGD ligands per square micrometer, cell response was observed to be significantly lower for individual YGRGDs than for ligands clustered in groups of nine with a cluster density of 2,300 YGRGD μm^{-2} . However, in our study, the clustering effect was not observed when lower global RGD densities were used; here clustering level did not show a significant effect on cell number and spreading. This is likely due to insufficient adhesive binding sites and no integrin clustering at low global density surfaces, which could potentially lead to low cell adhesion, cell quiescence or even apoptosis [62]. Similar to our findings, Benitez et al. also reported that ligand clustering influences integrin-dependent signals in a manner that significantly depends on both global and local ligand densities [63].

The clustering level also influenced the ALP activity of hMSCs, where highly clustered surfaces can significantly upregulate ALP level in hMSCs as compared to low clustered surfaces. The difference in ALP production was well-aligned with the difference we observed in hMSCs morphology and spreading. It can then be speculated that cells with more spread morphology and stronger adhesions undergo osteogenic differentiation. This result aligns with previously published data, in which larger, and increased numbers of focal adhesions formed on smaller nanopacings promoted higher levels of mechanical tension, therefore, biased the commitment of hMSCs to an osteogenic fate through the enhanced mechanotransduction [64]. Indeed, previous studies have reported that focal adhesions emerge as diverse protein networks which not only provide structural integrity connecting the ECM to the intracellular actin cytoskeleton but also transmit signaling pathways crucial to cell differentiation [65]. The exact signaling mechanisms linking focal adhesions with the commitment of hMSCs to the osteogenic lineage are still not well understood. However several studies have suggested that the FAK \rightarrow ERK \rightarrow Runx2 signaling pathway constitutes a crucial element of the transduction machinery controlling this process [66, 67]. In summary, our findings suggested that RGD ligand clustering level also had an effect on hMSCs adhesion and differentiation, and such effects of RGD ligand clustering are dependent on global ligand density.

4. Conclusions

In conclusion, we fabricated a series of biointerfaces based on RGD-modified MSN to study the effect of RGD global density and nanoscale clustering level on stem cell morphology, focal adhesion, and differentiation. Distinct differences in hMSCs

morphology and spreading were observed as the average global RGD density changed. The nanoscale RGD ligand clustering level could be tuned and a higher RGD ligand clustering level led to an enhanced focal adhesion and osteogenic differentiation even when the global RGD density remained consistent. This suggested that nanoscale ligand clustering level could be a crucial factor to be considered to optimize RGD incorporation into biomaterials. Our findings highlight the importance of the nanoscale ligand clustering in biomaterial design to the regulation of stem cell response. Ligand clustering could be more beneficial to enhance cell adhesion than randomly increasing ligand density. We expect the knowledge gained from this study to accelerate the development of more functional materials to support stem cell-based regenerative therapies.

For future application, the fabricated MSN-RGD platform is not limited to the study of RGD-integrin interaction, but also allows the incorporation of other ligands to probe other ligand-induced stem cell processes. The possibility to tune the surface chemistry of MSN makes them versatile platforms that may be engineered to display multiple epitopes to study nanoscale ligand crosstalk. Moreover, our MSN with clustered RGD can also be easily incorporated into biomaterials to enhance their (stem) cell adhesion properties and/or improve tissue integration.

5. Experimental Section

5.1. Materials

Tetraethyl orthosilicate (TEOS, 98%), triethanolamine (TEA), cetyltrimethylammonium chloride (CTAC), 3-aminopropyl triethoxysilane (APTES), ammonium fluoride, hydrochloric acid (37%), m-dPEG@12-NHS ester (PEG-CH₃), ammonium nitrate, phosphate-buffered saline (PBS), fetal bovine serum (FBS) and ascorbic acid 2-phosphate sesquimagnesium salt hydrate (ASAP) were purchased from Sigma Aldrich. RGDC peptides were purchased from Sanbio. RGD-FAM was commercially synthesized by GenScript. Absolute ethanol, paraformaldehyde (PFA), minimum essential medium alpha GlutaMAX (αMEM), bovine serum albumin (BSA), Triton X-100 were purchased from VWR. 5/6-carboxyfluorescein succinimidyl ester (FITC-NHS), CyQUANT™ cell proliferation assay kit and Mal-PEG12-NHS were purchased from ThermoFisher Scientific. Alkaline phosphatase (ALP) assay kit and recombinant Alexa Fluor® 647 anti-vinculin antibody were purchased from Abcam. Penicillin and streptomycin were obtained from Gibco Life

Technologies. Alexa Fluor™ 488 Phalloidin and Alexa Fluor™ 647 Phalloidin were purchased from Fisher Scientific.

5.2. Synthesis and characterization of MSN_{NH_2} , $MSN-PEG$ and $MSN-RGD$

Synthesis of MSN_{NH_2} was based on a sol-gel co-condensation process as previously reported [68]. To synthesize MSN_{NH_2} , a mixture of 1.73 g tetraethyl orthosilicate (TEOS) and 14.3 g triethanolamine (TEA) was heated to 90 °C under static conditions for 20 min (Solution 1). Solution 2 was prepared by adding 100 mg of ammonium fluoride (NH₄F), 2.41 ml of cetyltrimethylammonium chloride (CTAC) to 22 ml of bi-distilled water (DIW) and heated to 60 °C for 10 min. Next, Solution 2 was quickly added to solution 1, and the mixture was stirred vigorously for 20 min, after which 138.2 mg TEOS was added to the mixture in four equal portions every 3 min, and stirred for 30 min. In the next, a mixture of 19.3 mg TEOS with either 20.5 mg 3-Aminopropyl triethoxysilane (APTES, in the case of $MSN-NH_2$) or 20.5 mg 3-mercaptopropyl triethylsilane (MPTES, in the case of $MSN-SH$) was added and stirred overnight at room temperature. The following day, particles were collected by centrifugation and washed once with ethanol, and then redispersed in an ethanolic ammonium nitrate solution. Then, the mixture was refluxed at 90 °C for 45 min. Afterwards, MSN were collected by centrifugation, washed once with ethanol, redispersed in 100 ml of a hydrochloric acid solution (HCl 37% in DIW), and refluxed again at 90 °C for 45 min. Finally, MSN were collected, re-dissolved in ethanol and kept at -20 °C for future use.

Conjugation of RGD onto MSN_{NH_2} was performed in two steps. First, MSN_{NH_2} were modified with NHS-PEG12-Mal linker to create $MSN-PEG_{mal}$. For this, 2 mg of MSN_{NH_2} were dispersed in 920 µl of PBS buffer (pH 8.25) and sonicated for 30 min at room temperature (RT). Then 80 µl of Mal-PEG12-NHS (5mM in DMSO) was added and the mixture was stirred for 4 h. After that, $MSN-PEG_{mal}$ was obtained by centrifugation and purified by subsequent washing with water. In the second step, the obtained $MSN-PEG_{mal}$ was re-dispersed in 600 µl of Tris-EDTA buffer (pH 7.4), followed by the addition of 400 µL or 200 µL of RGDC peptides (2 mg/ml in water) to create MSN with high-clustered or low-clustered RGD, respectively. Then the RGD coupling reaction was carried out by continuous stirring the mixture overnight at RT. Finally, $MSN-RGD$ were collected by centrifugation, followed by washing, and then stored at 4 °C.

To quantify RGD grafting ratio, FAM-labeled RGD peptides (RGD-FAM) were used for the reaction as described above instead of using RGDC peptides.

After RGD coupling reaction, unbound RGD-FAM peptides were collected and quantitatively calculated by fluorescence intensity measurement at $\lambda_{ex} = 488 \pm 14$ nm, $\lambda_{em} = 535 \pm 30$ nm. A standard curve prepared from RGD-FAM was used for calibration.

MSN-PEG was also created and used as a blank control in this study. For this, appropriate amounts of m-dPEG12-NHS ester linker (5mM in DMSO) were added to MSN_{NH_2} suspension and stirred for 4 h. After that, excess linkers were removed by double-washing in water. MSN-PEG were collected by centrifugation and stored at 4 °C.

The zeta potential of MSN_{NH_2} , MSN-PEG, and MSN-RGD_H were analyzed using Malvern Zetasizer Nano (Malvern Panalytical, UK). For this, nanoparticles were suspended in Milli-Q water at 0.5 mg/ml concentration and sonicated for 30 min. The morphology and size of MSN_{NH_2} , MSN-PEG, and MSN-RGD_H were examined using transmission electron microscopy (TEM, JEM-100CX II, Japan). Nanoparticles that suspended in absolute ethanol at 0.5 mg/ml concentration were dropped onto a copper grid and air-dried at RT overnight before imaging. Particle size was determined using ImageJ.

5.3. Preparation and characterization of MSN based films

MSN films were prepared using spin-coating. Immediately prior to spinning, coverslips with a diameter of 22 mm were surface-cleaned in 1M HCl in 50 % ethanol and activated with O₂ plasma treatment (Plasma Cleaner, Diener Electronics Femto PCCE) at 0.4 bar, 5 sscm O₂, 70 W, 10 min. MSN-PEG were collected by centrifugation (14000 rpm, 20°C, 10 min) and dispersed in bi-distilled water at a concentration of 40 mg/ml. Various ethanol-water solvents including 0%, 50% and 70% of ethanol have been used to disperse MSN-RGD to optimize nanoparticle dispersibility and spin coating homogeneity. To prepare MSN films with various global RGD densities at high clustering level, different ratios of MSN-PEG and MSN-RGD_H dispersant were mixed accordingly and a volume of 25 μ l of the mixture was pipetted centrally on a coverslip and spun at 2100 rpm for 20 sec on a tabletop spin coater. Similarly, MSN films with low clustering level were created by mixing appropriate proportion of MSN-RGD_L with MSN-PEG for spin coating. The obtained films were stored dry at 4°C. The spin coating quality and film homogeneity were assessed by optical pictures. To further characterize the films, 3D laser scanning microscopy (Keyence VR-3000 3D Profilometer, Keyence, Japan) was used to assess film roughness and thickness. SEM (Teneo, FEI, US)

imaging was used to analyze the surface properties of the films and assess the coating homogeneity. For SEM analysis, spin-coated MSN films were sputtered with a 2-nm layer of iridium and imaged at 25000 x and 10000 x magnification. WCA of MSN films was measured by a sessile drop technique at room temperature using a contact angle goniometer (Drop shape Analyzer DSA25, Kruss, Germany). For this, nanoparticle spin coated coverslips and uncoated coverslips were fixed on a stage of the goniometer. A droplet of 5 μ l water dropped onto the films and the values were read after 1 minute.

5.4. hMSCs *in vitro* cell culture

hMSCs were obtained from one donor with informed consent and cultured in α MEM medium with the addition of 10% (v/v) FBS, 0.2 mM ASAP at 37 °C, 5% CO₂ in a humidified atmosphere. Cells before passage 6 were used for the experiments. Cell seeding densities varied depending on the individual experiment and detailed information can be found in each experimental section.

5.5. Cell morphology on films and image analysis

Cell morphology on MSN films was evaluated by staining hMSCs for F-actin and nuclei using Alexa Fluor™ 647 Phalloidin and 4', 6 diamidino-2-phenylindole (DAPI). hMSCs were seeded onto the films at a density of 3000 cells cm⁻² and 1000 cells cm⁻² for culturing 1 day and 3 days, respectively. Before staining, cells were rinsed with PBS and fixed with 4% PFA for 15 min. After three times of washing with PBS, samples were incubated with freshly-prepared Triton X-100 (0.2% (vol/vol) in PBS) for 10 min and blocked with blocking buffer (4% (w/v) BSA and 0.05% (v/v) Tween in PBS) for 1h at RT. After blocking, the cells were stained with Alexa Fluor™ 647 Phalloidin (1:40 in PBS) overnight at 4°C, followed by DAPI staining (1:100 in PBS) for 15 min. Then the films were rinsed with PBS, mounted on a glass slide with mounting media (Dako) and imaged using a Nikon Eclipse Ti-E microscope (Nikon Instruments Europe BV, the Netherlands) at 20x objectives.

Quantitative analysis of cell morphology was performed using cell profiles as we have done previously [31, 69]. The attached cell number was determined by applying Otsu adaptive thresholding method on the DAPI channels. The cell morphology was analyzed by applying Otsu adaptive thresholding method on both DAPI and Phalloidin channel. The parameters describing cell morphology were

quantified in terms of cell spreading area (the number of pixels occupied) and form factors (numbers closer to 1 describes rounder cells)

5.6. Cell focal adhesion on films

Cell focal adhesion was also analyzed using immunohistochemical staining. hMSCs were seeded onto MSN films at a density of 1500 cells cm^{-2} . Briefly, after 5 days of culture, hMSCs were fixed with 4% PFA for 10-15 min, permeabilized with Triton X-100 (0.2% (vol/vol) in PBS) for 10 min and blocked with blocking buffer (4% (w/v) BSA and 0.05% (v/v) Tween in PBS) for 1h at RT. After that, cells were incubated with Alexa Fluor® 647 Anti-Vinculin antibody (1:200 in blocking buffer) overnight at 4°C, followed by washing three times with PBS. To visualize actin bundles and nuclei, hMSCs were stained with Alexa Fluor™ 488 Phalloidin (1:40 in PBS) for 1 h and DAPI (1:100 in PBS) for 15 min at RT, respectively. After gently rinsing with PBS, samples were mounted Dako® and imaged with a Nikon Eclipse Ti-E microscope (Nikon Instruments Europe BV, the Netherlands) using a 40x objective. Images were further processed to assess the length and area of vinculin using NIS-Elements AR Analysis 5.30 with a custom-made pipeline.

5.7. Computer simulations

We used Python 3.8 to create a 2D grid (2000 × 2000) on which we could place circles with a diameter of 70 nm to represent MSN particles coating a 2D surface. RGD containing MSN particles were distributed on the surface randomly among other MSN particles using the function “random.sample” from the Python random module. For each simulation, we repeated the random coatings a hundred times in order to avoid any sampling bias. Using the coating simulations we aimed to answer two main questions:

- 1) What percent of MSN-RGD particles need to be used in order to obtain sufficient aggregation between RGD particles to provide the basis for optimal focal adhesion formation?
- 2) What is the main difference between low and high local density MSN-RGD particles in terms of the RGD spacing and particle aggregation?

For the first question, we simulated surface coatings for 10%, 25%, 50% and 75% of MSN-RGD particles. A representative example of nanoparticles random distribution on surfaces is shown in Figure 2a. Note that we use a mean field approximation on the MSN nanoparticles. Any RGD ligand that is attached to the MSN has no specific location- the dimensions on the nanoparticle itself are invalid.

We defined MSN-RGD particles as “neighbors” if they were at most 70 nm apart from one another (surface-to-surface Euclidean distance). We then reported the mean ratio of MSN-RGD particles with at least one neighbor over the total number of MSN-RGD particles for each wt% composition. We also reported the average number of neighbors per MSN-RGD particle (average of 100 coatings) in each wt% to provide an idea of the aggregate size of the RGD peptides in each setup. Additionally, we investigated the effect of the nanoparticle size on RGD ligand distribution at a certain RGD global density (25% RGD). Same as calculating the number of the “neighbors”, we adjusted the diameter of the circles, which in turn recalculated the position of each MSN nanoparticle and how many nanoparticles could fit within a 2000 × 2000 nm surface. We then placed RGD particles at random locations, until a global density of 25% is achieved. We then identified RGD-MSN particles that had a RGD-MSN neighbour within the cut-off distance of 70 nm.

For the second question, we introduced a metric called the effective distance, which indicates the average distance between any two MSN-RGD particles on the 2D surface. Biologically, the effective distance corresponds to the distance a cell needs to span in order to adhere to any two RGD carrying particle. To simulate the high local density MSN-RGD particles, we assumed they carried twice as many RGD peptides as the low local density MSN-RGD particles did. The average distance between any RGD particles is then calculated as: sum of all distances between RGD ligands (Figure 5a). For the high density clustering, due to mean field approximation, we assume that the distance between two RGD nanoparticles on the same MSN particle can be safely neglected. Again, due to mean field approximation, the distance between any two ligands on two different MSN is always same. We then compared how the effective distance changes between the low and high local density setups. We repeated these simulations for varying surface sizes in order to make sure the results were not affected by the choice of surface size.

5.8. Alkaline Phosphatase Assay

Osteogenic differentiation of hMSCs was evaluated by measuring ALP levels after 14 days of culture using alkaline phosphatase kit (Abcam) according to the manufacturer’s instructions. The CyQuant cell proliferation was used to determine DNA content for the normalization of ALP levels. hMSCs were seeded onto MSN films at a density of 4000 cells cm⁻². For cell seeding, 250 µl of cell

suspension was carefully pipetted on the films, or uncoated glass coverslips (negative control), and cells were left to adhere for 4 h. After 4 h of incubation, the cells were refreshed with 2 ml of basic medium or osteogenic medium (basic medium supplemented with 10 nM dexamethasone). After 14 days of culture, cells were harvested from the films or uncoated glass, rinsed with PBS and then divided into two portions. One portion was used to measure ALP levels and another one was used to measure DNA content.

To measure ALP levels, cells were resuspended in appropriate volumes of Assay Buffer provided in the kit. Then samples were incubated with MUP substrate (5 mM) at 25°C for 30 min in dark. After that, Stop Solution was added to the samples and fluorescent signal was measured on a spectrophotometer at 360 nm. ALP values were normalized with total DNA content per sample and expressed as an x-fold increase compared to the negative control.

To measure DNA content, cells were frozen-thawed for three cycles at -80 °C and then digested by incubating with Proteinase K solution (1 mg/ml in Tri-EDTA buffer, pH 8.0) overnight at 56°C. After another three cycles of freezing-thawing at -80 °C, the Proteinase K digested samples were lysed with RNase-containing lysis buffer for 1h at RT. Afterward, the cell lysate was mixed with GR-dye solution (provided in the CyQuant kit, 1:200 in lysis buffer). After 15min of incubation, the fluorescent signal was measured with a spectrophotometer at $\lambda_{ex} = 485 \pm 10$ nm, $\lambda_{em} = 530 \pm 20$ nm. Absolute DNA amounts were calculated using the standard curve prepared following the supplier's instructions.

5.9. Statistical analysis

All data was statistically analyzed using one-way analysis of variance (ANOVA) followed by a Turkey's multiple comparison post hoc test. All data was expressed as the mean \pm standard deviation. For all figures the following p-values apply: *p < 0.05; **p < 0.01; ***p < 0.001. A difference with a p-value less than 0.05 was considered statistically significant.

Authorship contribution statement

Xingzhen Zhang: Conceptualization, Methodology, Validation, Formal analysis, Investigation, Writing—original draft, Visualization. Zeynep Karagöz: Software, Visualization, Writing—review & editing. Sangita Swapnasrita: Software, Visualization, Writing—review & editing. Pamela Habibovic: Writing—review & editing, Supervision. Aurélie Carlier: Resources, Writing—review & editing. Sabine

van Rijt: Conceptualization, Investigation, Writing–review & editing, Supervision, and Project administration.

Conflict of Interest Statement

The authors declare no conflict of interest.

Acknowledgements

This research was financially supported by the Gravitation Program “Materials Driven Regeneration”, funded by the Dutch Research Council NWO (024.003.013). The authors would like to thank Dr. Timo Rademakers for technical assistance with microscopy imaging analysis. The authors also would like to thank Lei He for help with TEM imaging. Xingzhen Zhang acknowledges Ke Song for assisting with Profilometer measurement. Xingzhen Zhang also acknowledges a bursary support from the China Scholarship Council.

Supporting Information

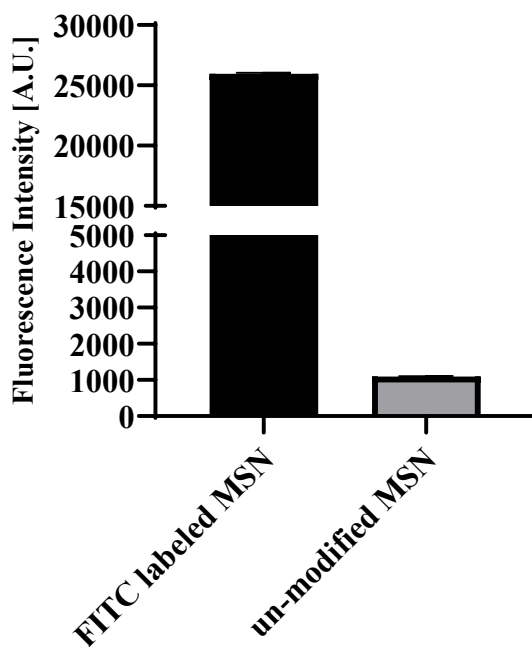


Figure S1. Fluorescence intensity (a.u.) of FITC-NHS labeled MSN_{NH_2} Un-modified MSN used as control.

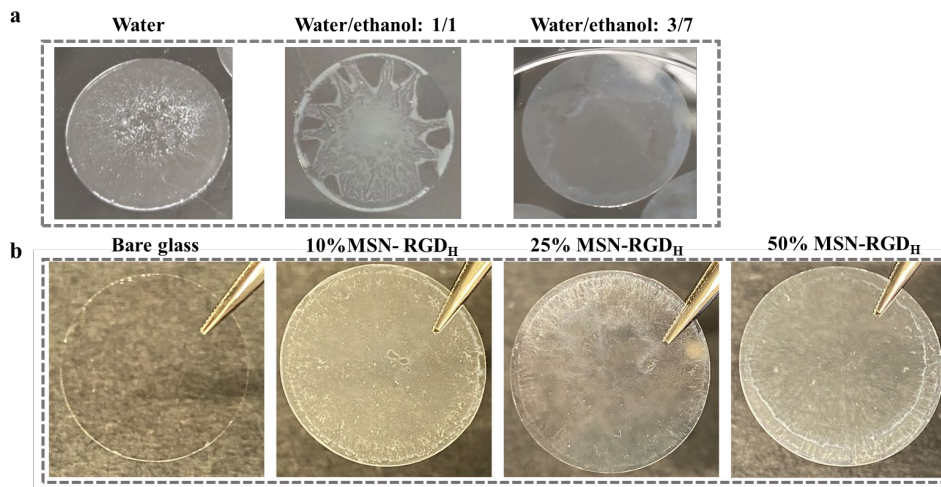


Figure S2. Optical image of MSN films. a) The effect of different ratios of ethanol/water as MSN-RGD_H dispersion solvent on spin coating quality. b) Optimized and homogenous surface coating of MSN surface obtained from different ratios of MSN-PEG and MSN-RGD_H.

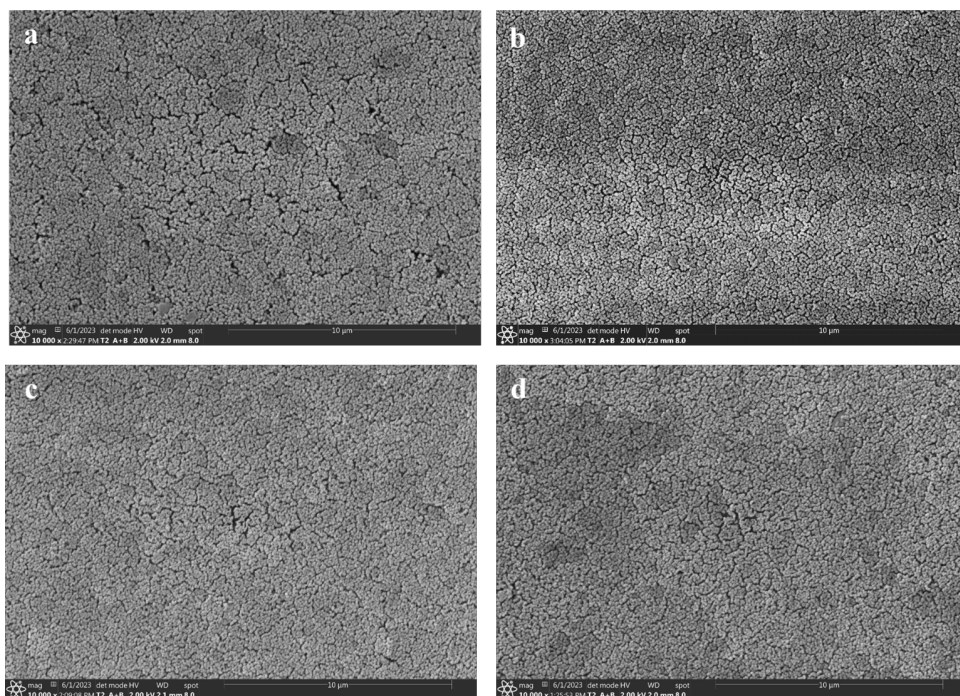


Figure S3. SEM images showing the homogenous surface structure of the MSN films made from a) 50% MSN-RGD_L, b) 25% MSN-RGD_H, c) 100% MSN-RGD_L, and d) 50% MSN-RGD_H nanoparticle compositions.

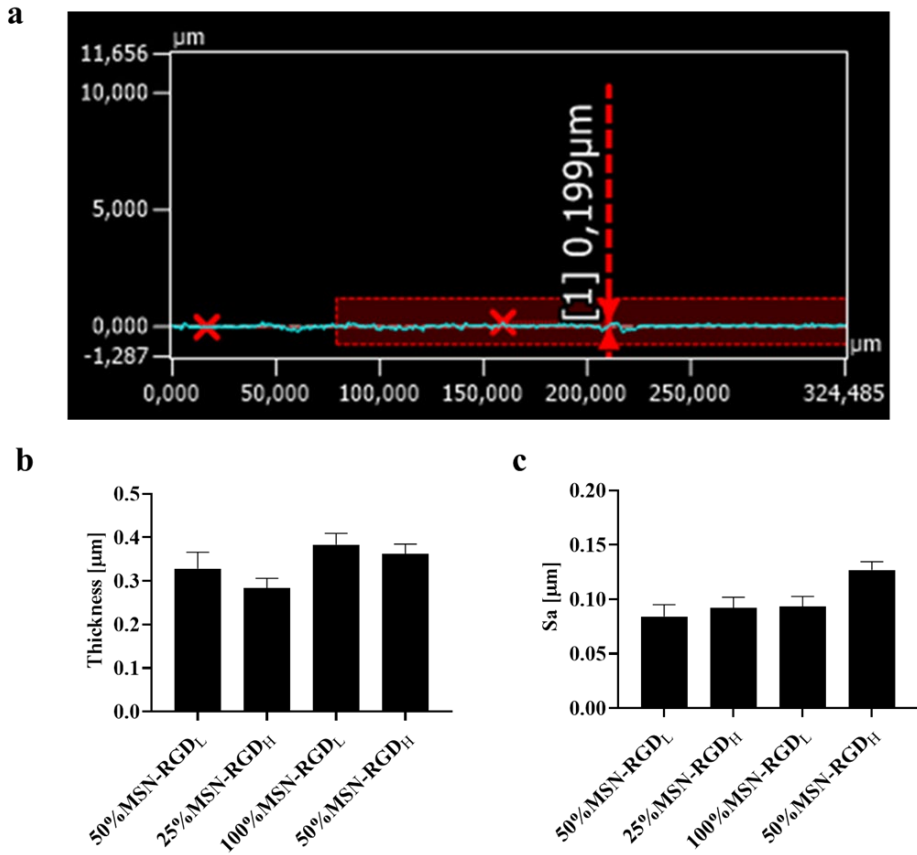


Figure S4. a) A representative 3D laser scanning microscopy image showing the smooth surface profile of the MSN film. b) Surface thickness and c) surface roughness.

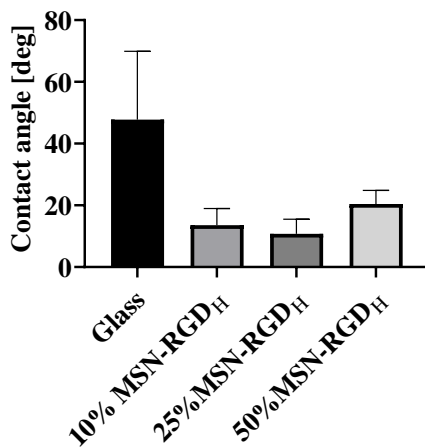


Figure S5. The water contact angle of glass substrates and different MSN films.

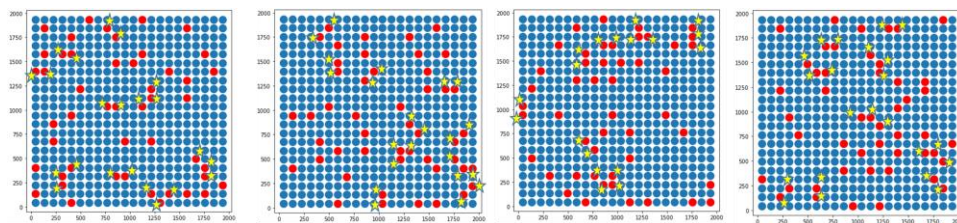


Figure S6. A schematic illustration showing four examples of random nanoparticle distribution on 10% MSN-RGD_H surface, 484 particles in total, 48 of them are MSN-RGD_H in red. The yellow stars indicate the RGD particles having another neighboring RGD particle within 70 nm distance.

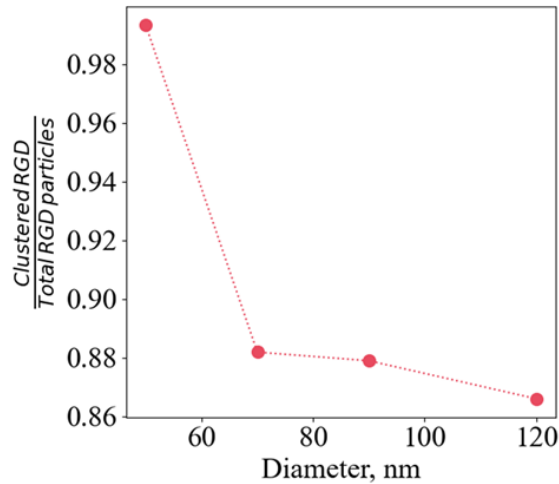


Figure S7. Computational description of how the size of the nanoparticle influences the ratio of MSN-RGD particles which have at least one other MSN-RGD within 70 nm distance (clustered RGD) over the total number of MSN-RGD particles on the surface.

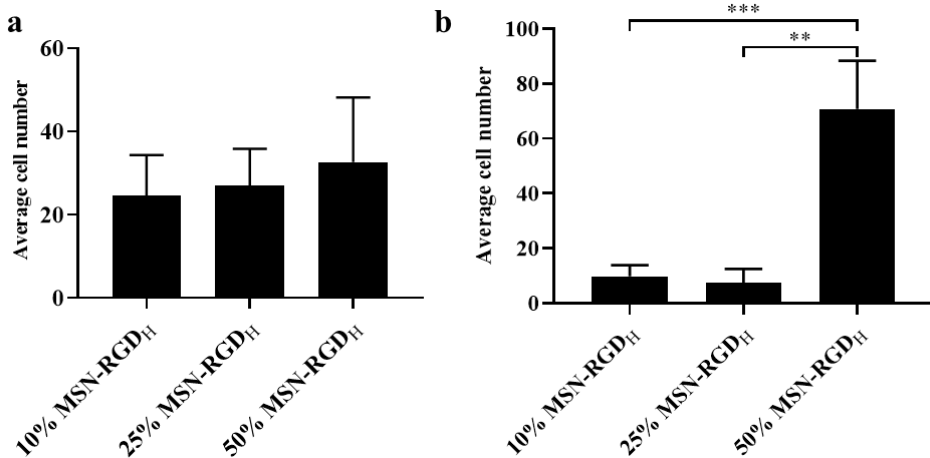


Figure S8. Effect of RGD global density on hMSC attachment. Quantification of attached cell number of hMSCs cultured on 10% MSM-RGD_H, 25% MSM-RGD_H and 50% MSM-RGD_H films for a) 1 day and b) 3 days. Data are expressed as the mean \pm SD (n=3). *p < 0.05; **p < 0.01; ***p < 0.001.

References

- [1] C. Trayford, D. Crosbie, T. Rademakers, C. van Blitterswijk, R. Nuijts, S. Ferrari, P. Habibovic, V. LaPointe, M. Dickman, S. van Rijt, Mesoporous Silica-Coated Gold Nanoparticles for Multimodal Imaging and Reactive Oxygen Species Sensing of Stem Cells, *ACS Appl Nano Mater* 5(3) (2022) 3237-3251.
- [2] W. Zakrzewski, M. Dobrzyński, M. Szymonowicz, Z. Rybak, Stem cells: past, present, and future, *Stem Cell Research & Therapy* 10(1) (2019) 68.
- [3] A. Brunet, M.A. Goodell, T.A. Rando, Ageing and rejuvenation of tissue stem cells and their niches, *Nature Reviews Molecular Cell Biology* (2022).
- [4] M. Ahmed, C. Ffrench-Constant, Extracellular Matrix Regulation of Stem Cell Behavior, *Curr Stem Cell Rep* 2(3) (2016) 197-206.
- [5] G.S. Hussey, J.L. Dziki, S.F. Badylak, Extracellular matrix-based materials for regenerative medicine, *Nature Reviews Materials* 3(7) (2018) 159-173.
- [6] M. Okawa, A. Tanabe, S. Ohta, S. Nagatoishi, K. Tsumoto, T. Ito, Extracellular matrix-inspired hydrogel of hyaluronan and gelatin crosslinked via a Link module with a transglutaminase reactive sequence, *Communications Materials* 3(1) (2022) 81.
- [7] D. Dems, R. Freeman, K.D. Riker, T. Coradin, S.I. Stupp, C. Aimé, Multivalent Clustering of Adhesion Ligands in Nanofiber-Nanoparticle Composites, *Acta Biomaterialia* 119 (2021) 303-311.
- [8] S.W. Lane, D.A. Williams, F.M. Watt, Modulating the stem cell niche for tissue regeneration, *Nat Biotechnol* 32(8) (2014) 795-803.
- [9] J. Nicolas, S. Magli, L. Rabbachin, S. Sampaolesi, F. Nicotra, L. Russo, 3D Extracellular Matrix Mimics: Fundamental Concepts and Role of Materials Chemistry to Influence Stem Cell Fate, *Biomacromolecules* 21(6) (2020) 1968-1994.
- [10] X. Zhang, S. van Rijt, 2D biointerfaces to study stem cell-ligand interactions, *Acta Biomater* 131 (2021) 80-96.
- [11] M. Camman, P. Joanne, O. Agbulut, C. Hélyary, 3D models of dilated cardiomyopathy: Shaping the chemical, physical and topographical properties of biomaterials to mimic the cardiac extracellular matrix, *Bioactive Materials* 7 (2022) 275-291.
- [12] Y.H. Tsou, J. Khoneisser, P.C. Huang, X. Xu, Hydrogel as a bioactive material to regulate stem cell fate, *Bioact Mater* 1(1) (2016) 39-55.
- [13] A. Tahlawi, M.E. Klontzas, M.C. Allenby, J.C.F. Morais, N. Panoskaltsis, A. Mantalaris, RGD-functionalized polyurethane scaffolds promote umbilical cord blood mesenchymal stem cell expansion and osteogenic differentiation, *J Tissue Eng Regen Med* 13(2) (2019) 232-243.

- [14] M.J. Dalby, N. Gadegaard, R.O. Oreffo, Harnessing nanotopography and integrin-matrix interactions to influence stem cell fate, *Nat Mater* 13(6) (2014) 558-69.
- [15] H. Donnelly, M. Salmeron-Sanchez, M.J. Dalby, Designing stem cell niches for differentiation and self-renewal, *Journal of the Royal Society, Interface* 15(145) (2018).
- [16] J.-P. Xiong, T. Stehle, R. Zhang, A. Joachimiak, M. Frech, S.L. Goodman, M.A. Arnaout, Crystal Structure of the Extracellular Segment of Integrin $\alpha V\beta 3$ in Complex with an Arg-Gly-Asp Ligand, *Science* 296(5565) (2002) 151-155.
- [17] M. Nieberler, U. Reuning, F. Reichart, J. Notni, H.J. Wester, M. Schwaiger, M. Weinmüller, A. Räder, K. Steiger, H. Kessler, Exploring the Role of RGD-Recognizing Integrins in Cancer, *Cancers (Basel)* 9(9) (2017).
- [18] H. Kang, H.J. Jung, D.S.H. Wong, S.K. Kim, S. Lin, K.F. Chan, L. Zhang, G. Li, V.P. Dravid, L. Bian, Remote Control of Heterodimeric Magnetic Nanoswitch Regulates the Adhesion and Differentiation of Stem Cells, *Journal of the American Chemical Society* 140(18) (2018) 5909-5913.
- [19] O.J. Mezu-Ndubuisi, A. Maheshwari, The role of integrins in inflammation and angiogenesis, *Pediatric Research* 89(7) (2021) 1619-1626.
- [20] G. Kocer, P. Jonkheijm, About Chemical Strategies to Fabricate Cell-Instructive Biointerfaces with Static and Dynamic Complexity, *Adv Healthc Mater* 7(14) (2018) e1701192.
- [21] A. Lagunas, I. Tsintzou, Y. Vida, D. Collado, E. Pérez-Inestrosa, C. Rodríguez Pereira, J. Magalhaes, J.A. Andrades, J. Samitier, Tailoring RGD local surface density at the nanoscale toward adult stem cell chondrogenic commitment, *Nano Research* 10(6) (2016) 1959-1971.
- [22] J. Li, Y. Chen, N. Kawazoe, G. Chen, Ligand density-dependent influence of arginine-glycine-aspartate functionalized gold nanoparticles on osteogenic and adipogenic differentiation of mesenchymal stem cells, *Nano Research* 11(3) (2018) 1247-1261.
- [23] E.A. Cavalcanti-Adam, T. Volberg, A. Micoulet, H. Kessler, B. Geiger, J.P. Spatz, Cell spreading and focal adhesion dynamics are regulated by spacing of integrin ligands, *Biophys J* 92(8) (2007) 2964-74.
- [24] S. Sankaran, E. Cavatorta, J. Huskens, P. Jonkheijm, Cell Adhesion on RGD-Displaying Knottins with Varying Numbers of Tryptophan Amino Acids to Tune the Affinity for Assembly on Cucurbit[8]uril Surfaces, *Langmuir* 33(35) (2017) 8813-8820.
- [25] F. Karimi, A.J. O'Connor, G.G. Qiao, D.E. Heath, Integrin Clustering Matters: A Review of Biomaterials Functionalized with Multivalent Integrin-Binding Ligands to Improve Cell Adhesion, Migration, Differentiation, Angiogenesis, and Biomedical Device Integration, *Adv Healthc Mater* 7(12) (2018) e1701324.

- [26] C.J. Brinkerhoff, J.J. Linderman, Integrin dimerization and ligand organization: key components in integrin clustering for cell adhesion, *Tissue Eng* 11(5-6) (2005) 865-76.
- [27] G. Maheshwari, G. Brown, D.A. Lauffenburger, A. Wells, L.G. Griffith, Cell adhesion and motility depend on nanoscale RGD clustering, *J Cell Sci* 113 (Pt 10) (2000) 1677-86.
- [28] X. Wang, C. Yan, K. Ye, Y. He, Z. Li, J. Ding, Effect of RGD nanospacing on differentiation of stem cells, *Biomaterials* 34(12) (2013) 2865-74.
- [29] K. Ye, X. Wang, L. Cao, S. Li, Z. Li, L. Yu, J. Ding, Matrix Stiffness and Nanoscale Spatial Organization of Cell-Adhesive Ligands Direct Stem Cell Fate, *Nano Letters* 15(7) (2015) 4720-4729.
- [30] Y. Peng, Q.-J. Liu, T. He, K. Ye, X. Yao, J. Ding, Degradation rate affords a dynamic cue to regulate stem cells beyond varied matrix stiffness, *Biomaterials* 178 (2018) 467-480.
- [31] X. Zhang, S. van Rijt, DNA modified MSN-films as versatile biointerfaces to study stem cell adhesion processes, *Colloids Surf B Biointerfaces* 215 (2022) 112495.
- [32] M. Vallet-Regí, F. Schüth, D. Lozano, M. Colilla, M. Manzano, Engineering mesoporous silica nanoparticles for drug delivery: where are we after two decades?, *Chemical Society Reviews* 51(13) (2022) 5365-5451.
- [33] P. Sutthavas, Z. Tahmasebi Birgani, P. Habibovic, S. van Rijt, Calcium Phosphate-Coated and Strontium-Incorporated Mesoporous Silica Nanoparticles Can Effectively Induce Osteogenic Stem Cell Differentiation, *Adv Healthc Mater* (2021) e2101588.
- [34] L. Andree, D. Barata, P. Sutthavas, P. Habibovic, S. van Rijt, Guiding mesenchymal stem cell differentiation using mesoporous silica nanoparticle-based films, *Acta Biomater* 96 (2019) 557-567.
- [35] Y. Arima, H. Iwata, Effect of wettability and surface functional groups on protein adsorption and cell adhesion using well-defined mixed self-assembled monolayers, *Biomaterials* 28(20) (2007) 3074-3082.
- [36] Z. Karagöz, L. Rijns, P.Y.W. Dankers, M. van Griensven, A. Carlier, Towards understanding the messengers of extracellular space: Computational models of outside-in integrin reaction networks, *Computational and Structural Biotechnology Journal* 19 (2021) 303-314.
- [37] Q. Liu, S. Zheng, K. Ye, J. He, Y. Shen, S. Cui, J. Huang, Y. Gu, J. Ding, Cell migration regulated by RGD nanospacing and enhanced under moderate cell adhesion on biomaterials, *Biomaterials* 263 (2020) 120327.
- [38] J. He, Q. Liu, S. Zheng, R. Shen, X. Wang, J. Gao, Q. Wang, J. Huang, J. Ding, Enlargement, Reduction, and Even Reversal of Relative Migration Speeds of Endothelial and Smooth Muscle Cells on Biomaterials Simply by Adjusting RGD Nanospacing, *ACS Appl Mater Interfaces* 13(36) (2021) 42344-42356.

- [39] S. Zheng, Q. Liu, J. He, X. Wang, K. Ye, X. Wang, C. Yan, P. Liu, J. Ding, Critical adhesion areas of cells on micro-nanopatterns, *Nano Research* 15(2) (2022) 1623-1635.
- [40] J. He, R. Shen, Q. Liu, S. Zheng, X. Wang, J. Gao, Q. Wang, J. Huang, J. Ding, RGD Nanoarrays with Nanospacing Gradient Selectively Induce Orientation and Directed Migration of Endothelial and Smooth Muscle Cells, *ACS Appl Mater Interfaces* 14(33) (2022) 37436-37446.
- [41] P. Peach, Bias in Pseudo-Random Numbers, *Journal of the American Statistical Association* 56(295) (1961) 610-618.
- [42] W.A. Comisar, N.H. Kazmers, D.J. Mooney, J.J. Linderman, Engineering RGD nanopatterned hydrogels to control preosteoblast behavior: A combined computational and experimental approach, *Biomaterials* 28(30) (2007) 4409-4417.
- [43] J. Yu, J. Huang, J.A. Jansen, C. Xiong, X.F. Walboomers, Mechanochemical mechanism of integrin clustering modulated by nanoscale ligand spacing and rigidity of extracellular substrates, *J Mech Behav Biomed Mater* 72 (2017) 29-37.
- [44] P. Kanchanawong, D.A. Calderwood, Organization, dynamics and mechanoregulation of integrin-mediated cell-ECM adhesions, *Nature Reviews Molecular Cell Biology* (2022).
- [45] M. Arnold, V.C. Hirschfeld-Warneken, T. Lohmüller, P. Heil, J. Blümmel, E.A. Cavalcanti-Adam, M. López-García, P. Walther, H. Kessler, B. Geiger, J.P. Spatz, Induction of cell polarization and migration by a gradient of nanoscale variations in adhesive ligand spacing, *Nano Lett* 8(7) (2008) 2063-9.
- [46] J.C. Kuo, Mechanotransduction at focal adhesions: integrating cytoskeletal mechanics in migrating cells, *J Cell Mol Med* 17(6) (2013) 704-12.
- [47] J.D. Humphries, P. Wang, C. Streuli, B. Geiger, M.J. Humphries, C. Ballestrem, Vinculin controls focal adhesion formation by direct interactions with talin and actin, *The Journal of cell biology* 179(5) (2007) 1043-1057.
- [48] E.K.F. Yim, E.M. Darling, K. Kulangara, F. Guilak, K.W. Leong, Nanotopography-induced changes in focal adhesions, cytoskeletal organization, and mechanical properties of human mesenchymal stem cells, *Biomaterials* 31(6) (2010) 1299-1306.
- [49] X. Wang, S. Li, C. Yan, P. Liu, J. Ding, Fabrication of RGD Micro/Nanopattern and Corresponding Study of Stem Cell Differentiation, *Nano Letters* 15(3) (2015) 1457-1467.
- [50] M.H. You, M.K. Kwak, D.H. Kim, K. Kim, A. Levchenko, D.Y. Kim, K.Y. Suh, Synergistically enhanced osteogenic differentiation of human mesenchymal stem cells by culture on nanostructured surfaces with induction media, *Biomacromolecules* 11(7) (2010) 1856-62.
- [51] B. Wang, W. Wang, Y. Yu, Y. Zhang, J. Zhang, Z. Yuan, The study of angiogenesis stimulated by multivalent peptide ligand-modified alginate, *Colloids Surf B Biointerfaces* 154 (2017) 383-390.

- [52] I. Bilem, P. Chevallier, L. Plawinski, E.D. Sone, M.C. Durrieu, G. Laroche, RGD and BMP-2 mimetic peptide crosstalk enhances osteogenic commitment of human bone marrow stem cells, *Acta Biomater* 36 (2016) 132-42.
- [53] D.S.H. Wong, J.N. Li, X.H. Yan, B. Wang, R. Li, L. Zhang, L.M. Bian, Magnetically Tuning Tether Mobility of Integrin Ligand Regulates Adhesion, Spreading, and Differentiation of Stem Cells, *Nano Letters* 17(3) (2017) 1685-1695.
- [54] A.U. Khan, R. Qu, T. Fan, J. Ouyang, J. Dai, A glance on the role of actin in osteogenic and adipogenic differentiation of mesenchymal stem cells, *Stem Cell Res Ther* 11(1) (2020) 283.
- [55] R. McBeath, D.M. Pirone, C.M. Nelson, K. Bhadriraju, C.S. Chen, Cell shape, cytoskeletal tension, and RhoA regulate stem cell lineage commitment, *Dev Cell* 6(4) (2004) 483-95.
- [56] W.J. Hadden, Y.S. Choi, The extracellular microscale governs mesenchymal stem cell fate, *J Biol Eng* 10 (2016) 16.
- [57] J.A. Rowley, D.J. Mooney, Alginate type and RGD density control myoblast phenotype, *J Biomed Mater Res* 60(2) (2002) 217-23.
- [58] R. Sivkova, J. Táborská, A. Reparaz, A. de Los Santos Pereira, I. Kotelnikov, V. Proks, J. Kučka, J. Svoboda, T. Riedel, O. Pop-Georgievski, Surface Design of Antifouling Vascular Constructs Bearing Biofunctional Peptides for Tissue Regeneration Applications, *Int J Mol Sci* 21(18) (2020).
- [59] F. Karimi, T.G. McKenzie, A.J. O'Connor, G.G. Qiao, D.E. Heath, Nano-scale clustering of integrin-binding ligands regulates endothelial cell adhesion, migration, and endothelialization rate: novel materials for small diameter vascular graft applications, *Journal of Materials Chemistry B* 5(30) (2017) 5942-5953.
- [60] S. Miyamoto, S.K. Akiyama, K.M. Yamada, Synergistic roles for receptor occupancy and aggregation in integrin transmembrane function, *Science* 267(5199) (1995) 883-5.
- [61] G. Maheshwari, G. Brown, D.A. Lauffenburger, A. Wells, L.G. Griffith, Cell adhesion and motility depend on nanoscale RGD clustering, *Journal of Cell Science* 113(10) (2000) 1677.
- [62] E.A. Cavalcanti-Adam, D. Aydin, V.C. Hirschfeld-Warneken, J.P. Spatz, Cell adhesion and response to synthetic nanopatterned environments by steering receptor clustering and spatial location, *Hfsp j* 2(5) (2008) 276-85.
- [63] P.L. Benitez, S. Mascharak, A.C. Proctor, S.C. Heilshorn, Use of protein-engineered fabrics to identify design rules for integrin ligand clustering in biomaterials, *Integr Biol (Camb)* 8(1) (2016) 50-61.
- [64] P.P. Han, J.E. Frith, G.A. Gomez, A.S. Yap, G.M. O'Neill, J.J. Cooper-White, Five Piconewtons: The Difference between Osteogenic and Adipogenic Fate Choice in Human Mesenchymal Stem Cells, *Acs Nano* 13(10) (2019) 11129-11143.

[65] C. Cimmino, L. Rossano, P.A. Netti, M. Ventre, Spatio-Temporal Control of Cell Adhesion: Toward Programmable Platforms to Manipulate Cell Functions and Fate, *Front Bioeng Biotechnol* 6 (2018) 190.

[66] M.J. Biggs, M.J. Dalby, Focal adhesions in osteoneogenesis, *Proc Inst Mech Eng H* 224(12) (2010) 1441-53.

[67] S. Huvneers, E.H. Danen, Adhesion signaling - crosstalk between integrins, Src and Rho, *J Cell Sci* 122(Pt 8) (2009) 1059-69.

[68] V. Cauda, A. Schlossbauer, J. Kecht, A. Zürner, T. Bein, Multiple Core-Shell Functionalized Colloidal Mesoporous Silica Nanoparticles, *Journal of the American Chemical Society* 131(32) (2009) 11361-11370.

[69] P. Sutthavas, P. Habibovic, S.H. van Rijt, The shape-effect of calcium phosphate nanoparticle based films on their osteogenic properties, *Biomaterials Science* 9(5) (2021) 1754-1766.

Chapter 5

Effects of ligand-presenting dynamics on stem cell adhesion and migration

Xingzhen Zhang¹, Stijn van Veen², Darya Hadavi³, Yuandi Zhao³, Marten Honing³, Pamela Habibović¹, Lorenzo Albertazzi², Sabine van Riemsdijk^{1*}

¹Department of Instructive Biomaterials Engineering, MERLN Institute for Technology Inspired Regenerative Medicine, Maastricht University, Maastricht, the Netherlands.

²Department of Biomedical Engineering and Institute for Complex Molecular Systems (ICMS), Eindhoven University of Technology, Eindhoven, the Netherlands.

³Maastricht Multimodal Molecular Imaging (MMI) Institute, Division of Imaging Mass Spectrometry, Maastricht University, Maastricht, the Netherlands.

EMBARGOED

Chapter 6

General Discussion

Tissue engineering, which applies methods from engineering and life sciences to create artificial constructs to direct tissue regeneration, has attracted the interest of many researchers with the hope to regenerate patient's own tissues and organs [1]. An important avenue of tissue engineering is the development of synthetic ECM-mimicking materials that can guide tissue formation and promote regenerative processes. Such materials should not only provide an appropriate physical environment, which mimics the mechanical and structural properties of the target tissue, but also provide adhesive ligands for cells to adhere, as well as for bioactive molecules that guide cellular behavior. In particular, developing material systems that direct specific cellular behavior is a major goal of biomaterials and tissue engineering technologies. One method to achieve this goal is to biofunctionalize materials with peptide ligands that bind to integrin receptors responsible for cell adhesion [2]. In the past decades, RGD tripeptide, which is the minimal motif required to specifically bind to integrin receptors, has been extensively utilized to modify different biomaterials, such as implants, scaffolds, and hydrogels, to promote cell adhesion and survival [3-5]. However, the mode of ligand incorporation in a material has significant impact on ligand functionality and subsequent cell-material interactions [6]. There are many important aspects to consider when functionalizing materials with adhesive peptides including ligand density, spacing and tether properties [7-9]. Thus, a comprehensive and systematic understanding of how ligand parameters influence cell behavior is essential in advancing the design and surface functionalization strategies of biomaterials. The aim of this thesis was to improve our fundamental understanding of ligand-integrin interactions in stem cells. To achieve this goal, in Chapter 2, we first provided an overview of the types of cell-instructive biointerfaces that have been developed to study the effect of ligand affinity, density, spacing, crosstalk and dynamicity on stem cell behavior. In Chapters 3-5, we investigate how the tether length, nanoclusters, and temporal kinetics of RGD regulate stem cell adhesion, migration and differentiation. In this current chapter, a general discussion of the results presented in Chapters 3-5 is presented from two perspectives. First, we discuss different strategies and techniques for engineering biointerfaces, and their advantages and limitations in comparison to our systems developed in this thesis. Then, we discuss the implications of our findings for biomaterial science and tissue engineering. Finally, we give an outlook and recommendations for future research using the platforms as developed in this thesis.

1. Strategies to fabricate biointerfaces to control ligand presentation

In the past years, advances in materials science and fabrication technologies have considerably promoted the design and development of biointerfaces with spatiotemporally controlled surface properties as valuable tools to study integrin-ligand interactions [10, 11]. In particular, the development of nanostructured platforms able to control ligand presentation at the order of nanometer-scale proved to be helpful in shedding light on how cells respond to nanoscale surface features. In previous studies, diverse techniques and approaches have been explored to control the spatial RGD arrangements at the nanoscale. These include nanolithography technique, recombinant protein technique, covalent surface grafting, and polymer-based approaches [12-15]. For example, Mark and co-workers used a nanoimprint lithography technique to fabricate nanoarray chips in which geometric arrangement patterns of ligands could be easily modified (Figure 1) [12]. The patterns were generated by electron beam lithography and then transferred into a poly(methyl methacrylate) (PMMA) film, followed by residual PMMA removal and metal evaporation through an angle-evaporated hard mask, lift-off, and thermal annealing to obtain spherical AuPd nanodots. The AuPd nanodots were treated with piranha solution and functionalized with thiolated PEG-biotin for the following cyclic RGDfK ligand conjugation. By applying different nanoimprint template molds for patterning, biochips with heterogeneous ligand patterns including arrangements of nanodots in dimers, trimers, and extended hexagons have been successfully created. In another study, a similar approach based on micellar diblock copolymer lithography has been used to pattern cell-adhesive gold nanodots with high precision at 28, 58, 73, and 85 nm spacing [16]. These studies provided valuable insights into various strategies to control the ligand nanospacing, nanopatterning and nanotopography. In particular, nanoimprint lithography, which is a high-throughput patterning technique, has shown great promise for precise control over nanoscale patterns. However, these come with certain limitations as well. On one hand, these techniques usually rely on expensive and specialized equipment or involve aggressive and complex fabrication processes. For instance, traditional covalent immobilization of ligands to glass substrates often require piranha treatment to activate the hydroxyl groups of glass surfaces [17]. Since piranha solution is extremely hazardous and reactive with many organic materials, handling piranha solutions requires specialized training, equipment and proper safety measures. Beyond the safety concerns,

piranha treatment can result in etching or roughening of the glass surface due to its strong oxidative nature, thereby potentially (negatively) influencing subsequent immobilization processes. In the case of nanolithography, surfaces are usually prepared by patterning with gold nanoparticles, which can hinder the observation of cell morphology using an optical microscope or a fluorescence microscope due to the low light transmittance of gold [18]. Moreover, these current techniques are limited in their capabilities to achieve control over nanoscale ligand clustering, which has been previously reported as a crucial factor in promoting integrin clustering and cell adhesion [19, 20]. To address this limitation, in Chapter 4, we presented a novel strategy to create biointerfaces based on RGD-modified silica nanoparticles (MSN-RGD), which enables high control over RGD ligand clustering level at the nanoscale on 2D surfaces. In our approach, mesoporous silica nanoparticles (MSN) were chemically functionalized with RGD peptides via an antifouling PEG linker. The RGD surface functionalization could be tuned by changing the ratios of MSN to RGD during synthesis, therefore allowing us to change the RGD clustering levels on MSN. Our approach provides numerous advantages over the previously established methods. The first one is the simplicity of the preparation process. In our method, using a simple blending and spin coating technique, homogenous MSN films with varied RGD clustering levels were successfully created and therefore ensure easy modulation of ligand nanoclusters. As previously reported [21], the particle size could be easily tuned, thereby enabling precise control over the size of ligand islands. Further, the average spacing between the clustered ligand islands can be easily changed by controlling the blending ratio of RGD-functionalized to nonfunctionalized MSN. As such, our method paves the way toward highly tunable ligand nanoclusters, which offers a promising tool to unravel the nanoscale cell-ligand interactions.

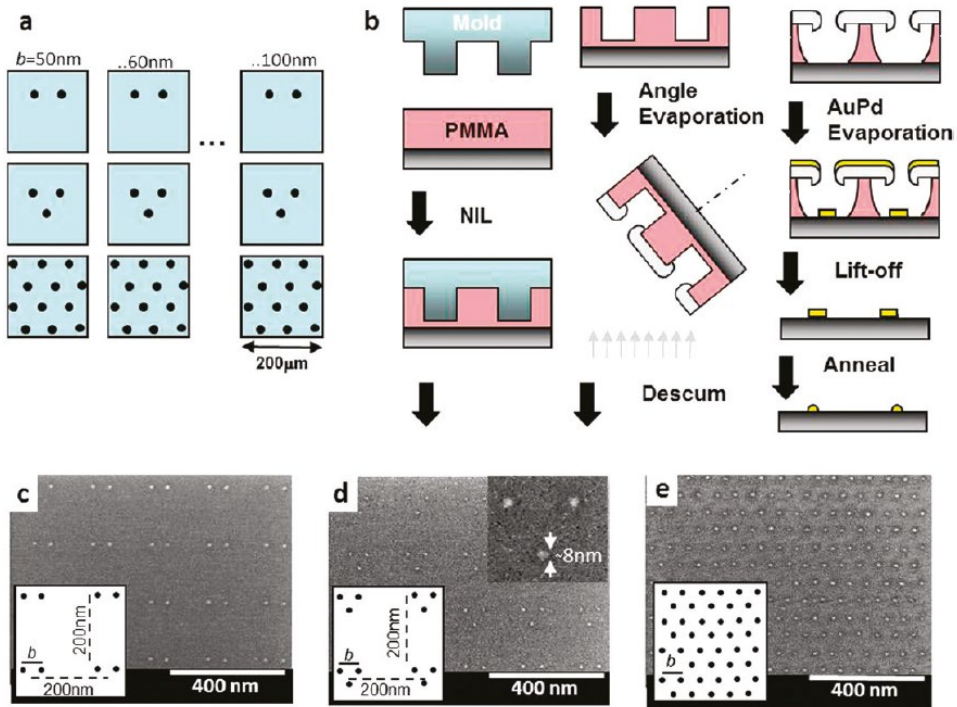


Figure 1. (a) Schematic view of a chip containing arrays of sub-10-nm functionalized nanodots, arranged in dimers, trimers, and extended hexagons with various interdot spacings. Each pattern extends over an area of $200\ \mu\text{m}$. (b) Schematic fabrication process flow of AuPd nanodot arrays. (c-e) SEM images of arrays of dimers, trimers, and extended hexagons, respectively. Reprinted with permission from ref. [12].

In addition to the above-mentioned nanoscale spatial arrangement of adhesion ligands, there is also growing interest in the development of platforms, which enable dynamic and temporal control over ligand presentation. The natural ECM undergoes complex dynamic remodelling, resulting in heterogeneity in ligand composition at the nanoscale *in vivo* [22]. To recapitulate the ECM dynamicity, different approaches and strategies have been explored to create dynamic platforms with smart surface properties capable of controlled display of bioactive ligands. Most current dynamic platforms are based on stimuli-responsive systems. Diverse responsive materials that can respond to physiochemical stimuli (e.g., light [23], chemicals [24], magnetism [25], and electric field [26]) together with various

chemical strategies (e.g., supramolecular chemistry [27], host-guest chemistry [28]) have been investigated to create well controlled and dynamic biointerfaces. These systems often need an external stimulus to change the surface properties, with a strategy to “switch” the ligands between an active and inactivate state [29]. For example, in the study by Cheuk and co-workers, a switchable surface was developed by modifying an electrode surface with a self-assembled monolayer (SAM) that has charged moieties or RGD ligands at their distal ends (Figure 2) [26]. Application of the same potential as the charged moiety caused the molecules to be repelled from the surface, which concealed the RGD peptides from cells. Conversely, the opposite potential resulted in the exposure of RGD. The surface could be switched from a cell-repulsive (inactive state) to cell-adhesive state (active state) by giving an electric stimulus. Although promising in controlling ligands reversibly, most of these strategies involve stimulus intervention to alter the tethering of RGD peptides and may possibly interfere with normal cellular events. In contrast to the previous systems, in Chapter 5, we described the fabrication of a novel dynamic platform using a DNA hybridization strategy to control RGD ligand presenting kinetics on single strand DNA-modified MSN surfaces (MSN-ssDNA). We showed that the surface RGD presenting kinetics could be tuned by altering the base pair length (9, 11 and 20 bp) of csDNA to which the RGD ligands were attached. A dynamic platform with high RGD kinetics was developed using 9 bp DNA constructs. DNA is an interesting engineering tool to spatiotemporally control the attachment of biomolecules onto surfaces, as highlighted in several previous studies where different strategies such as toehold-mediated DNA strand displacement and DNA hairpin conformation switching have been explored to reversibly control and spatially arrange bioactive signal onto surfaces [30-32]. These studies usually rely on competitive hybridization/dehybridization. In contrast to the previous strategy, our approach provides the first evidence for controlling dynamics of RGD presentation by exploiting the DNA spontaneous and intrinsic binding and dissociation processes. Furthermore, we envisage that the high programmable nature of DNA also offers possibilities to present multiple ligands in one system to probe dynamic ligand synergy in the future research.

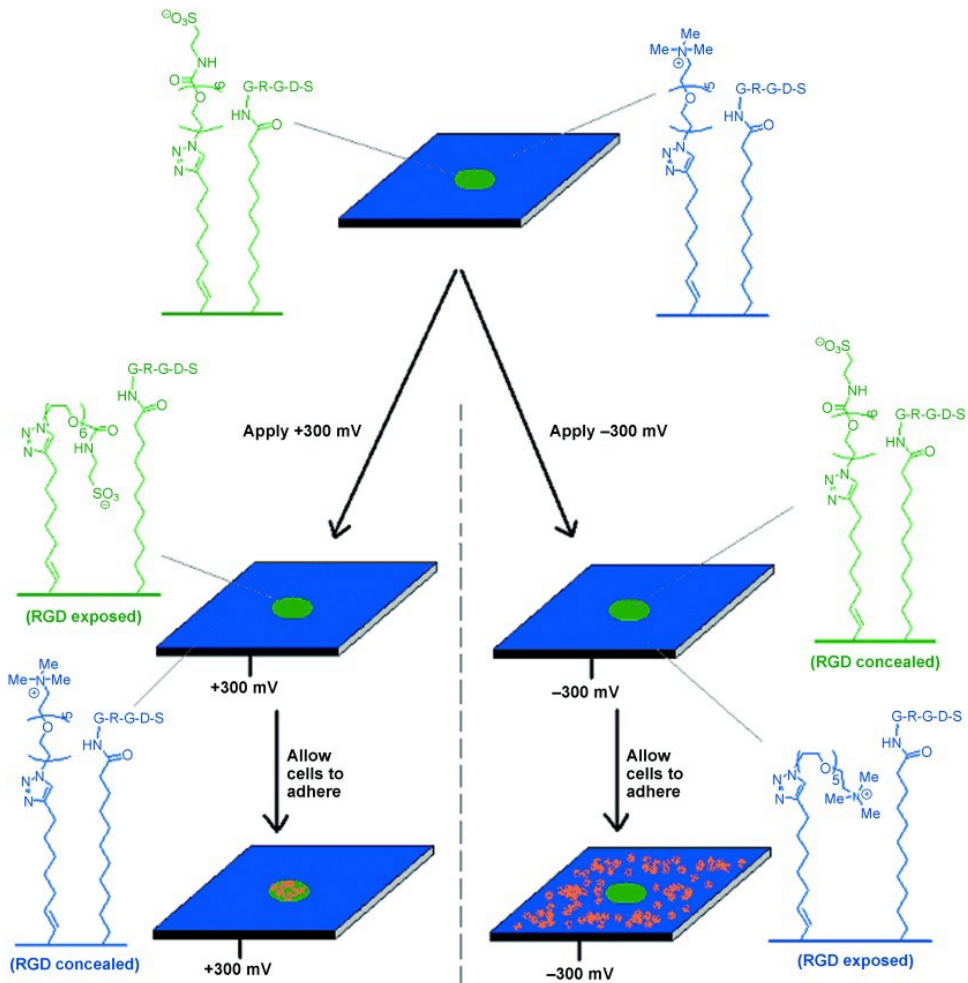


Figure 2. The design principle of the potential-induced switchable surfaces for regulation of ligand presentation. Reprinted with permission from ref. [26].

2. The importance of RGD presentation to control stem cell adhesion

The interaction between adhesion ligands and integrin receptors is of great importance in regulating stem cell processes, including cell adhesion, migration, differentiation, proliferation, and survival [33, 34]. Specifically, ligand presentation mode (e.g., spacing, clustering) alters how cells adhere to a material surface, and defines cell fate through changes in both cell biochemistry and cell morphology

[35]. For example, Steven et al. have shown that the nature of the chemical bond by which RGD ligands were immobilized to the surface could influence cell behavior. In this study, RGD peptides were either attached via thiol-maleimide covalent or supramolecular naphthol-cucurbit[8]uril non-covalent bonds to tetra(ethylene glycol)-based self-assembled surfaces [36]. They found that surfaces coated with non-covalent bound RGD peptides induced a more robust focal adhesion development and mechanobiological response with higher levels of mechanosensitive transcription factors SFR and EGR-1 in fibroblasts, compared to surfaces with covalently bound RGD peptides. Moreover, the importance of RGD presentation has also been shown in studies investigating RGD spacing [37], RGD organization (ordered or disordered patterns) [38], or RGD presentation as either cyclic or linear tripeptides [39]. Therefore, in Chapters 3-5 of this thesis, we further added to the design space of RGD peptides where we investigated how the immobilization linker length, nanoclustering and dynamics of RGD peptides influence stem cell behavior. In this section, we discuss how the knowledge gained from these studies is important for tissue engineering applications where we aim to use ligand functionalization to improve the biological performance of synthetic biomaterials. Although this thesis focuses on stem cells, in this part, we expand our discussion with other types of cells that have been used in the tissue engineering field.

In chapter 3 of the thesis, we studied the effect of the tether length of RGD peptides on RGD functionality and stem cell adhesion processes [40]. We used PEG linkers at varying chain lengths (PEG6, PEG8, PEG12) creating three different MSN-ssDNA films. We chose PEG as it is the most used anti-fouling linker to tether ligands onto surfaces [41-43]. Our results showed that PEG chain length has a substantial impact on RGD-stem cell interactions. A longer PEG linker appeared to be more efficient in reducing non-specific cell attachment. More interestingly, a longer PEG linker also improved RGD functionality, as evidenced by enhanced cell adhesion with a more spread cell morphology. These findings are in line with a previous study by Lee et al. who reported that an increase in spacer arm length led to enhanced cell spreading and proliferation in both 2D and 3D culturing systems due to an improved accessibility of the RGD peptides to cells with a longer chain [44]. Our study confirmed that PEG chain length is a crucial factor influencing stem cell adhesion to peptide sequences. An appropriate PEG length is required to decouple non-specific interactions and achieve optimal RGD presentation. One common issue upon implantation of a biomaterial is the

nonspecific protein and cell fouling on the surfaces of biomaterials, resulting in inflammation, foreign-body response, and even the loss of the implants functions [45]. To solve this issue, anti-fouling strategies have been applied to minimize the immune response or bacterial infections of biomaterials [46, 47]. The knowledge obtained from this study is useful to determine the optimal spacer length to ensure specific cell adhesion to biomaterials and scaffolds.

In Chapter 4, we fabricated four MSN films using high and low-clustered RGD on MSN to investigate the influence of RGD nanoclustering level and global densities on stem cell adhesion and differentiation. Our results demonstrated that both RGD global density and nanoclustering level are crucial variables to regulate stem cell behavior. In line with a previous report [48], we observed enhanced cell adhesion and spreading when RGD global density increased. When we kept global RGD densities the same, surfaces with more highly clustered RGD promoted cell spreading, focal adhesion formation and expression of alkaline phosphatase in hMSCs. It has been previously reported that a full cell adhesion response requires two criteria to be fulfilled: (1) the integrin receptors must be occupied by a ligand and (2) the integrin receptors must be clustered within the cell membrane [20, 49]. Integrin-binding ligands in a clustered format aided in achieving both of these criteria, thus resulting in enhanced integrin clustering and the formation of focal complexes [50]. As such, the observed enhanced focal adhesion to the surface with a higher ligand clustering level may be related to a higher level of cellular integrin clustering. Several earlier studies have reported the importance of ligand clustering in regulating cell adhesion [51-53]. For example, in the study by Fatemeh et al., improved adhesion and migration of endothelial cells was observed on nano-clustered surfaces compared to random surfaces [50]. Our results together with the previous studies suggested that ligand nano-clustering is a key player in regulating cell behavior. We expect that nano-clustering of peptide ligands would be a promising strategy for next generation biomaterials with improved functionality in tissue engineering, as it was recently highlighted that the incorporation of clustered bioadhesive ligands could improve adhesion and spreading of fibroblast cells on composite hydrogels [54] or promote robust implant-tissue integration [55].

Given the dynamic nature of natural ECM, in chapter 5, we fabricated a dynamic platform with tunable RGD presenting kinetics to investigate the effect of ligand dynamics on stem cell behavior. The results of this study showed that surfaces with low RGD kinetics led to enhanced stem cell adhesion and spreading

resulting in a more elongated cell morphology, and promoted cell migration compared to surfaces with high RGD kinetics. Previously, several research groups have investigated the influence of ligand dynamics on stem cell adhesion, migration and differentiation [17, 56-58]. When comparing these studies with our research results, some interesting similarities are observed. In the study by Dexter et al., it has been demonstrated that a rotary surface inhibited stem cell adhesion, spreading, and actin cytoskeleton formation compared to a static surface [59]. In another study, Bian's group showed that the mobile RGD presentation delayed the early adhesion and spreading of hMSCs, leading to compromised osteogenic differentiation at a later stage when compared to static surfaces with restricted RGD tether mobility [17]. We speculated that such an effect could be explained by the altered ligand-integrin-binding kinetics [60]. Studying ligand dynamics provides valuable insights into the dynamic behavior and therapeutic implications of ligand-receptor interactions. A full understanding of cell responses to their dynamic environment should help researchers developing better ECM-mimicking biomaterials for modulating cell behavior in tissue engineering.

3. Future perspective

The design and fabrication of instructive synthetic biointerfaces has significantly advanced our fundamental understanding of integrin-matrix interactions. In particular in the field of tissue engineering and regenerative medicine, knowledge on how stem cells respond to specific cues can help researchers rationally design bioactive materials. Despite these tremendous advancements in the development of biointerfaces, there are still many challenges that need to be addressed. First, many previous studies including ours used RGD peptides. Different ligand types can result in drastically different cellular behavior. Therefore, exploring the effect of other integrin-binding ligands is of interest too. In Chapter 3, we developed a versatile biointerface based on MSN-ssDNA films. Since DNA hybridization is highly programmable and tunable, one powerful advantage of our design is that different types of ligands or even multiple ligands can easily be introduced into the platform. Therefore, such a biointerface is a promising platform for the study of other types of integrin binding ligands and ligands crosstalk. In addition, since soluble bioactive factors can be easily loaded in the mesopores of MSN, this system also allows for the simultaneous study of soluble factors as well as immobilized ligands in regulating stem cell processes. Moreover, beyond the

biochemical cues, the nanoscale surface topography is also an important factor in influencing stem cell fate. Since the MSN morphology and size can be easily tuned as reported previously [61], we envisage that the developed MSN films also be explored to study the interaction of nanotopographical features with stem cells in the future. Finally, in the current thesis, the impact of ligand immobilization strategies has only been explored on stem cells. However, the developed MSN films also hold high potential to be used for other biomedical applications for the study of other types of cells. For example, the dynamic platforms developed in Chapter 5 can be adapted to study metastasis of primary cancer, which is mediated by detachment of cells from a solid tumor and resettlement of the detached tumor cells in a new site. Additionally, the platform is also applicable for the study of other dynamic biological processes such as bacterial chemotaxis and mobility.

References

- [1] H. Shin, S. Jo, A.G. Mikos, Biomimetic materials for tissue engineering, *Biomaterials* 24(24) (2003) 4353-4364.
- [2] N. Huettnner, T.R. Dargaville, A. Forget, Discovering Cell-Adhesion Peptides in Tissue Engineering: Beyond RGD, *Trends in Biotechnology* 36(4) (2018) 372-383.
- [3] U. Hersel, C. Dahmen, H. Kessler, RGD modified polymers: biomaterials for stimulated cell adhesion and beyond, *Biomaterials* 24(24) (2003) 4385-4415.
- [4] J. Yu, A.R. Lee, W.H. Lin, C.W. Lin, Y.K. Wu, W.B. Tsai, Electrospun PLGA fibers incorporated with functionalized biomolecules for cardiac tissue engineering, *Tissue Eng Part A* 20(13-14) (2014) 1896-907.
- [5] S.W. Kang, B.H. Cha, H. Park, K.S. Park, K.Y. Lee, S.H. Lee, The effect of conjugating RGD into 3D alginate hydrogels on adipogenic differentiation of human adipose-derived stromal cells, *Macromol Biosci* 11(5) (2011) 673-9.
- [6] S.L. Bellis, Advantages of RGD peptides for directing cell association with biomaterials, *Biomaterials* 32(18) (2011) 4205-10.
- [7] S.J. Attwood, E. Cortes, A.W.M. Haining, B. Robinson, D. Li, J. Gautrot, A. del Río Hernández, Adhesive ligand tether length affects the size and length of focal adhesions and influences cell spreading and attachment, *Scientific Reports* 6(1) (2016) 34334.
- [8] G. Bae, M.S. Kim, R. Thangam, T.M. Koo, W.Y. Jang, J. Yoon, S.B. Han, L. Yang, S.Y. Kim, N. Kang, S. Min, H. Hong, H.E. Fu, M.J. Ko, D.H. Kim, W.K. Jeong, D.H. Kim, T.H. Kim, J.W. Choi, K.B. Lee, R. Paulmurugan, Y. Zhu, H.J. Kim, J. Lee, J.S. Kim, A. Khademhosseini, Y.K. Kim, H. Kang, Receptor-Level Proximity and Fastening of Ligands Modulates Stem Cell Differentiation, *Advanced Functional Materials* 32(30) (2022).
- [9] T. Satav, J. Huskens, P. Jonkheijm, Effects of Variations in Ligand Density on Cell Signaling, *Small* 11(39) (2015) 5184-99.
- [10] W. Li, Z. Yan, J. Ren, X. Qu, Manipulating cell fate: dynamic control of cell behaviors on functional platforms, *Chem Soc Rev* 47(23) (2018) 8639-8684.
- [11] Y. Ma, X.H. Tian, L. Liu, J.M. Pan, G.Q. Pan, Dynamic Synthetic Bionterfaces: From Reversible Chemical Interactions to Tunable Biological Effects, *Accounts Chem. Res.* 52(6) (2019) 1611-1622.
- [12] M. Schwartzman, M. Palma, J. Sable, J. Abramson, X. Hu, M.P. Sheetz, S.J. Wind, Nanolithographic Control of the Spatial Organization of Cellular Adhesion Receptors at the Single-Molecule Level, *Nano Letters* 11(3) (2011) 1306-1312.
- [13] G. Roman, M. Martin, P.S. Joachim, Block copolymer micelle nanolithography, *Nanotechnology* 14(10) (2003) 1153.
- [14] J.A. Deeg, I. Louban, D. Aydin, C. Selhuber-Unkel, H. Kessler, J.P. Spatz, Impact of Local versus Global Ligand Density on Cellular Adhesion, *Nano Letters* 11(4) (2011) 1469-1476.

- [15] E.A. Cavalcanti-Adam, T. Volberg, A. Micoulet, H. Kessler, B. Geiger, J.P. Spatz, Cell spreading and focal adhesion dynamics are regulated by spacing of integrin ligands, *Biophys J* 92(8) (2007) 2964-74.
- [16] M. Arnold, E.A. Cavalcanti-Adam, R. Glass, J. Blümmel, W. Eck, M. Kantslehner, H. Kessler, J.P. Spatz, Activation of integrin function by nanopatterned adhesive interfaces, *Chemphyschem* 5(3) (2004) 383-8.
- [17] D.S.H. Wong, J.N. Li, X.H. Yan, B. Wang, R. Li, L. Zhang, L.M. Bian, Magnetically Tuning Tether Mobility of Integrin Ligand Regulates Adhesion, Spreading, and Differentiation of Stem Cells, *Nano Letters* 17(3) (2017) 1685-1695.
- [18] Q. Chen, D. Zhang, J. Gu, H. Zhang, X. Wu, C. Cao, X. Zhang, R. Liu, The Impact of Antifouling Layers in Fabricating Bioactive Surfaces, *Acta Biomater* (2021).
- [19] L.Y. Koo, D.J. Irvine, A.M. Mayes, D.A. Lauffenburger, L.G. Griffith, Co-regulation of cell adhesion by nanoscale RGD organization and mechanical stimulus, *J Cell Sci* 115(Pt 7) (2002) 1423-33.
- [20] S. Miyamoto, S.K. Akiyama, K.M. Yamada, Synergistic roles for receptor occupancy and aggregation in integrin transmembrane function, *Science* 267(5199) (1995) 883-5.
- [21] L. Chen, X. Zhou, C. He, Mesoporous silica nanoparticles for tissue-engineering applications, *Wiley Interdiscip Rev Nanomed Nanobiotechnol* (2019) e1573.
- [22] C. Khatua, S. Min, H.J. Jung, J.E. Shin, N. Li, I. Jun, H.W. Liu, G. Bae, H. Choi, M.J. Ko, Y.S. Jeon, Y.J. Kim, J. Lee, M. Ko, G. Shim, H. Shin, S. Lee, S. Chung, Y.K. Kim, J.J. Song, V.P. Dravid, H. Kang, In Situ Magnetic Control of Macroscale Nanoligand Density Regulates the Adhesion and Differentiation of Stem Cells, *Nano Lett* 20(6) (2020) 4188-4196.
- [23] Y. Guo, R. Yan, X. Wang, G. Liang, A. Yang, J. Li, Near-Infrared Light-Controlled Activation of Adhesive Peptides Regulates Cell Adhesion and Multidifferentiation in Mesenchymal Stem Cells on an Up-Conversion Substrate, *Nano Lett* 22(6) (2022) 2293-2302.
- [24] J.N. Roberts, J.K. Sahoo, L.E. McNamara, K.V. Burgess, J. Yang, E.V. Alakpa, H.J. Anderson, J. Hay, L.A. Turner, S.J. Yarwood, M. Zelzer, R.O. Oreffo, R.V. Ulijn, M.J. Dalby, Dynamic Surfaces for the Study of Mesenchymal Stem Cell Growth through Adhesion Regulation, *ACS Nano* 10(7) (2016) 6667-79.
- [25] H. Kang, H.J. Jung, D.S.H. Wong, S.K. Kim, S. Lin, K.F. Chan, L. Zhang, G. Li, V.P. Dravid, L. Bian, Remote Control of Heterodimeric Magnetic Nanoswitch Regulates the Adhesion and Differentiation of Stem Cells, *Journal of the American Chemical Society* 140(18) (2018) 5909-5913.
- [26] C.C. Ng, A. Magenau, S.H. Ngalim, S. Ciampi, M. Chockalingham, J.B. Harper, K. Gaus, J.J. Gooding, Using an electrical potential to reversibly switch surfaces between two states for dynamically controlling cell adhesion, *Angew Chem Int Ed Engl* 51(31) (2012) 7706-10.

- [27] J. Brinkmann, E. Cavatorta, S. Sankaran, B. Schmidt, J. van Weerd, P. Jonkheijm, About supramolecular systems for dynamically probing cells, *Chem Soc Rev* 43(13) (2014) 4449-69.
- [28] L. Feng, W. Li, J. Ren, X. Qu, Electrochemically and DNA-triggered cell release from ferrocene/beta-cyclodextrin and aptamer modified dual-functionalized graphene substrate, *Nano Research* 8(3) (2015) 887-899.
- [29] J. Robertus, W.R. Browne, B.L. Feringa, Dynamic control over cell adhesive properties using molecular-based surface engineering strategies, *Chem Soc Rev* 39(1) (2010) 354-78.
- [30] R. Meyer, S. Giselbrecht, B.E. Rapp, M. Hirtz, C.M. Niemeyer, Advances in DNA-directed immobilization, *Curr Opin Chem Biol* 18 (2014) 8-15.
- [31] R. Hager, A. Arnold, E. Sevcsik, G.J. Schütz, S. Howorka, Tunable DNA Hybridization Enables Spatially and Temporally Controlled Surface-Anchoring of Biomolecular Cargo, *Langmuir* 34(49) (2018) 15021-15027.
- [32] R. Freeman, N. Stephanopoulos, Z. Alvarez, J.A. Lewis, S. Sur, C.M. Serrano, J. Boekhoven, S.S. Lee, S.I. Stupp, Instructing cells with programmable peptide DNA hybrids, *Nat Commun* 8 (2017) 15982.
- [33] M.F. Brizzi, G. Tarone, P. Defilippi, Extracellular matrix, integrins, and growth factors as tailors of the stem cell niche, *Curr Opin Cell Biol* 24(5) (2012) 645-51.
- [34] D. Docheva, C. Popov, W. Mutschler, M. Schieker, Human mesenchymal stem cells in contact with their environment: surface characteristics and the integrin system, *J Cell Mol Med* 11(1) (2007) 21-38.
- [35] M.J. Dalby, N. Gadegaard, R.O. Oreffo, Harnessing nanotopography and integrin-matrix interactions to influence stem cell fate, *Nat Mater* 13(6) (2014) 558-69.
- [36] S. A. Vermeulen, Advancing the cell culture landscape: the instructive potential of artificial and natural geometries. [Doctoral Thesis, Maastricht University]. Maastricht University, 2020.
- [37] X. Wang, C. Yan, K. Ye, Y. He, Z. Li, J. Ding, Effect of RGD nanospacing on differentiation of stem cells, *Biomaterials* 34(12) (2013) 2865-74.
- [38] J. Huang, S.V. Grater, F. Corbellini, S. Rinck, E. Bock, R. Kemkemer, H. Kessler, J. Ding, J.P. Spatz, Impact of order and disorder in RGD nanopatterns on cell adhesion, *Nano Lett* 9(3) (2009) 1111-6.
- [39] P.W. Kämmerer, M. Heller, J. Brieger, M.O. Klein, B. Al-Nawas, M. Gabriel, Immobilisation of linear and cyclic RGD-peptides on titanium surfaces and their impact on endothelial cell adhesion and proliferation, *Eur Cell Mater* 21 (2011) 364-72.
- [40] X. Zhang, S. van Rijt, DNA modified MSN-films as versatile biointerfaces to study stem cell adhesion processes, *Colloids Surf B Biointerfaces* 215 (2022) 112495.

- [41] K. Ye, X. Wang, L. Cao, S. Li, Z. Li, L. Yu, J. Ding, Matrix Stiffness and Nanoscale Spatial Organization of Cell-Adhesive Ligands Direct Stem Cell Fate, *Nano Letters* 15(7) (2015) 4720-4729.
- [42] B. Cao, Z. Li, R. Peng, J. Ding, Effects of cell–cell contact and oxygen tension on chondrogenic differentiation of stem cells, *Biomaterials* 64 (2015) 21-32.
- [43] Q. Chen, S. Yu, D. Zhang, W. Zhang, H. Zhang, J. Zou, Z. Mao, Y. Yuan, C. Gao, R. Liu, Impact of Antifouling PEG Layer on the Performance of Functional Peptides in Regulating Cell Behaviors, *J Am Chem Soc* 141(42) (2019) 16772-16780.
- [44] J.W. Lee, Y.J. Park, S.J. Lee, S.K. Lee, K.Y. Lee, The effect of spacer arm length of an adhesion ligand coupled to an alginate gel on the control of fibroblast phenotype, *Biomaterials* 31(21) (2010) 5545-5551.
- [45] D. Zhang, Q. Chen, C. Shi, M. Chen, K. Ma, J. Wan, R. Liu, Dealing with the Foreign-Body Response to Implanted Biomaterials: Strategies and Applications of New Materials, *Advanced Functional Materials* 31(6) (2021) 2007226.
- [46] I. Francolini, C. Vuotto, A. Piozzi, G. Donelli, Antifouling and antimicrobial biomaterials: an overview, *Apmis* 125(4) (2017) 392-417.
- [47] Z.K. Zander, M.L. Becker, Antimicrobial and Antifouling Strategies for Polymeric Medical Devices, *ACS Macro Letters* 7(1) (2018) 16-25.
- [48] J.A. Rowley, D.J. Mooney, Alginate type and RGD density control myoblast phenotype, *J Biomed Mater Res* 60(2) (2002) 217-23.
- [49] F. Karimi, A.J. O'Connor, G.G. Qiao, D.E. Heath, Integrin Clustering Matters: A Review of Biomaterials Functionalized with Multivalent Integrin-Binding Ligands to Improve Cell Adhesion, Migration, Differentiation, Angiogenesis, and Biomedical Device Integration, *Adv Healthc Mater* 7(12) (2018) e1701324.
- [50] F. Karimi, T.G. McKenzie, A.J. O'Connor, G.G. Qiao, D.E. Heath, Nano-scale clustering of integrin-binding ligands regulates endothelial cell adhesion, migration, and endothelialization rate: novel materials for small diameter vascular graft applications, *Journal of Materials Chemistry B* 5(30) (2017) 5942-5953.
- [51] G. Maheshwari, G. Brown, D.A. Lauffenburger, A. Wells, L.G. Griffith, Cell adhesion and motility depend on nanoscale RGD clustering, *J Cell Sci* 113 (Pt 10) (2000) 1677-86.
- [52] P.L. Benitez, S. Mascharak, A.C. Proctor, S.C. Heilshorn, Use of protein-engineered fabrics to identify design rules for integrin ligand clustering in biomaterials, *Integr Biol (Camb)* 8(1) (2016) 50-61.
- [53] K.Y. Lee, E. Alsberg, S. Hsiang, W. Comisar, J. Linderman, R. Ziff, D. Mooney, Nanoscale Adhesion Ligand Organization Regulates Osteoblast Proliferation and Differentiation, *Nano Lett* 4(8) (2004) 1501-1506.
- [54] D. Dems, R. Freeman, K.D. Riker, T. Coradin, S.I. Stupp, C. Aimé, Multivalent Clustering of Adhesion Ligands in Nanofiber-Nanoparticle Composites, *Acta Biomaterialia* 119 (2021) 303-311.

- [55] T.A. Petrie, J.E. Raynor, D.W. Dumbauld, T.T. Lee, S. Jagtap, K.L. Templeman, D.M. Collard, A.J. García, Multivalent integrin-specific ligands enhance tissue healing and biomaterial integration, *Sci Transl Med* 2(45) (2010) 45ra60.
- [56] W. Du, D.T. Zhang, X.M. Wang, T.C. Ren, C.Y. Gao, Mediating the Migration of Mesenchymal Stem Cells by Dynamically Changing the Density of Cell-selective Peptides Immobilized on beta-Cyclodextrin-modified Cell-resisting Polymer Brushes, *Chin. J. Polym. Sci.* 38(2) (2020) 126-136.
- [57] L. Liu, X. Tian, Y. Ma, Y. Duan, X. Zhao, G. Pan, A Versatile Dynamic Mussel-Inspired Biointerface: From Specific Cell Behavior Modulation to Selective Cell Isolation, *Angew Chem Int Ed Engl* 57(26) (2018) 7878-7882.
- [58] S. Min, M.J. Ko, H.J. Jung, W. Kim, S.-B. Han, Y. Kim, G. Bae, S. Lee, R. Thangam, H. Choi, N. Li, J.E. Shin, Y.S. Jeon, H.S. Park, Y.J. Kim, U.K. Sukumar, J.-J. Song, S.-K. Park, S.-H. Yu, Y.C. Kang, K.-B. Lee, Q. Wei, D.-H. Kim, S.M. Han, R. Paulmurugan, Y.K. Kim, H. Kang, Remote Control of Time-Regulated Stretching of Ligand-Presenting Nanocoils In Situ Regulates the Cyclic Adhesion and Differentiation of Stem Cells, *Advanced Materials* 33(11) (2021) 2008353.
- [59] Q. Zhou, J. Chen, Y. Luan, P.A. Vainikka, S. Thallmair, S.J. Marrink, B.L. Feringa, P. van Rijn, Unidirectional rotating molecular motors dynamically interact with adsorbed proteins to direct the fate of mesenchymal stem cells, *Sci Adv* 6(5) (2020) eaay2756.
- [60] C. An, X. Wang, F. Song, J. Hu, L. Li, Insights into intercellular receptor-ligand binding kinetics in cell communication, *Front Bioeng Biotechnol* 10 (2022) 953353.
- [61] J.M. Rosenholm, J. Zhang, M. Linden, C. Sahlgren, Mesoporous silica nanoparticles in tissue engineering--a perspective, *Nanomedicine (Lond)* 11(4) (2016) 391-402.

Chapter 7

Impact

In this chapter, we discuss the (potential) impact of the research results described in the thesis on the state of the art scientific knowledge and applications within and across disciplines of tissue engineering and regenerative medicine. In addition, we also discuss the societal and economic relevance of our research findings.

By combining principles from cell biology, engineering, and materials science, the field of tissue engineering and regenerative medicine provides unprecedented opportunities to restore, maintain, or improve the functions of injured tissues and organs damaged by aging, cancer and other diseases [1, 2]. It aims to engineer functional tissues/constructs that can be implanted into the body to promote natural healing processes, and ultimately improve patients' quality of life. In 2006, the first engineered tissue, specifically an engineered bladder, was successfully implanted into human patients [3]. The engineered bladder was created using a combination of the patients' own cells and a biodegradable scaffold, allowing it to grow and integrate with the natural tissues in the body [4]. This groundbreaking achievement marked a significant milestone in the field of regenerative medicine and tissue engineering, and has further spurred the development of experimental therapies and increased public expectations. Enthusiasm about the far-reaching potential of tissue engineering created a gap between expectations and the (speed of) translation of experimental technologies into clinical practice. Currently, there are still many challenges to overcome in the process leading from bench to bedside. Specifically, creating biomaterials and tissue engineered constructs with tailored and controllable interaction with the biological environment of the body remains a core challenge. To address this challenge, it is of utmost importance to obtain a full understanding of how cells interact with their environment. This knowledge could help researchers engineer better biomaterials that mimic the native environment or adopt to it, improving tissue and organ repair and regeneration, and offering potential treatments for various degenerative diseases and injuries. Therefore, we anticipate that the contributions of this thesis to the understanding of how ligand immobilization strategies influence stem cell-material interactions may be valuable to a broad scientific community and will eventually accelerate the clinical translation of regenerative medicine products.

Since the discovery of fibronectin and the role it plays in cell adhesion, there has been increasing interest in the use of ECM proteins for promoting cell adhesion in tissue engineered constructs. In particular, RGD, which has been

identified as the minimal binding domain of fibronectin, has become the most widely used ligand for material functionalization to improve cell adhesion [5]. However, other cell adhesion peptides (CAPs), have also been investigated. CAPs including RGD, represent an interesting alternative to the use of natural ECM macromolecules, because they are easy to manufacture at a high purity in automated peptide synthesizers, and are well characterized. As such, CAPs have had a great impact on the design of cell culture platforms, implants, and wound dressings. Despite their potential, the full scope of functions exhibited by various CAPs is not yet comprehensively understood [6]. Biointerfaces with the capability to present biomolecules specifically and flexibly such as the one developed in Chapter 3 (DNA modified MSN films), are promising platforms to systematically study their biological functions. By finely controlling the presentation of these ligands, researchers can gain insights into cell adhesion mechanisms, signaling pathways, and cellular responses, ultimately contributing to the advancement of regenerative medicine and tissue engineering strategies by the creation of new biomaterial design rules.

The MSNs used in this study can also be used themselves in biomedical applications as coatings or components in biomaterials. Surface coating technology is a promising strategy for the creation of highly biocompatible and functional biomaterials, including medical devices and scaffolds for regenerative medicine. For example, coating techniques have been used to improve the osteoconductivity of bone implants and bone fillers. Silica nanoparticles could be used as potential coating materials [7]. In the past few years, silica nanoparticles have entered clinical trials for a variety of biomedical applications, including oral drug delivery, diagnostics, plasmonic resonance and photothermal ablation therapy. Preliminary results indicate the safety, efficacy and viability of silica nanoparticles under these clinical scenarios [8]. In this thesis, the synthesized silica nanoparticles have only been used for coating glass surfaces. However, considering their good biocompatibility and potential drug delivery capacity, MSN may be suitable for coating a wide range of biomaterials. Especially, in Chapter 4, we developed MSN functionalized with highly clustered of RGD ligands, which has been shown to enhance stem cell adhesion. Such MSN coatings may thus be used to enable proper cell adhesion to biomaterials and enhance their integration with the surrounding tissue. In addition to the coating approach, MSN can also be incorporated into biomaterials as chemical crosslinkers to increase their bioactivity or mechanical properties [9, 10], which are crucial for their clinical applicability. For

example, hydrogels are a promising class of materials in tissue regeneration [11]. However, hydrogel often lacks the mechanical strength required for load-bearing applications like bone regeneration. Several studies have reported that incorporating MSN into the hydrogel matrix allows for the development of hybrid material with improved structural integrity and mechanical properties [12, 13]. Additionally, another interesting study has demonstrated that RGD-modification of MSN remarkably enhanced cell adhesion on an alginate hydrogel compared to a MSN-NH₂- incorporated hydrogel [14]. Therefore, the functionalized MSN developed in the thesis holds the potential for a wide range of applications, such as serving as a coating material for biomedical devices or as additives to create hybrid biomaterials with additional functionalities, demonstrating their potential clinical and economic impact.

The study of cells on surfaces is relevant in several scientific disciplines. In the current thesis, we empathize the usefulness of synthetic biointerfaces in understanding stem cell-material interactions in the regenerative medicine field. In Chapter 5, we explored a novel strategy based on DNA hybridization to create a dynamic biointerface. This paves the way towards the fabrication of advanced ECM-mimicking biomaterials with dynamic complexity associated with complex cell processes. Beyond regenerative medicine, dynamic platforms also hold high potential to be used for other applications such as cell-based disease diagnosis. Work performed by Lei and co-workers nicely demonstrated this concept [15]. In this work, a flexible dynamic interface was developed. Different peptides were successfully introduced for various applications from dynamic modulation of stem cell adhesion behavior to selective isolation of tumor cells. Currently, most dynamic systems are focused on *in vitro* studies. There is still a long way to go to translate the dynamic systems to clinical applications. To speed up the translation process, further efforts should be directed towards evaluation of the efficacy and long-lasting operation of the dynamic platforms both *in vitro* and *in vivo*, as well as their cost and scalability [16].

References

- [1] S. Mantha, S. Pillai, P. Khayambashi, A. Upadhyay, Y. Zhang, O. Tao, H.M. Pham, S.D. Tran, *Smart Hydrogels in Tissue Engineering and Regenerative Medicine*, *Materials* 12(20) (2019) 3323.
- [2] F. Berthiaume, T.J. Maguire, M.L. Yarmush, *Tissue Engineering and Regenerative Medicine: History, Progress, and Challenges*, *Annual Review of Chemical and Biomolecular Engineering* 2(1) (2011) 403-430.
- [3] E. Jacques, E.J. Suuronen, *The Progression of Regenerative Medicine and its Impact on Therapy Translation*, *Clin Transl Sci* 13(3) (2020) 440-450.
- [4] A. Atala, *Tissue engineering of human bladder*, *British Medical Bulletin* 97(1) (2011) 81-104.
- [5] N. Huettner, T.R. Dargaville, A. Forget, *Discovering Cell-Adhesion Peptides in Tissue Engineering: Beyond RGD*, *Trends Biotechnol* 36(4) (2018) 372-383.
- [6] Q. Chen, S. Yu, D. Zhang, W. Zhang, H. Zhang, J. Zou, Z. Mao, Y. Yuan, C. Gao, R. Liu, *Impact of Antifouling PEG Layer on the Performance of Functional Peptides in Regulating Cell Behaviors*, *J Am Chem Soc* 141(42) (2019) 16772-16780.
- [7] X. Lin, J. Chen, Y. Liao, J.L. Pathak, H. Li, Y. Liu, *Biomimetic Calcium Phosphate Coating as a Drug Delivery Vehicle for Bone Tissue Engineering: A Mini-Review*, *Coatings* 10(11) (2020) 1118.
- [8] T.I. Janjua, Y. Cao, C. Yu, A. Popat, *Clinical translation of silica nanoparticles*, *Nature Reviews Materials* 6(12) (2021) 1072-1074.
- [9] A. Zengin, J.P.O. Castro, P. Habibovic, S.H. van Rijt, *Injectable, self-healing mesoporous silica nanocomposite hydrogels with improved mechanical properties*, *Nanoscale* 13(2) (2021) 1144-1154.
- [10] A.K. Gaharwar, C. Rivera, C.J. Wu, B.K. Chan, G. Schmidt, *Photocrosslinked nanocomposite hydrogels from PEG and silica nanospheres: structural, mechanical and cell adhesion characteristics*, *Mater Sci Eng C Mater Biol Appl* 33(3) (2013) 1800-7.
- [11] S. Cascone, G. Lamberti, *Hydrogel-based commercial products for biomedical applications: A review*, *Int J Pharm* 573 (2020) 118803.
- [12] S. Yang, J. Wang, H. Tan, F. Zeng, C. Liu, *Mechanically robust PEGDA-MSNs-OH nanocomposite hydrogel with hierarchical meso-macroporous structure for tissue engineering*, *Soft Matter* 8(34) (2012) 8981-8989.
- [13] X. Sun, Z. Ma, X. Zhao, W. Jin, C. Zhang, J. Ma, L. Qiang, W. Wang, Q. Deng, H. Yang, J. Zhao, Q. Liang, X. Zhou, T. Li, J. Wang, *Three-dimensional bioprinting of multicell-laden scaffolds containing bone morphogenic protein-4 for promoting M2 macrophage polarization and accelerating bone defect repair in diabetes mellitus*, *Bioactive Materials* 6(3) (2021) 757-769.

- [14] N.S. Kehr, E.A. Prasetyanto, K. Benson, B. Ergün, A. Galstyan, H.-J. Galla, Periodic Mesoporous Organosilica-Based Nanocomposite Hydrogels as Three-Dimensional Scaffolds, *Angewandte Chemie International Edition* 52(4) (2013) 1156-1160.
- [15] L. Liu, X. Tian, Y. Ma, Y. Duan, X. Zhao, G. Pan, A Versatile Dynamic Mussel-Inspired Biointerface: From Specific Cell Behavior Modulation to Selective Cell Isolation, *Angew Chem Int Ed Engl* 57(26) (2018) 7878-7882.
- [16] W. Li, Z. Yan, J. Ren, X. Qu, Manipulating cell fate: dynamic control of cell behaviors on functional platforms, *Chem Soc Rev* 47(23) (2018) 8639-8684.

Summary

ECM-mimicking 2D biointerfaces that offer high control over surface properties are an important tool to improve our understanding of stem cell-material interactions. In this thesis, we focus on the design and fabrication of a new type of synthetic 2D biointerface based on mesoporous silica nanoparticles (MSN) to study how ECM adhesive ligand presentation parameters influence stem cell regenerative processes. Chapter 2 describes a literature review on the development of synthetic biointerfaces to study (stem) cell adhesion processes. This review focuses on the design of static biointerfaces with predefined biochemical signals and how these can be optimized towards the creation of dynamic biointerfaces that can spatiotemporally control ligand display. In the future outlook of Chapter 2, we highlight that one core challenge in the design of biointerfaces is to mimic the dynamicity and nanoscale features of natural ECM ligand presentation. In Chapters 3-5, we present novel strategies to address this challenge using MSN to tune the dynamic and clustered RGD ligand presentation at the nanoscale. To ensure specific interaction of the bioactive ligands with stem cell integrin receptors, the effect of PEG length on its anti-fouling property and RGD presentation is investigated in Chapter 3. The results demonstrated that RGD ligand immobilized on a longer PEG chain length is more favorable in terms of reducing non-specific cell attachment without negatively affecting RGD-cell interaction. Based on this result, a long PEG chain length was selected to prepare MSN films for the following studies. Next, in Chapter 4, we investigated the influence of RGD clustering level on stem cell morphology, adhesion and differentiation. We found that a higher RGD ligand clustering level led to enhanced focal adhesions and osteogenic differentiation of human mesenchymal stromal cells (hMSCs) even when the global RGD density remained consistent. In Chapter 5, we increased the MSN biointerface complexity to mimic the dynamicity of the ECM. A novel strategy based on DNA hybridization was explored to control ligand display kinetics. High RGD kinetics showed a negative effect on stem cell adhesion and migration. In Chapter 6, we summarize the main findings obtained in this thesis, give a general discussion of the results and provide future perspectives. In the last part of the thesis, we explore the scientific and social impact of our findings and potential future commercial applications of the system developed in this thesis.

In conclusion, the results described in the present thesis shed light upon the importance of adhesive ligand parameters for the regulation of stem cell adhesion, survival, migration and differentiation. Increased understanding on these processes will improve the clinical translation of stem cell-based therapies by helping tissue engineers to rationally design better performing bioactive biomaterials. Furthermore, this thesis also provides valuable insights into strategies to tune adhesion ligand presentation, which is a step forward toward uncovering the mechanisms underlying integrin-mediated cellular signaling pathways.

Samenvatting

2D-biointerfaces die de liganden van het ECM nabootsen met veel controle over oppervlakte-eigenschappen, zijn een belangrijk hulpmiddel om ons begrip van stamcel-materiaal interacties te verbeteren. In dit proefschrift richten we ons op het ontwerpen en ontwikkelen van een nieuw type synthetische 2D bio-interface op basis van mesoporeuze silica nanodeeltjes (MSN) om te bestuderen hoe de presentatie van ECM liganden stamcel regeneratieprocessen beïnvloeden. Hoofdstuk 2 beschrijft een literatuuroverzicht over de ontwikkeling van synthetische bio-interfaces om (stam)cel adhesieprocessen te bestuderen. De review richt zich op het ontwerp van statische bio-interfaces met vooraf gedefinieerde biochemische signalen en hoe deze kunnen worden geoptimaliseerd voor het creëren van dynamische bio-interfaces. In dit Hoofdstuk 2 benadrukken we ook dat een uitdaging bij het ontwerpen van bio-interfaces het nabootsen van de dynamische en specifieke biochemische signalen op nanoschaal is. In de hoofdstukken 3-5 presenteren we nieuwe strategieën om deze uitdaging aan te gaan met behulp van MSN om de dynamische en geclusterde RGD-ligandpresentatie op nanoschaal af te stemmen. Om zeker te zijn van een specifieke interactie van de bioactieve liganden met stamcel-integrine receptoren, wordt het effect van de PEG-lengte en de RGD-presentatie op specifieke stamcel adhesie onderzocht in Hoofdstuk 3. De resultaten toonden aan dat RGD-liganden geïmmobiliseerd op een langere PEG-ketenlengte gunstiger is in termen van het verminderen van niet-specifieke cel hechting zonder de RGD-cel interactie negatief te beïnvloeden. Op basis van dit resultaat werd een lange PEG-ketenlengte geselecteerd om MSN-films te maken voor de volgende onderzoeken. Vervolgens hebben we in Hoofdstuk 4 de invloed van RGD-clusteringniveau op stamcelmorfologie, adhesie en differentiatie onderzocht. We ontdekten dat een hogere RGD-ligand clusteringniveau leidde tot verbeterde focale adhesies en osteogene differentiatie van menselijke mesenchymale stromale cellen (hMSC's), zelfs wanneer de globale RGD-dichtheid consistent bleef. In hoofdstuk 5 hebben we de complexiteit van de MSN bio-interface verhoogd om de dynamiek van de ECM na te kunnen bootsen. Een nieuwe strategie op basis van DNA-hybridisatie werd onderzocht om de kinetiek van ligand display te beheersen. Hoge RGD-kinetiek toonde een negatief effect op

stamceladhesie en migratie. In Hoofdstuk 6 vatten we de belangrijkste bevindingen van dit proefschrift samen, geven we een algemene discussie over de resultaten, en geven we toekomstperspectieven. In het laatste deel van het proefschrift onderzoeken we de wetenschappelijke en maatschappelijke impact van onze bevindingen en mogelijke toekomstige commerciële toepassingen van het systeem dat in dit proefschrift is ontwikkeld.

Concluderend, de resultaten beschreven in dit proefschrift werpen licht op het belang van hoe adhesieve liganden gepresenteerd worden voor de regulatie van stamceladhesie, overleving, migratie en differentiatie. Een beter begrip van deze processen zal de klinische vertaling van op stamcellen gebaseerde therapieën verbeteren door onderzoekers in het veld van regeneratieve geneeskunde te helpen bij het rationeel ontwerpen van beter presterende bioactieve biomaterialen. Bovendien biedt dit proefschrift ook waardevolle inzichten in strategieën hoe de presentatie van liganden het beste afgestemd kunnen worden, wat een stap voorwaarts is in de richting van het blootleggen van de mechanismen die ten grondslag liggen aan integrine-gemedieerde cellulaire signaalroutes.

List of Publications

Xingzhen Zhang, Sabine van Rijt. 2D Biointerfaces to Study Stem Cell-ligand interactions. *Acta Biomaterialia*. 2021, 131, 80-96.

Xingzhen Zhang, Sabine van Rijt. DNA modified MSN-films as versatile biointerfaces to study stem cell adhesion processes. *Colloids and Surfaces B: Biointerfaces*. 2022, 215, 112495.

Xingzhen Zhang, Zeynep Karagöz, Sangita Swapnasrita, Pamela Habibović, Aurélie Carlier, and Sabine van Rijt. Development of mesoporous silica nanoparticle based films with tunable arginine-glycine-aspartate peptides global density and clustering levels to study stem cell adhesion and differentiation. *ACS Applied Materials & Interfaces*. 2023, 15 (32), 38171–38184.

Xingzhen Zhang, Stijn van Veen, Darya Hadavi, Yuandi Zhao, Maarten Honing, Pamela Habibović, Lorenzo Albertazzi, Sabine van Rijt. Effects of ligand-presenting dynamics on stem cell adhesion and migration. (Submitted to *Small*, in revision).

Scientific communications

- Chemistry as Innovating Science (CHAINS 2020, the Netherlands), Poster Presentation.
- 6th World Congress 2021 Tissue Engineering and Regenerative Medicine International Society (TERMIS 2021, Maastricht, the Netherlands), Oral Presentation.
- 30th Annual Meeting of the Netherlands Society for Biomaterials and Tissue Engineering (NBTE 2022, De Werelt, the Netherlands), Poster Presentation.
- 13th International workshop on Engineering of Functional Interfaces (EnFI 2022, Maastricht, the Netherlands), Oral and Poster Presentation.
- 32nd Annual Conference of the European Society for Biomaterials (ESB 2022, Bordeaux, France), Poster Presentation.

Acknowledgements

At long last, I come to the point of writing the acknowledgments, which I've been thinking about many times since I started writing my thesis. Pursuing a Ph.D. is not an easy process, and I am greatly thankful to those who have been by my side along my Ph.D. journal.

Foremost, I would like to thank my supervisors Dr. Sabine van Rijt and Professor Pamela Habibović for giving me the opportunity of doing my Ph.D. under their supervision. Dear Pamela, I want to express my sincere gratitude for your invaluable feedback on my papers and thesis chapters. Your suggestions have been very helpful and instructive. I understand you've been quite occupied with your new role, and I'm always impressed by your prompt response and efficient feedback. Dear Sabine, you are not just an awesome supervisor; you have also become a dear friend, adding a shining light to my life. When I lost confidence at the beginning of my PhD, you encouraged me. When things were not working in the lab, you guided me through, and helped me with finding a solution. You had the ability and power to catch interesting points from experiments and results that I could not see. Your solid knowledge of biomaterials and chemistry has been proven very valuable to my research. I am very grateful for all your patience, feedback, suggestions and comments on my writing and presentation skills. Besides, I like all the little sketches you drew during our regular meetings, from the chemical structure of mesoporous silica nanoparticles to various chemical reactions. This really helps the discussion and has brought so much fun to our meetings.

Besides my supervisors, I also would also like to thank the members of my thesis evaluation committee Prof. Roman Truckenmüller, Prof. Pascal Jonkheijm, Prof. Carmen Bartic, Dr. Ingrid Dijkgraaf and Dr. Matt Baker for taking the time to critically evaluate and provide feedback on this thesis.

My sincere thanks also goes to our research collaborators Dr. Aurélie Carlier, Zeynep Karagöz, Sangita Swapnasrita, Hamidreza Jafarinia, Prof. Lorenzo Albertazzi, Stijn van Veen, Prof. Maarten Honing, Dr. Darya Hadavi, Yuandi Zhao.

Many thanks to all the members of the Nanogroup, past and present, who have made it a great place to work: Por, Aygul, Chloe, Lei, Gerli, Lotte, Dina, Lin, Jin,

Valentino, Ana, Aida, Matthias, Darragh. Thank you all for helping and supporting me during my PhD: from providing me with advice during our group meetings to all the great time we have spent together during our group outings.

In addition, my thanks are also extended to all my other colleagues and friends at MERLN. I would like to acknowledge all the lab managers: Timo, Eva, Denis, Dennie and Marloes for their assistance in the laboratory, and for putting effort to provide a safe and nice working environment. Yousra, Francis, Francesca, David, Steven, Maryam, Martyna, Filipa, Maria José, Asli, Jaehyeon, Vinidhra, Fiona, Clarissa, Betzabeth, Claudia, Shivesh, Tristan, Monize, Carlos, Carolin, Sami, Tim, Adrian, Kike, Ivo and other MERLNers.... Thank you all for your help throughout my PhD journey.

Many special thanks goes to my Chinese friends who I met at MERLN. Jiaping, Lei, Hongjuan, Ke, Wen, Luo, Qiang, Zhengdong, Hao, Fangzhou. Thank you for offering help. Wishing you the best of luck with your time at MERLN. 感谢李老师在 工作, 科研, 实验和生活上总是热心地给予我们帮助和提供宝贵的建议, 感谢李老师帮我融入 MERLN 以及邀请我们去乌特勒支做客。感谢何磊和洪娟经常邀请我们一起聚餐, 打牌, 玩狼人杀以及一起周边游玩。感谢宋柯无私的分享 protocol 和借给我试剂, 还有平时一起午饭时对科研和工作的探讨。感谢陈文对我实验上提供的建议和帮我测流变。感谢罗娇和蓓陪我去市中心吃饭和赏夜景, 还有经常一起喝咖啡。感谢政栋和方舟邀请我们去你家吃火锅。感谢邬浩对我在 Photoshop 上提供技术支持。除此之外, 我还想感谢 Yonggang, Dongqin, Tianyu, Tianran, 感谢你们在我刚开始加入 MERLN 时的陪伴和帮助, 希望你们在国内的生活一切顺利。

Siyu (孙思雨), I enjoyed the time I spent with you. From our first meeting in Jinan in 2016 to the present day in Maastricht, our friendship has grown stronger with each passing year. You are always a good listener. It's great to know that I can tell you everything anytime. Thank you for helping and supporting me in the past eight years, and for taking care of Duoduo. My dear friends Zhanzhe Wu (吴瞻哲), Meizheng Li (李美铮), and your adorable cat GOGO, you have a special place in my heart. Your culinary skills have brought us so much delight with your delicious Chinese dishes such as Xian noodles, fish broth hotpot, Chinese BBQ, and more. Now, as you've started a new chapter of life in Amsterdam. I can't wait to hear about your exciting experiences in fishing. My neighbor and my drinking mate, Jiaojing Xu (许蛟婧), we had so many late night chats, where you shared with me your interest in archery, the traditional Chinese dresses and historical books. We had so much fun together. Thank you for taking care of Duoduo. Wenbo (吴文博),

Shan (王珊), Yingyi (吴映谊), Lisi (关丽斯), Wei (罗维), Wenting (油文亭), Xiuxiang (檀秀香), Hongxing (罗鸿幸), Yongchan (永婵), Panjun (高盼君), Longping (姚陇平), Qian (武谦), Shunxin (靳顺鑫), JIngnan (竞男), Min (邓敏), Feijie (飞杰) Xiaodi (张笑迪), we all moved to Maastricht and started our PhD journeys around the same time. I'm grateful to the countless memorable moments we've shared. From the heartwarming dinners and fun Chinese new year parties to the cherished little chats, every interaction with you has been a treasured part of my time here. I'd also like to express my gratitude to my other Chinese friends who I met at the beginning of my PhD journey and helped me settle into life in Maastricht: Qian (罗倩), Jun (万俊), Shanshan (王珊珊), Ying (龚英), Shengshi (黄盛世), Huajie (刘华杰), and Meng (张锰). Ning (安宁), I wish you all the very best in your endeavors. Cui (翠), Armando and your lovely baby (小馒头), thank you for inviting me to the barbecue party in your backyard with all people from Synapse. 云鹏、小松, 俊雄, 娟芝和桂翔, thank you for inviting us to dinners.

Lastly, I would like to thank my family, especially my parents, sister and brother. My greatest thanks goes to my partner **Jinmi** and my cat **DuoDuo**. Your presence has filled my life with immeasurable joy and happiness.

Curriculum Vitae

Xingzhen Zhang was born on the 7th of August 1992 in the Yanshi District of Luoyang, an industrial city in central Henan province of China. In 2015, she received her Bachelor's degree in Pharmacy at Shandong University, China. After that, she continued her Master's study in Pharmaceutics at the same University under the supervision of Professor Guangxi Zhai. Her master thesis was about the development of multifunctional nanoparticles for controlled and targeted drug delivery to treat glioma. During this phase, she received accolades such as the title of Outstanding Graduate Student of Shandong University and the prestigious First Class Academic Scholarship of Shandong University. In 2018, she was granted a scholarship by the China Scholarship Council, which provided her with the opportunity to pursue her Ph.D. studies abroad. Initially, she spent a year at the department of Psychiatry and Neuropsychology within the School for Mental Health and Neuroscience. Subsequently, she moved to the department of Instructive Biomaterials Engineering within the MERLN Institute for Technology-Inspired Regenerative Medicine. Under the supervision of Dr. Sabine van Rijt and Professor Pamela Habibovic, Xingzhen Zhang dedicated her Ph.D. research to the design and development of nanoparticle-based biointerfaces for studying stem cell-ligand interactions. The results of her research are described in this thesis.